UNIVERSITY OF VERONA
DEPARTMENT OF BIOTECHNOLOGY

Graduate School of Natural Sciences and Engineering
Doctoral Program in Biotechnology

XXX Cycle

Biochemical characterization of ornithine aminotransferase and cystathionine γ-lyase from *Toxoplasma gondii*: possible targets for drug development?

S.S.D. BIO/10

Coordinator: Prof. Massimo Delledonne
Tutor: Prof. Paola Dominici
Co-Tutor: Dr. Alessandra Astegno

Doctoral Student: Dr. Elena Maresi

Abstract

Toxoplasmosis is a widespread parasitic disease caused by *Toxoplasma gondii*, an obligate intracellular protozoa belonging to the phylum Apicomplexa. Toxoplasmosis is a major public health problem, infecting one-third of humans worldwide. Due to the fact that no effective vaccine is currently available and treatment is based on drugs for which resistance is emerging, there is an urgent need to discover novel drug targets that are exploitable for the design of new therapeutics against the pathogen.

A recent proteomic analysis of partially sporulated oocysts of *T. gondii* showed that oocysts have a greater capability of de novo amino acid biosynthesis, shedding light on several stage-specific proteins whose functional profile is in accord with the oocyst need to resist various environmental stresses [1]. Herein, we focused our attention on two enzymes belonging to these putative oocyst/sporozoite-specific protein group: the ornithine aminotransferase (OAT) and the cystathionine γ-lyase (CGL). OAT is involved in the polyamine metabolism and catalyzes the reversible conversion of L-ornithine (L-orn) into glutamate-5-semialdehyde and glutamate, while CGL catalyzes the cleavage of L-cystathionine (L-cth) to L-cysteine (L-cys), α-ketobutyrate and ammonia in the reverse transsulfuration pathway. Despite the central metabolic roles of these enzymes, the functionality of none of them has so far been investigated. Herein, a biochemical characterization of OAT and CGL from *T. gondii* has been performed, in order to expand the very limited knowledge about the polyamine and cysteine metabolism of the parasite and to explore the possible use of these enzymes as novel drug targets against toxoplasmosis.

Analysis of spectral and kinetic properties of TgOAT revealed that the enzyme is largely similar to OATs from other species regarding its general transamination mechanism and spectral properties of PLP; however, it does not possess a specific ornithine aminotransferase activity, but exhibits both N-acetylornithine (AcOrn) and γ-aminobutyric acid (GABA) transaminase activity, highlighting its possible role both in arginine and GABA metabolism *in vivo*. The presence of Val79 in the active site of TgOAT in place of Tyr, as in its human counterpart, provides the necessary room to accommodate AcOrn and GABA, resembling the active site arrangement of GABA transaminases. Moreover, mutation of Val79 to Tyr resulted in a change of substrate preference between GABA, AcOrn and L-orn, suggesting a key role of Val79 in defining substrate specificity.

The purified TgCGL is a functional enzyme which splits L-cth almost exclusively at the CγS bond to yield L-cys. This finding likely implies that the reverse transsulfuration pathway is operative in the parasite. The enzyme displays only marginal reactivity toward L-cys, which is

also a mixed-type inhibitor of TgCGL activity, therefore indicating a tight regulation of cysteine intracellular levels in the parasite. Structure-guided homology modelling revealed two striking amino acid differences between human and TgCGL active sites (Glu59 and Ser340 in human to Ser77 and Asn360 in toxoplasma). Mutation of these two residues to the corresponding residues in human revealed their importance in modulating both substrate and reaction specificity of the parasitic enzyme.

Altogether our findings could be considered as a first step toward exploring the possible use of TgOAT and TgCGL as an anti-toxoplasmosis drug targets.

Table of Contents

Abstract 6
Abbreviations/Acronyms 10

CHAPTER 1 12
GENERAL INTRODUCTION 12
1. *Toxoplasma gondii*, the causative agent of toxoplasmosis 14
2. Toxoplasmosis. 16
3. Pyridoxal 5'-phosphate enzymes 18
4. PLP-dependent enzymes as drug targets. 20
5. Aims 22

CHAPTER 2 23
UNIQUE SUBSTRATE SPECIFICITY OF ORNITHINE AMINOTRANSFERASE FROM *TOXOPLASMA GONDII* 24
1. INTRODUCTION 25
1.1 Polyamine metabolism 25
1.2 Ornithine aminotransferase 26
2. EXPERIMENTAL 31
2.1 Materials 31
2.2 Protein production 31
2.3 Size exclusion chromatography (SEC) 32
2.4 Determination of equilibrium dissociation constant of PLP for TgOAT and V79Y variants 33
2.5 Steady state analysis 33
2.6 Pre-steady state analysis 34
2.7 Spectroscopic measurements 34
2.8 Molecular modelling studies 35
2.9 Isothermal titration calorimetry (ITC) 35
3. RESULTS 37
3.1 Production of recombinant TgOAT 37
3.2 Spectral properties of recombinant TgOAT 38
3.3 Steady state kinetic studies 40
3.4 Absorption changes of TgOAT in the presence of substrates 42
3.5 Rapid-scanning stopped-flow kinetics 43
3.6 Reaction of TgOAT with β-chloro-L-alanine 45
3.7 V79Y variant 46
3.8 Molecular modelling 49

3.9 Regulation of TgOAT activity by reduced TgTrx....51
4. DISCUSSION....55

CHAPTER 3....58
THE TRANSSULFURATION ENZYME CYSTATHIONINE Γ-LYASE IS FUNCTIONAL IN *TOXOPLASMA GONDII*....59
1. INTRODUCTION....60
1.1 Sulfur-containing amino acids metabolism....60
1.2 Cystathionine γ-lyase....62
2. EXPERIMENTAL PROCEDURES....65
2.1 Protein production....65
2.2 Size exclusion chromatography (SEC)....65
2.3 Apo-proteins preparation....66
2.4 Limited proteolysis....66
2.5 Differential scanning calorimetry....66
2.6 Enzyme activity assays....66
2.7 Inhibition assays....67
2.8 Spectroscopic measurement....68
2.9 Statistical analysis....68
2.10 Thin layer chromatography....68
2.11 Molecular modelling studies....68
3. RESULTS....70
3.1 Expression and purification of recombinant TgCGL....70
3.2 Properties of recombinant TgCGL....70
3.3 Steady State Kinetic Parameters of TgCGL....72
3.4 Molecular modelling....77
3.5 N360S variant....79
3.6 S77E variant....82
4. DISCUSSION....85

GENERAL CONCLUSIONS....87

Appendix....88
References....90

Abbreviations/Acronyms

AcOAT	N-acetylornithine aminotransferase
AcOrn	N-acetylornithine
ADC	Arginine decarboxylase
AdoMet	S-adenosylmethionine
AdoMetDC	S-Adenosylmethionine decarboxylase
BCA	β-chloro-L-alanine
CBL	Cystathionine β-lyase
CBS	Cystathionine β-synthase
CD	Circular dichroism
CGL	Cystathionine γ-lyase
CGS	Cystathionine γ-synthase
CS	Cysteine synthase
dcAdoMet	Decarboxylated S-adenosylmethionine
DSC	Differential scanning calorimetry
DTNB	5,5′-dithiobis-(2-nitrobenzoic acid)
DTT	DL-Dithiothreitol
EDTA	Ethylenediaminetetraacetic acid
GABA	γ-aminobutyric acid
GABA-AT	γ-aminobutyric acid aminotransferase
GOX	Glutamate oxidase
IPTG	Isopropyl β-D-1-thiogalactopyranoside
ITC	Isothermal titration calorimetry
L-cth	L-cystathionine
L-cys	L-cysteine
LDH	lactate dehydrogenase
L-hcys	L- homocysteine
L-orn	L-ornithine
MBP buffer	MOPS, bicine, proline buffer
NADH	β-Nicotinamide adenine di nucleotide
OAS	O-acetylserine
OAT	Ornithine aminotransferase
ODC	Ornithine decarboxylase
P5C	Δ^1-pyrroline-5- carboxylate

PAG	DL-proparglyglycine
PAO	Polyamine oxidase
PDB	Protein Data Bank
PLP	Pyridoxal 5’-phosphate
PMP	Pyridoxamine 5′-phosphate
POSP	Putative oocyst/sporozoite-specific protein
SDS-PAGE	Sodium dodecyl sulfate polyacrylamide gel electrophoresis
SEC	Size exclusion chromatography
SHMT	Hydroxymethyltransferase
SPDS	Spermidine synthase
SPMS	Spermine synthase
SSAT	Spermidine/spermine N-acetyltransferase
Trx	Thioredoxin
UV	Ultraviolet
UV-Vis	Ultraviolet-Visible
wt	wild-type
α-KG	α-ketoglutarate

Chapter 1

General introduction

The main topic of this Ph.D. thesis is the biochemical characterization of ornithine aminotransferase (Chapter 2) and cystathionine γ-lyase (Chapter 3) from *Toxoplasma gondii*. For each enzyme, a brief introduction on the metabolism in which the enzyme is involved and known features of the enzyme is given.

The following sections will give an overview on basic features of *Toxoplasma gondii* and the general mechanism of action of PLP-dependent enzymes.

1. *Toxoplasma gondii*, the causative agent of toxoplasmosis

Toxoplasma gondii is an obligate intracellular protozoa that belongs to the phylum Apicomplexa, precisely to the coccidian subclass. As all the apicomplexa parasites, *T. gondii* possesses a unique organelle called the apicoplast. The apicoplast has a secondary endosymbiotic origin and is essential for the survival of the parasite. However, the specific functions of this organelle are not fully clarified. Thanks to the genome projects underway for *T. gondii* and *Plasmodium falciparum*, it is known that the apicoplast is involved in the fatty acid biosynthesis and in the synthesis of isopentenyl diphosphate (IPP), a precursor of isoprenoids. Moreover, subsequent data showed that the apicoplast of these parasites makes iron sulfur complexes and cooperates with the mitochondrion in the synthesis of haem [2].

T. gondii has a complex life cycle consisting of different phases of sexual and asexual reproduction and uses felidae and warm-blooded vertebrates, i.e., mammals and birds, as final or intermediate hosts, respectively.

There are three infective stages of *T. gondii*: a rapidly dividing invasive tachyzoite, a slowly dividing bradyzoite contained in tissue cysts, and an environmental stage, the sporozoite, contained in oocysts [3].

Oocysts are produced during the parasite's sexual cycle that occurs in the intestine of definitive host. Oocysts are excreted through cat feces in the environment, where sporulation takes place and sporozoites become infective. Upon oral uptake of sporulated oocysts by new hosts, sporozoites transform to tachyzoites that actively penetrate all nucleated cells and replicate rapidly by repeated endodyogeny. The tachyzoite form causes tissue destruction and is therefore responsible for clinical manifestations of the disease. The consequent immune-response of the host is accompanied by the formation of tissue cysts in which bradyzoites multiply slowly by endodyogeny. Tissue cysts are the terminal life-cycle stage in the intermediate hosts and are found in the retina, brain, skeletal and heart muscles. Bradyzoites could persist inside cysts for the life of the host or they could be released from cysts, transform back into tachyzoites that reinvade host cells. If ingested by a definitive host the bradyzoites proliferate in epithelial cells of the small intestine. After this asexual multiplication, the sexual phase of the life cycle is restored (Figure 1)[4,5].

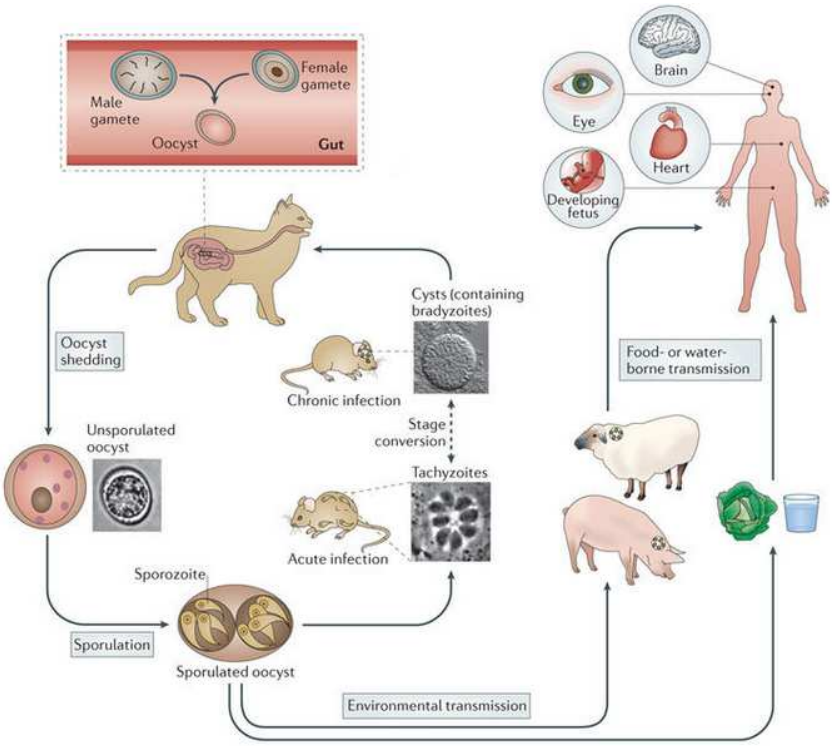

Figure 1. The complex life cycle of Toxoplasma gondii [6].

During the developmental transition of these three phases, *T. gondii* modifies its metabolism, and morphology, to adapt to the environmental changes during its life cycle. Regarding the energy metabolism, significant differences were found between bradyzoites and tachyzoites. Bradyzoites lack a functional TCA (tricarboxylic acid) cycle and respiratory chain. Pyruvate kinase and lactate dehydrogenase (LDH) activities are higher in bradyzoites, suggesting that lactate production is the major metabolic pathway for energy generation during latency. In contrast, tachyzoites use both mitochondrial oxidative phosphorylation and glycolysis to generate ATP [7]. The parasite expresses different stage-specific isoforms of some enzymes in order to adjust glycolysis fluxes to accommodate proliferation or dormancy. *T. gondii* possesses two isoenzymes of LDH, LDH1 and LDH2, which are respectively tachyzoite- and bradyzoite-specific [7]. Moreover, two stage-specific enolase (ENO) have been described. *In vitro* analysis revealed that the tachyzoite-specific ENO2 has a higher specific activity at V_{max} and a lower denaturation temperature than those of the bradyzoite-specific ENO1. These enzymatic properties are in agreement with the metabolic and physiological needs of the parasite during differentiation [8].

Due to the difficulty in producing and working with oocysts, the sporozoite is the less biochemically characterized among the infectious stages of *T. gondii*. Recent proteomic analysis revealed that the metabolic proteins of freshly sporulated sporozoites may be more

similar to tachyzoites than to bradyzoites. Indeed, the ENO2 and LDH1 isoforms, that predominate in tachyzoites, were detected in oocysts [9]. Moreover, *T. gondii* oocysts were found to possess all the enzymes of both glycolytic and TCA cycle, differing from tachyzoites for the expression of isoenzymes of citrate synthase and phosphoenolpyruvate carboxykinase [1].

It is known that in *T. gondii* the TCA cycle is not coupled to glycolysis, as the pyruvate dehydrogenase complex is specifically localized to the apicoplast and not to the mitochondrion [10]. Proteomic data suggested that oocysts generate mitochondrial acetyl-CoA, necessary to feed the TCA cycle, through the β-oxidation of fatty acids and the degradation of branched amino acids. Alternatively, intracellular tachyzoites presumably use the enzyme acetyl-CoA synthetase (TGME49_066640), which could produce acetyl-CoA from the acetate scavenged from host cell mitochondria, to fuel the TCA cycle [1].

Other interesting stage-specific differences were found in amylopectin metabolism and amino acid metabolism [1]. *T. gondii* stores glucose in cytoplasmic granules of amylopectin, found to be more abundant in oocysts and bradyzoites than tachizoytes [11]. Oocysts uniquely express a 4-α-glucanotransferase, resulting in an increase of amylopectin debranching and glucose mobilization. This feature is in agreement with the additional demand of energy typical of the oocyst's sporulation process.

Regarding amino acid metabolism, oocysts specifically express enzymes with a key role in the synthesis of 6 non essential amino acids, i.e., proline, alanine, threonine, cysteine, lysine and tyrosine, underlying the capability of oocysts to adapt to the nutrient-poor extracellular environment.

2. Toxoplasmosis.

Toxoplasmosis is a zoonotic disease of medical and veterinary importance with worldwide distribution [12]. Seroprevalence varies widely between different countries (from 10 to 80%) and often within a given country. As for animals, seroprevalence in human is affected by many factors, like climatic and anthropogenic factors, including dietary, social or cultural habits, quality of water and sanitation coverage [3, 4].

There are essentially two ways of transmission: the vertical and the horizontal transmission.

The vertical or congenital transmission occurs during pregnancy, when the tachyzoites might cross the placenta and infect fetus. Congenital toxoplasmosis may cause abortion, neonatal death, or fetal abnormalities [12]. The horizontal transmission of *T. gondii* may occurs through the infection by one of the three life-cycle stages of the parasite, i.e. oocysts, tissue

cysts or tachyzoites. Tachyzoites, which are very sensitive to environmental conditions, can be transmitted by transplantation of organs or by consumption of unpasteurized milk. In general, the majority of horizontal transmissions is caused by ingestion of one of the two persistent stages of *T. gondii*, i.e. tissue cysts in infected meat and oocysts in food or water contaminated with cat faece. In particular, sporulated oocysts are a significant source of infection for intermediate hosts, as they are very resistant to environmental conditions. They are distributed through wind, rain, or harvested feeds and they remain infectious in moist soil or sand more than a year. Sporulated oocysts also are highly impermeable and, therefore, are also very resistant to disinfectants [5].

In immunocompetent individuals, *T. gondii* infection is asymptomatic in more than 80% of cases. On the other hand, toxoplasmosis is always life threatening in immunocompromised patients. Clinical manifestations include serious encephalitis, mental status changes, seizures, motor deficits, sensory abnormalities, speech abnormalities, hemiparesis and neuropsychiatric findings [3, 12].

Drug treatment is usually not necessary in asymptomatic hosts, except in children younger than 5 years. The most effective treatment for acute cases of toxoplasmosis is the combination of pyrimethamine and sulfadiazine, which have a synergic action and target two different enzymes along the folate synthesis pathway. In congenital toxoplasmosis, spiramycin is used either alone, in order to prevent fetal infection, or combined with sulfadiazine and pyrimethamine when there is substantive evidence of fetal infection. Other current therapies include the use of clindamycin, atovaquone or azithromycin [12].

However, these regimens are inadequate for the treatment of toxoplasmosis for a variety of reasons. First of all, they only control the proliferative tachyzoite stage and are unable to eliminate the cyst stage of the parasite. Then, the combination of these drug result to be toxic and have significant side effects, including hypersensitivity, bone marrow suppression, and teratogenic effects. Moreover, these treatments are no selective for toxoplasmosis therapy as they were used in the treatment of other apicomplexan disease prior to being repurposed [13]. All these motives, in addition to the emerging of parasite drug resistance, suggest that a better understanding of unique *T. gondii* developmental physiology, metabolism, molecular structure and virulence is required to facilitate the design of novel inhibitors against parasite.

3. Pyridoxal 5'-phosphate enzymes

Pyridoxal 5'-phosphate (PLP) enzymes are characterized by their involvement in different metabolic pathways due to their ability to catalyze a wide repertoire of reactions. Almost all PLP-dependent enzymes are associated with biochemical pathways that involve amino acids, but they also play key roles in the replenishment of one-carbon units, synthesis and degradation of biogenic amines, synthesis of tetrapyrrolic compounds and metabolism of amino-sugars [14].

Despite the variety of catalyzed transformations by the PLP-enzymes, the mechanisms of reaction share several common features. In all PLP-dependent enzymes acting on amino acid substrates, the cofactor is covalently bound to the ε-amino group of an active-site lysine residue through an imine linkage, forming the so-called internal aldimine. Through transimination, the ε-amino group of the lysine residue is exchanged with the α-amino group of the amino acid substrate to form the planar external aldimine. Both types of aldimines react reversibly with primary amines in a transaldimination reaction, with formation of a geminal diamine intermediate, allowing either binding of substrates or release of products (Scheme 1).

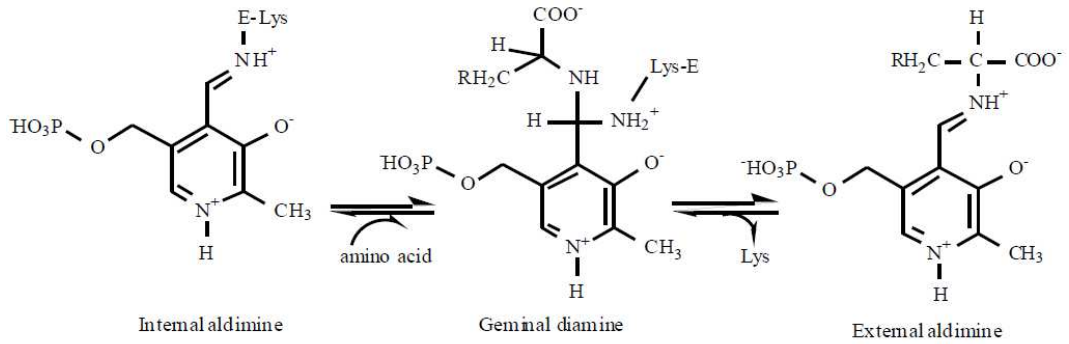

Scheme 1. Structures of internal aldimine, the geminal diamine and the external aldimine (adapted from [15]).

The external aldimine is the common central intermediate for all PLP-catalyzed reactions with amino acids. The cleavage of one of the three bonds at Cα gives rise to the quinonoid intermediates; the net negative charge arising from the heterolytic cleavage of sigma bonds is delocalized by the extensive conjugation of the π-electrons of the pyridine ring of the cofactor, that acts as an electron silk [15].

An important factor for the reaction specificity is the orientation of the bonds at Cα of the substrate moiety in the external aldimine adduct. Dunathan [16] pointed out that the bond in the substrate amino acid to be broken by a PLP-dependent enzyme should lie in a plane perpendicular to the plane of the cofactor-imine π system. This would minimize the transition

state energy by allowing maximum σ-π overlap between the breaking bond and the ring-imine π system. It could also provide the geometry closest to that of the planar quinonoid intermediate to be formed, thus minimizing molecular motion in the approach to the transition state.

PLP-catalyzed reactions may be classified as reactions proceeding through (Figure 2):

- Deprotonation: dissociation of the α-hydrogen from the Schiff base leads to a quinonoid-carbanionic intermediate that can react in several ways: i) racemisation, reprotonation at Cα but without stereospecificity (e.g. alanine racemase); ii) transamination, protonation of C4' of PLP to form a ketimine intermediate that undergoes hydrolysis to pyridoxamine phosphate (PMP) and an α-oxo acid (e.g. aspartate aminotransferase); or iii) β- (or γ-) elimination and replacement, when a good leaving group is present in the β (or γ) position of the amino acid it can be eliminated (e.g. tryptophanase and tryptophan synthase).
- Elimination of CO_2: loss of the carboxyl group from external aldimine that most commonly leads to the protonation at the original site of decarboxylation followed by breakup of the Schiff base (e.g. glutamic acid decarboxylase).
- Side chain cleavage: Schiff base side chains undergo aldol cleavage. Conversely, a side chain can be added by β condensation. The best known enzyme of this group is serine hydroxymethyltransferase.

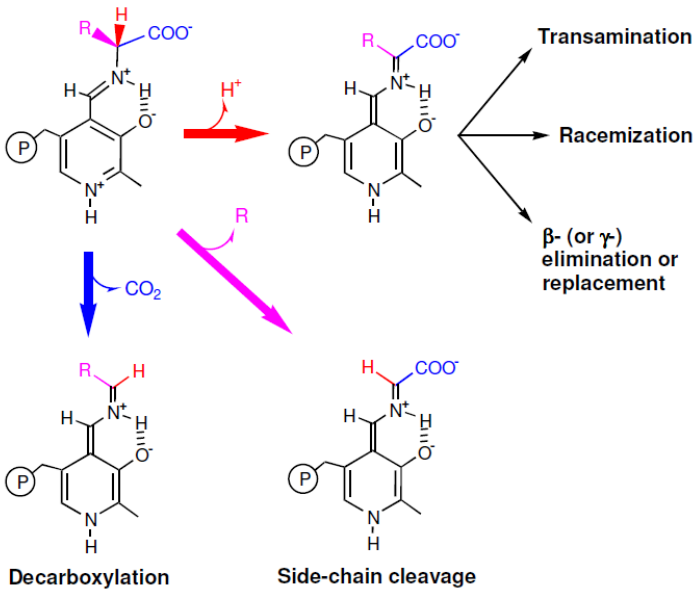

Figure 2. A schematic view of the different reaction types catalyzed by PLP-dependent enzymes that act on amino acids [17].

Due to their common mechanistic features, PLP-dependent enzyme often catalyze different chemical reactions, showing 'catalytic promiscuity'. This feature may have played a

fundamental role in divergent evolution and diversification of catalytic properties. Ancestral enzymes were probably able to catalyze several reactions, but gene duplication and evolutionary pressure may have worked to modify enzymes' active sites so as to confer narrower substrate and reaction specificity [18].

Initially, PLP-dependent enzymes have been classified into five distinct structural groups [19], which presumably correspond to five independent evolutionary lineages originated very early in the evolution (before the three biological kingdoms diverged) from different protein ancestors [20]. These families have been named from their more representative enzyme. The aspartate aminotransferase family corresponds to fold type I and contains the majority of structurally determined PLP-dependent enzymes, consisting of aminotransferases, decarboxylases as well as of enzymes that catalyze α,β- and α,γ-eliminations. Its members are catalytically active as homodimers, although they may assemble into higher order complexes, and their active site lies at on the dimer interface. The tryptophan synthase β-subunit family corresponds to the fold type II and differ from those of fold Type I in that the active sites are composed entirely of residues from one monomer, with additional regulatory domains. The bacterial alanine racemase family corresponds to the fold type III. These enzymes are obligate dimers, as each monomer contributes residues to both active sites. In enzymes of the D-amino acid aminotransferase family, fold type IV, the cofactor binds with its *re* side facing the protein rather than the active-site pocket as in the fold-type I family, accounting for the difference in stereochemistry of the products in the D-amino acid reaction. The enzymes of fold type V, e.g. glycogen phosphorylase, are mechanistically distinct in utilizing the cofactor phosphate group for catalysis. Subsequently, two more groups were identified by Percudani and Perracchi, fold type VI and fold type VII that are represented by D-lysine 5,6-aminomutase and lysine 2,3-aminomutase respectively, and contains enzymes whose structures are unlike all other PLP-dependent enzymes [17].

4. PLP-dependent enzymes as drug targets.

A consequence of their widespread metabolic distribution is that a number of these enzymes are current drug targets. For example, inhibitors of L-DOPA (L-3,4-dihydroxyphenylalanine) decarboxylase are used in the treatment of Parkinson's disease [21], alanine racemase has been identified as antibacterial drug target [22] and inhibitors of γ-aminobutyric acid aminotransferase (GABA-AT) are used in the treatment of epilepsy [23].

PLP-dependent enzymes are also intimately involved in the metabolic pathways of protozoa [24]. However, so far only serine hydroxymethyltransferase (SHMT) and ornithine

decarboxylase (ODC) have been targeted to develop clinically useful anti-protozoan drugs. Therefore, future studies are required to explore the potential of the other enzymes as anti-protozoan drug targets.

Recent analysis for PLP-dependent enzymes suggests three types of emergent drug targets: (1) enzymes that are present only in pathogens; (2) enzymes common to both humans and pathogens that possess different properties, allowing to discriminate each other; (3) enzymes related to a specialized parasitic life style (distinct host cells or particular life cycle phase). All these groups of enzymes identify targets that may be of interest in the development and design of species-specific therapeutics [24, 25].

Regarding the third group of drug targets, a recent proteomic analysis of partially sporulated oocysts of *T. gondii* identified a subset of proteins specifically expressed at the oocyst/sporozoite stage of the parasite. Among these putative oocyst/sporozoite-specific proteins (POSPs), four PLP-dependent enzymes were found. In particular, the oocyst resulted to differ from the tachyzoite for the expression of ornithine aminotransferase (OAT, TGME49_069110), an enzyme that takes part in the synthesis of proline and polyamine metabolism. The POPS subset also included three enzymes involved in the biosynthesis of cysteine: cystathionine β-synthase (CBS, TGME49_059180), cystathionine γ-lyase (CGL, TGME49_112930) and cysteine synthase (CS, TGME49_078910). This analysis provided proteomic evidence that the capability of de novo amino acid biosynthesis is modulated between oocysts and tachyzoites, with oocysts showing a greater persistence than tachyzoites. This feature is in accordance with the adaptation of *T. gondii* oocysts to the nutrient-poor and stressing extracellular environment.

5. Aims

This thesis aims to give a detailed biochemical description of two enzymes from *T. gondii*, the ornithine aminotransferase (TgOAT) and the cystathionine γ-lyase (TgCGL), in order to expand the very limited knowledge about the polyamine and cysteine metabolism of the parasite and to explore the possible use of these enzymes as novel drug targets against toxoplasmosis.

We overexpressed the proteins in *E. coli* and we isolated the recombinant enzyme as His-tagged proteins. The kinetic parameters of main and secondary activities were evaluated by steady state and pre-steady state analysis. In particular, pre-steady state analysis has been performed in collaboration with Prof. Mariarita Bertoldi from University of Verona. Moreover, we analyzed oligomeric state, ligand-induced spectral transitions and protein stability through an array of biochemical and biophysical techniques, such as UV-Vis and fluorescence spectroscopy, circular dichroism spectroscopy, size exclusion chromatography, limited proteolysis and differential scanning calorimetry. After a preliminary biochemical characterization, mutagenesis studies were performed to identify the key residues in the active sites that are responsible for reaction and substrate specificity.

Collaboration with Dr. Alessandro Paiardini, researcher at Sapienza University of Rome, was established in order to perform molecular modelling analysis to understand at a molecular level the structure/function relationship, substrate binding and catalytic mechanism of the enzymes.

Chapter 2

Unique substrate specificity of ornithine aminotransferase from *Toxoplasma gondii*

Abstract

Toxoplasma gondii is a protozoan parasite of medical and veterinary relevance responsible for toxoplasmosis in humans. As an efficacious vaccine remains a challenge, chemotherapy is still the most effective way to combat the disease. In search for novel druggable targets, herein we performed a thorough characterization of the putative PLP-dependent enzyme TgOAT. We overexpressed the protein in *E. coli* and analyzed its molecular and kinetic properties by UV-Vis absorbance, fluorescence, and CD spectroscopy, in addition to kinetic studies of both the steady state and pre-steady state. TgOAT is largely similar to OATs from other species regarding its general transamination mechanism and spectral properties of PLP; however, it does not show a specific ornithine aminotransferase activity as its homologs, but exhibits both AcOrn and GABA transaminase activity in vitro, suggesting a role in both arginine and GABA metabolism in vivo. The presence of Val79 in the active site of TgOAT in place of Tyr, as in its human counterpart, provides the necessary room to accommodate AcOrn and GABA, resembling the active site arrangement of GABA transaminases. Moreover, mutation of Val79 to Tyr results in a change of substrate preference between GABA, AcOrn and L-orn, suggesting a key role of Val79 in defining substrate specificity. The findings that TgOAT possesses parasite-specific structural features as well as differs in substrate specificity from its human homolog make it an attractive target for antitoxoplasmosis inhibitor design that can be exploited for chemotherapeutic intervention.

This work was published in the Biochemical Journal (2017) DOI: 10.1042/BCJ20161021

1. INTRODUCTION

1.1 Polyamine metabolism

Polyamines are aliphatic hydrocarbon chains with one or more amine groups. Their positive charge at physiological pH enables their interaction with polyanionic molecules such as DNA, RNA, phospholipid head groups in cell membrane or cell wall components. Due to their variety in terms of molecular structure, valence and prevalence, polyamines undertake different roles in the cells such as survival, growth, gene expression, stress response, cell differentiation and parasidic activity [26].

In Eukariota the biosynthesis of polyamines typically starts with the conversion of arginine to ornithine by arginase and the subsequent decarboxylation of ornithine by ODC to form putrescine. S-Adenosylmethionine decarboxylase (AdoMetDC) produces decarboxylated S-adenosylmethionine (dcAdoMet) which, then gives its aminopropyl group to putrescine for spermidine and spermine synthesis. Spermidine synthase (SPDS) and spermine synthase (SPMS), respectively, catalyse the latter two reactions. An alternative biosynthetic pathway that characterized Bacteria and plants is the arginine decarboxylase (ADC) pathway. ADC converts arginine into agmatine, which is consequently converted into putrescine by agmantinase (Figure 3).

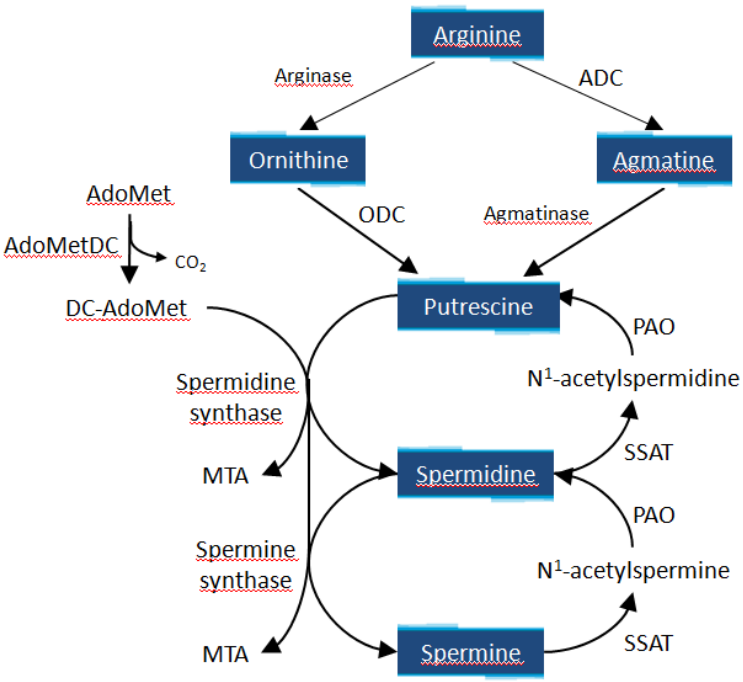

Figure 3. Reactions and enzymes involved in polyamine metabolism. MTA, methylthioadenosine.

The polyamine metabolism is highly divergent among Protozoa. In *Trypanosoma brucei* and Leishmania parasites, putrescine and spermidine are synthesized by ODC, AdoMetDC and SPDS. Differently, *Trypanosoma cruzi* lacks ODC, but does express both AdoMetDC and SPDS, implying that once putrescine is transported into the parasite, it can be converted into spermidine and spermine by the promiscuous activity of SPDS [27]. Moreover, published data have shown that *Cryptosporidium parvum* has a plant-like pathway that utilizes ADC [28], whereas in *P. falciparum* ODC and AdoMetDC enzymes were components of a bifunctional protein [29].

Interference with polyamine metabolism has been successfully exploited in the clinical treatment of West African sleeping sickness originated by *Trypanosoma brucei gambiense* by using α- difluoromethylornithine (DFMO, Eflornithine), a derivative of ornithine that can irreversibly inactivate ODC [30–32]. Furthermore, AdoMetDC, and SPDS have been chemically validated as a drug target in the major protozoan parasites and many specific irreversible inhibitors have been synthetized [27, 33–36]. These results prompted the idea that polyamine metabolism may be an important drug target also in other protozoan parasites responsible for global diseases, including *T. gondii*.

Recent studies suggest that toxoplasma lacks a forward-directed polyamine biosynthestic pathway. Indeed, it is devoid of the activity of two essential enzymes for polyamine metabolism such as ODC and ADC, and therefore is auxotrophic for polyamines [37, 38]. *T. gondii* has previously been shown to have a high affinity putrescine transporter, demonstrating the ability to scavenge host-derived putrescine [39]. This protozoan synthesizes polyamines by a retroconversion pathway from spermidine to spermine and putrescine via spermidine/spermine N-acetyltransferase (SSAT) and polyamine oxidase (PAO) [38]. Even if polyamine metabolism has not been deeply investigated in *T. gondii*, it is known that the parasite, as Plasmodium, possesses the polyamine-related PLP-enzyme OAT which is involved in ornithine homeostasis, control of polyamine levels and synthesis, and mitosis.

1.2 Ornithine aminotransferase

OAT (E.C. 2.6.1.13) is a strongly conserved enzyme found in almost all eukaryotic organisms, from protozoans to humans, and from fungi to higher plants.

OAT, like every PLP-dependent transaminase, operates via a “ping-pong” mechanism that requires two half reactions to complete one catalytic cycle of transamination. In the first part of the reaction, L-orn binds to the pyridoxal form of the holo-enzyme (OAT–PLP) with the formation of L-glutamate-γ-semialdehyde, which then cyclizes spontaneously to Δ^1-pyrroline-

5- carboxylate (P5C), yielding the pyridoxamine form of the enzyme (OAT–PMP). The second half-transamination proceeds through the reaction of α-ketoglutarate (α-KG) with OAT–PMP to reform OAT–PLP and release L-glutamate (see Scheme 2). P5C is further converted into proline.

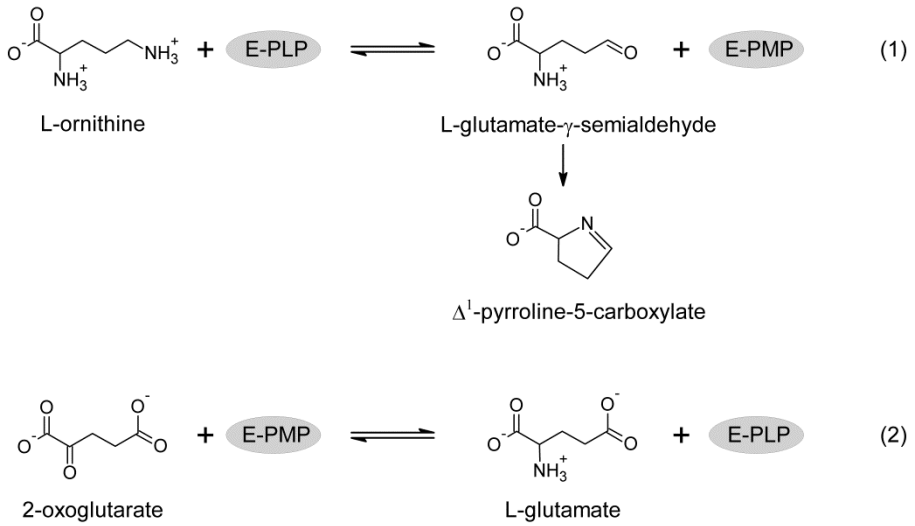

Scheme 2. Overview of the two half-transamination reactions catalysed by OAT.

The human OAT is synthesized as a 49 kDa precursor in the cytosol and it is then imported into mitochondria where it reaches the functional conformation upon removal of an N-terminal mitochondrial targeting sequence (residues 1–25) producing a ~45 kDa mature protein [40]. In the PDB databank, six crystal structures of this enzyme, both ligand-free [41] and in complex with different substrate analogues [42, 43], are present. These crystallographic studies showed that the human enzyme assume an hexameric assembly consisting of three homodimers hold together principally by electrostatic interactions. The dimer belongs to the fold type I class of PLP-enzymes and it was suggested that it could represent the functional unit of the enzyme [41]. In the active site, the PLP cofactor is fixed at the interface between subunits and forms an internal aldimine via a Schiff base bond with the catalytic Lys.

Crystal structures of human OAT complexed with inhibitors elucidate the exact mechanism for the specific ω-transaminase reaction of the enzyme: the α-carboxylate of L-orn is bound by R180 with the non-reacting α-amino group held between the OH groups of Y55 and Y85, while R413 interacts with E235 in order to arrange the δ-amino group of L-orn for transimination. In particular, the glutamate residue is important for neutralizing the positive charge of the R413 through a salt bridge during the first half-reaction, when there is an

internal PLP-lysine aldimine as the substrate approaches. This closed system allows productive binding of L-orn to OAT and restrains the binding of α-KG that are required for the second half-reaction. On the other hand, when there is an external PMP during the second half-reaction, this hydrogen bond network is weakened, and the salt bridge opens up to allow α-KG to interact with R413 (Figure 4) [43].

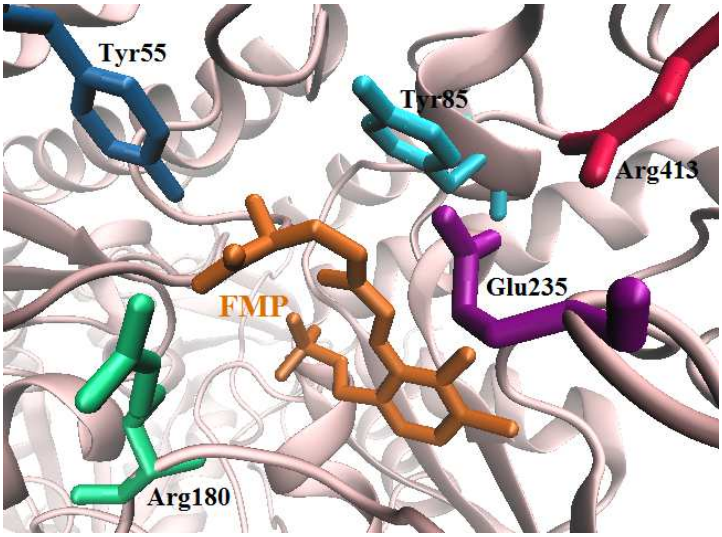

Figure 4. Structure of the active site of hOAT in complex with the inhibitor 5-fuoromethylornithine (5FMOrn). FMP is the inhibitor adduct formed between PLP and 5FMOrn. PDB ID code 2OAT. The figure is carried out using VMD (Visual Molecular Dynamics).

Interestingly, in *T. gondii*, OAT has been recently identified as a protein specifically expressed at the oocyst/sporozoite stage [1]. Inhibition of a polyamine-related, stage-specific protein, whose functional behavior is associated to the adaptation of *T. gondii* oocysts to multiple extracellular environmental stresses, could constitute an efficacious strategy for treating the parasitic infection.

Despite the presence of eight spatial structures of TgOAT in Protein Data Bank (PDB ID code 4NOG at 1.2 Å; PDB ID code 4ZLV at 1.8 Å; PDB ID code 4ZWM at 2.3 Å; PDB ID code 5EAV at 1.6 Å; PDB ID code 5EQC at 2.2 Å; PDB ID code 5DJ9 at 1.55Å; PDB ID code 5E5I at 1.7 Å; PDB ID code 5E3K at 1.7Å), functional information regarding this enzyme is still lacking.

Herein, in order to evaluate the TgOAT as a potential target for structure-based selective inhibitor design, significant progress in the spectroscopic characterization of the enzyme OAT from *T. gondii* ME49 and in the determination of its catalytic properties has been made.

A previous study, describing the different substrate specificities between human OAT and human GABA-AT, demonstrated that Tyr55 and Tyr85 in human OAT were major contributors to the productive binding of L-orn. In particular, Tyr85 was found to be a major

determinant of specificity towards L-orn with respect to GABA [44]. Notably, Tyr85 in human OAT is replaced by isoleucine in GABA-AT.

Sequence alignment of OAT from different organisms indicated that both of these tyrosines are highly conserved. However Tyr85 (human OAT numbering) is substituted by Val79 in TgOAT (Figure 5). Thus, a further aim of this study was to determine the contribution of Val79 to the specificity of the TgOAT enzyme by mutating the valine residue to tyrosine.

```
T. gondii          ----------MATKSDGSASAAAEGGARKTNIEAYRDGLKLKTEEDFFACDRQYVCQNYA       50
H. sapiens         MFSKLAHLQRFAVLSRGVHSSVA----SATSVATKKTVQGPPTSDDIFEREYKYGAHNYH       56
P. falciparum      ----------------------------------MDFVKELKSSQDYMNNELTYGAHNYD       26
P. vivax           ----------------------------------MDFIKELKSSQDYMNNELTYGAHNYD       26
P. sativum         ----MAATRQVQCLMRRV-----CRGTRTF--AVATQSNASSSSQTIIDKEHQHSAHNYH       49
S. cerevisiae      -----------------------------------MSEATLSSKQTIEWENKYSAHNYH       24
B. brevis          ----------------------------------------MSKTNVVIEQTEKFGAHNYH       20
                                                          . .  :    . .:**

T. gondii          PVPVVISKGKGARVWDINGNEYYDFLAGVSSLSQGHCHPRVIAALCRQAERLTLTLRAFG       110
H. sapiens         PLPVALERGKGIYLWDVEGRKYFDFLSSYSAVNQGHCHPKIVNALKSQVDKLTLTSRAFY       116
P. falciparum      PIPVVLKRGKGVFVYDIEDRRYYDFLSAYSSVNQGHCHPDILNAMINQAKKLTICSRAFF       86
P. vivax           PIPVVLKRGSGVFVYDIEDRRYYDFLSAYSSVNQGHCHPNILNAMINQAKKLTICSRAFF       86
P. sativum         PLPIVFAHAKGSSVWDPEGNKYIDFLSGYSAVNQGHCHPKILKALHDQADRLTVSSRAFY       109
S. cerevisiae      PLPVVFHKAKGAHVWDPEGKLYLDFLSAYSAVNQGHCHPHIIKALTEQAQTLTLSSRAFH       84
B. brevis          PLPIVISKAEGVWVHDPEGNKYLDMLSAYSALNQGHRHPRIIQALKDQADKVTLTSRAFY       80
                   *:*:.: :..*  : * :.. * *:*:. *::.*** ** :: *:  *.. :*:  ***

T. gondii          NDVTGPACRFMAEMFGYDRVLLMNTGAEAGESALKIARKWAYEVKEIPPDSAKVILCNNN       170
H. sapiens         NNVLGEYEEYITKLFNYHKVLPMNTGVEAGETACKLARKWGYTVKGIQKYKAKIVFAAGN       176
P. falciparum      SDSLGVCERYLTNLFGYDKVLMMNTGAEASETAYKLCRKWGYEVKKIPENSAKIIVCNNN       146
P. vivax           SDSLGVCERYLTTLFGYDKVLMMNTGAEANETAYKMCRKWGYEVKKIPENEAKIIVCNNN       146
P. sativum         NDRFPVFAEYLTALFGYDMVLPMNTGAEGVETALKLARKWGYEKKKIPNDEALIVSCCGC       169
S. cerevisiae      NDVYAQFAKFVTEFFGFETVLPMNTGAEAVETALKLARRWGYMKKNIPQDKAIILGAEGN       144
B. brevis          NDQLGEFYEKLSAVTGKEMILPMNTGAEAVETALKAVRRWAYDVKKVPENQAEIIVCEGN       140
                   .:      . :: . . . :* ****.*. *:* *  *:*.*  * :   .* :: . .

T. gondii          YWGRTITACSSSTTFD-CYNNFGPFTPGF------ELIDYDDVGALEEALKD---PNVAA       220
H. sapiens         FWGRTLSAISSSTDPT-SYDGFGPFMPGF------DIIPYNDLPALERALQD---PNVAA       226
P. falciparum      FSGRTLGCVSASTDKK-CKNNFGPFVPNF------LKVPYDDLEALEKELQD---PNVCA       196
P. vivax           FSGRTLGCVSASTDRK-CKNNFGPFVPNF------LKVPYDDLEALEVELQD---PNVCA       196
P. sativum         FNGRTLGVISMSCDNE-ATRGFGPLMPGH------LKVDFGDAEAIERIF-KEKGDRVAA       221
S. cerevisiae      FHGRTFGAISLSTDYEDSKLHFGPFVPNVASGHSVHKIRYGHAEDFVPILESPEGKNVAA       204
B. brevis          FHGRTVTVTSFSSAEE-YRRGFGPFTPGF------KIIPYGDIEALKQAI-T---PNTAA       189
                   : ***.   * *         ***: *.         : :..   :   :      ...*

T. gondii          FFVEPIQGEGGVNVPKPGYLKRAHELCRSKNVLLIVDEIQTGLCRTGRLLAADH--DEVH       278
H. sapiens         FMVEPIQGEAGVVVPDPGYLMGVRELCTRHQVLFIADEIQTGLARTGRWLAVDY--ENVR       284
P. falciparum      FIVEPVQGEAGVIVPSDSYFPGVASLCKKYNVLFVADEVQTGLGRTGKLLCTHH--YGVK       254
P. vivax           FVVEPIQGEAGVILPSDGYFKGVEALCKKYNVLFVADEVQTGLGRTGKLLCTYH--YGVR       254
P. sativum         FILEPIQGEAGVVIPPDGYLKAVRDLCSKYNVLMIADEIQTGLARTGKMLACDW--EDVR       279
S. cerevisiae      IILEPIQGEAGIVVPPADYFPKVSALCRKHNVLLIVDEIQTGIGRTGELLCYDHYKAEAK       264
B. brevis          FMLEPIQGEAGIIIPQEGFLKQAQEVCKANNVLLVSDEIQTGFGRTGKMFASDW--ENVV       247
                   :.:**:***.*: :*  .::  .  :*   :**:: **:***: ***. :.       .

T. gondii          PDILLLGKSLSAGVVPISAVMGRADVMDVLKPGTHGSTFGGNPLACAVAVEALTVLKDEK       338
H. sapiens         PDIVLLGKALSGGLYPVSAVLCDDDIMLTIKPGEHGSTYGGNPLGCRVAIAALEVLEEEN       344
P. falciparum      PDVILLGKALSGGHYPISAILANDDVMLVLKPGEHGSTYGGNPLAAAICVEALKVLINEK       314
P. vivax           PDVILLGKALSGGHYPISAILANNDVMLVLKPGEHGSTYGGNPLAAAICVESLNVLINEK       314
P. sativum         PDVVILGKALGGGILPVSAVLADKDVMLCIKPGQHGSTFGGNPLASAVAIAALEVIKEER       339
S. cerevisiae      PDIVLLGKALSGGVLPVSCVLSSHDIMSCFTPGSHGSTFGGNPLASRVAIAALEVIRDEK       324
B. brevis          PDMYIMGKALGGGVFPISAVAADKEILSVFEPGSHGSTFGGNPLGCAVAVAAMDVLADEG       307
                   **: ::**:*..*  *:*.:    :::  : ** ****:*****.. :.: :: *: :*
```

```
T. gondii          LADRAERLGAQFRDCLRRELYGKVPWIKEIRGRGLLNAVEVDS-D--AIDPNDVVMKLKE       395
H. sapiens         LAENADKLGIILRNELMK--LP-SDVVTAVRGKGLLNAIVIKETK--DWDAWKVCLRLRD       399
P. falciparum      LCENADKLGAPFLQNLKEQLKD-SKVVREVRGKGLLCAIEFKN-D--LVNVWDICLKFKE       370
P. vivax           LSENADRLGGPFLKALKEELKD-SKIVREVRGRGLLCAIEFRN-D--IINVWDICLKFKE       370
P. sativum         LTERSTKLGGELLGLLHKIQKKHPEHVKEVRGKGLFIGVELNSESLSPVSGFELSEKLKE       399
S. cerevisiae      LCQRAAQLGSSFIAQLKALQAKSNGIISEVRGMGLLTAIVIDPSKANGKTAWDLCLLMKD       384
B. brevis          LVQRSLEMGAYFMEKLKE---INNPIIKEIRGRGLFIGLELTTAA------RPYCEKLKE       358
                   * :.: .:*  :   *          :  :** **: .: .               :::

T. gondii          NGILSKPTRGRVMRFIPPLVITDEEHRDATTRIIKSFLAVEEERKK--------------       441
H. sapiens         NGLLAKPTHGDIIRFAPPLVIKEDELRESIEIINKTILSF--------------------       439
P. falciparum      NGLITRSVHDKTVRLTPPLCITKEQLDECTEIIVKTVKFFDDNL----------------       414
P. vivax           NGLITRSVHDKTIRLTPPLCITKEQLDECLEIISKTVKYFDDRL----------------       414
P. sativum         RGVLAKSTHDTIIRFTPPLCISADEIQQGSKALAEVLEIDLPLLKKTKPKDAVPLAGPSP       459
S. cerevisiae      HGLLAKPTHDHIIRLAPPLVISEEDLQTGVETIAKCIDLL--------------------       424
B. brevis          LGLLCKETHETTIRFAPPLVISKEDLDWAIDRIKQVLHVTE------------------       399
                    *:: : .:   :*: *** *. ::       : : .

T. gondii          ----------         441
H. sapiens         ----------         439
P. falciparum      ----------         414
P. vivax           ----------         414
P. sativum         CDRCGRLVYG         469
S. cerevisiae      ----------         424
B. brevis          ----------         399
```

Figure 5. Sequence alignment of OAT from different organisms. Black shading indicates the PLP-binding lysine. Gray shading indicates Tyr55 (human OAT numbering) which is conserved in OATs. The target residue for mutational analysis is highlighted in yellow. The OATs used in this alignment (NCBI accession number) are XP_002365604.1, *T. gondii* ME49; AAA59959.1, *H. sapiens*; AAA16481.1, *P. falciparum*; EDL46384.1, *P. vivax*; ABZ10818.1, *P. sativum*; ONH76070.1, *S. cerevisiae*; WP_012685950.1, *B. brevis*. All sequence alignments were carried out using the Clustal OMEGA program.

2. EXPERIMENTAL

2.1 Materials

PLP, L-Ornithine, γ-Aminobutyric acid, α-Ketoglutaric acid, Nα-Acetyl-L-ornithine, β-Chloro-L-alanine, L-Glutamate Oxidase, o-Dianisidine, Peroxidase, L-Lactic Dehydrogenase, IPTG, and NADH were purchased from Sigma.

2.2 Protein production

The complete cDNA of TgOAT (accession number: XM_002365563) in pUC57 vector was obtained from Genscript Corporation with a tag of six His at the C-terminal. The gene was subcloned into the expression vector pET21a, which was used for the heterologous expression of TgOAT in *E. coli* BL21(DE3) Codon plus cells. After growing cell cultures at 37°C to an absorbance at 600 nm of 0.6, expression was induced with 0.5 mM IPTG at 24°C for 20 h. Cell were then harvested by centrifugation, resuspended in 20 mM sodium phosphate pH 8, 300 mM sodium chloride and 1X protease inhibitor EDTA free and lysed by sonication. After centrifugation for 30 min at 30,000×g, the supernatant was loaded onto an Ni-affinity column equilibrated with 20 mM sodium phosphate at pH 8, 300 mM sodium chloride, and 10 mM imidazole. The imidazole concentration was increased to 500 mM in a linear gradient and soluble TgOAT eluted between 100 and 200 mM imidazole. The fractions containing TgOAT were pooled and, after addition of 100 μM PLP, were concentrated. Elution imidazole and unbound PLP were removed by extensive washing with 20 mM sodium phosphate buffer, pH 8, using Vivaspin concentrators (Sartorius).

The concentration of monomer was calculated with the extinction coefficient $\varepsilon_{280\ nm}$ = 40255 M^{-1} cm^{-1} (http://web.expasy.org/protparam/). PLP content in the holo-enzyme was calculated by addition of 0.1 M NaOH and using $\varepsilon_{388\ nm}$ = 6600 M^{-1} cm^{-1}. The yield from a standard purification was approximately 45 mg/L culture.

Generation of the N-terminally truncated TgOAT variant, without the first 16 residues, was performed by PCR (Polymerase chain reaction) amplification using the pET21a-TgOAT construct (forward primer 5'-CATATGGCTAGGAAAACGAACATTGAAGCTTACC-3'; reverse primer 5'-GGATCCTCAGTGGTGGTGGTGGTGGTGTTTTTTG-3'). The resulting DNA fragment was inserted into pET21a at the NdeI/BamHI sites and used to transform the *E. coli* strain BL21(DE3) Codon Plus.

Generation of V79Y, C179S, C187S, and the double mutant C179S C187S TgOAT was carried out by site specific mutagenesis on the N-terminally truncated pET21a-TgOAT

construct using the QuikChange® site-directed mutagenesis kit (Agilent Technologies). The sequence of the mutated plasmid was verified by DNA sequence analysis.

Expression and purification of all variants were carried out as described for full length wild-type TgOAT. The yield from a one-litre purification was approximately 50 mg for the N-terminally truncated form and 35 mg for other mutants.

The PLP- and PMP-form of the variants were prepared incubating the enzyme with α-KG and L-orn, respectively, for 20 min at room temperature and washing the excess substrates using Vivaspin concentrators (Sartorius). The complete conversion in the two forms was then monitored by an absorption spectrum.

The coding sequence for thioredoxin from *T. gondii* (TgTrx, accession number: XM_002370147) was cloned as C-terminal 6xHis-fusion construct in *E. coli* expression vector pET11 using NdeI and BamHI restriction sites. Protein expression was carried out by growing freshly transformed *E. coli* BL21(DE3) cells in LB (Luria-Bertani) medium at 37°C to an OD of 0.6 at 600 nm; after induction with 0.5 mM IPTG, cells were grown for 4 hours, harvested by centrifugation, resuspended in extraction buffer (20 mM sodium phosphate pH 8, 300 mM sodium chloride, and 10 mM imidazole and 1X protease inhibitor EDTA free), and lysed by sonication. The cell debris was removed by centrifugation (35,000 ×g for 20min) and the supernatant was loaded onto an Ni-affinity column equilibrated with 20 mM sodium phosphate at pH 8, 300 mM sodium chloride and 10 mM imidazole. The imidazole concentration was increased stepwise, first to 70 mM to remove nonspecifically bounded proteins, and then to 500 mM to elute the enzyme. Monomer concentration was determined from the calculated extinction coefficient (ε_{280nm} = 8543 M^{-1} cm^{-1}; http://web.expasy.org/protparam/). The yield from a standard purification was approximately 20 mg/L culture.

TgTrx was reduced trough incubation with fresh made DTT solution (1 mM) for 2 h at RT. Excess DTT was removed by extensive washing with 20 mM Hepes pH 8, using Vivaspin concentrators. To prepare oxidized forms, the proteins were reacted with freshly prepared H_2O_2 (1.1 molar equivalent) for 15 min at room temperature [45].

2.3 Size exclusion chromatography (SEC)

The oligomeric state of TgOAT was investigated by size exclusion chromatography using Superdex 200 HR 10/300 GL column. Protein elution was performed at a flow of 0.5 ml/min in 50 mM sodium phosphate pH 8.5, 150 mM sodium chloride. The calibration curve of the column was obtained following the protocol in [46].

2.4 Determination of equilibrium dissociation constant of PLP for TgOAT and V79Y variants

The apo-proteins were obtained by purification from *E. coli* without addition of PLP. The apo-form showed no absorbance between 320 - 500 nm. The holo-enzyme was easily reconstituted by the addition of exogenous PLP to the apo-protein.

The K_D^{PLP} was obtained by monitoring the change of intrinsic fluorescence of the apo-protein (1μM) in the presence of increasing concentrations of PLP (0.01-10 μM) in 50 mM Bis-Tris propane pH 8, at 25 °C. The K_D^{PLP} value was calculated using the following eq:

$$Y = Y_{max}\frac{e_0 + l_0 + K_d - \sqrt{[(e_0 + l_0 + K_d)^2 - 4e_0 l_0]}}{2e_0} \quad (1)$$

where e_0 and l_0 are the concentrations of TgOAT dimer and PLP respectively, K_d is the equilibrium dissociation constant, Y is the fluorescence change at the PLP concentration l_0, while Y_{max} is the fluorescence change at saturating PLP concentrations.

2.5 Steady state analysis

Transaminase activity of TgOAT was detected via (i) the GOX-coupled assay and (ii) the ninhydrin assay following the procedures described in [47] and [48], respectively. Briefly, in the GOX-assay a reaction mixture containing L-orn, 5 mM α-KG (or 2 mM for V79Y), 50 μM PLP, 1 μM TgOAT and 50 mM Hepes pH 8 was incubated at 37 °C for 7 min. After addition of 14 mM phosphoric acid followed by incubation at 90°C for 2 minutes to stop the reaction, the mixture was centrifuged.

Then, the mixture was incubated for 90 min at 37 °C in the presence of GOX (0.015 units), 0.75 mM o-dianisidine, and peroxidase (2.25 units). After addition of sulfuric acid (3.36 mM), absorbance was measured at 530 nm. A standard curve was prepared with known concentrations of L-glutamate (10-500 μM) supplemented in the reaction mixture, in the presence of 50 μM PLP, 5 mM α-KG, and 14 mM phosphoric acid (Appendix, Figure A1). The determination of K_m and v_{max} of the substrates was performed varying the concentration of one substrate and keeping the other at a constant concentration value.

In the ninhydrin assay TgOAT was added to an assay reaction mixture containing 50 mM Hepes pH 8, pyruvate or oxaloacetate as substrate, 50 mM L-orn, 0.05 mM PLP, and incubated for 30 min at 37 °C. Then, 0.6 M HCl and 0.26% (wt/vol) ninhydrin were added to stop the reaction and the samples were heated for 5 min at 100 °C. After resuspending the pellet in 1.5 ml 99% ethanol, the absorbance was measured at 510 nm.

The β-lyase activity of TgOAT towards BCA was detected as described previously [49] by monitoring pyruvate formation via NADH-dependent lactate dehydrogenase.

The Michaelis-Menten equation was used in modelling of data and determination of kinetic parameters of TgOAT activity.

For α-KG, data were fit to a non-hyperbolic curve that considers substrate inhibition:

$$\frac{v}{E_t} = \frac{k_{cat}}{1 + (K_m/S) + (S/K_i)} \quad (2)$$

where v is the reaction rate, E_t is the total enzyme concentration, K_m is the Michaelis-Menten constant, S is the substrate concentration, k_{cat} is the rate constant, and K_i is inhibition constant.

The inhibition mode of putrescine and spermidine with respect to L-orn was determined from Lineweaver Burk plot. The K_i value was calculated from the secondary plot [50].

The kinetic experiments were carried out at least in triplicate, and reported values represent means ± S.E.M of two or more independent determinations using different batches of protein that were purified separately. Data fitting was carried out with OriginPro8 (OriginLab).

2.6 Pre-steady state analysis

The reaction of TgOAT-PLP (10 μM) or TgOAT-PMP (10 μM) with various concentrations of L-orn (1-100 mM) or α-KG (0.1- 10 mM) were performed in 20 mM sodium phosphate buffer, pH 8 at 12°C in 200 μl. In both reactions, 500 absorbance spectra were collected between 250-550 nm on a J&M Tidas 16256 diode array detector (Molecular Kinetics) using a BioLogic SFM300 instrument, with a dead-time of 3.6 ms at a flow rate of 12 mL/s. The determination of rate constants was performed by following changes at 416 or 331 nm using the non-linear regression equation

$$A_t = A_\infty + \Delta A e^{-k_{obs}} \quad (3)$$

where A_t is the absorbance at time t, A_∞ is the final absorbance, ΔA is the amplitude of the phase, k_{obs} is the measured observed rate constant. Global fitting of the absorbance spectra were performed using SpecFit, and single wavelength increases or decreases were analyzed with Biokine 4.01 (Biologic) software.

2.7 Spectroscopic measurements

Absorption spectra were collected with a Jasco-V560 UV-Vis spectrophotometer (Easton, Maryland, USA), using 20 μM enzyme in a buffer solution containing 50 mM Bis-Tris propane pH 8.

CD spectra were carried out on a Jasco J-710 spectropolarimeter (Easton, Maryland, USA) at 25 °C in 20 mM sodium phosphate pH 8. Protein concentration was ~ 30 μM in a cuvette with a path length of 1 cm. Spectra were recorded as described in [51].

Fluorescence emission spectra were obtained with a Jasco FP8200 spectrofluorometer (Easton, Maryland, USA) at a protein concentration varying from 1 to 10 μM in 50 mM Bis-Tris propane pH 8 at 25 °C upon tryptophans excitation at 280 nm or upon cofactor excitation at 331 or 415 nm. Spectra of blanks were subtracted from each spectrum of samples containing protein.

2.8 Molecular modelling studies

The crystal structure of TgOAT in its internal aldimine form (PDB ID code 4ZLV) was used to generate the V79Y form of the enzyme, using the "mutagenesis" tool of PyMol [52], followed by energy minimization with the BIOPOLYMER package from InsightII (V.2000, MSI, Los Angeles), as already described [53].

The Dundee PRODRG2 Server [54] was employed to build the energy minimized three-dimensional structures of the PLP-GABA, PLP-L-Orn and PLP-AcOrn external aldimines complexes, which were then docked into the active site of wild-type and V79Y form of TgOAT, using the template-based molecular docking approach of Molegro Virtual Docker (MVD) software (®CLCbio). The flexible torsions of external aldimines were automatically distinguished by MVD, and then checked manually in terms of consistency. A search space of 15 Å radius was used for docking, which was centred on the active site. The internal aldimine form of PLP , as present in 4ZLV, was used as the pharmacophoric group for docking based on the template. If an atom of the ligand matched a group definition, a weighted score depending on its distance to the centers of the group was given. A grid-based MolDock score (resolution 0.30 Å) was utilized as a scoring function, while MolDock SE was used for the docking algorithm [55]. A total of 10 runs were used for each ligand. Similar poses (RMSD ≤ 1.0 Å) were clustered, and the one with the best score was considered to be representative. The remaining docking parameters were fixed at default values. Following docking, energy optimization of hydrogen bonds was carried out.

2.9 Isothermal titration calorimetry (ITC)

All ITC experiments were performed on a TA Instrument Nano-ITC (New Castle, Delaware, USA). TgTrx binding to TgOAT was evaluated by titrating 2 μl of 2 mM TgTrx solution into the reaction cell (200 μL) containing 150 μM protein dissolved in 20 mM sodium phosphate

buffer, pH 8 at 25 °C. Prior to each titration Trx and OAT solutions were equilibrated to 25 °C and degassed. The baseline from a buffer blank titration was subtracted from the raw data.

3. RESULTS

3.1 Production of recombinant TgOAT

Recombinant full-length TgOAT was highly unstable, rapidly losing its activity during purification or storage. Efforts to stabilize the enzyme activity, including addition of glycerol, EDTA, PLP, reducing agents, freezing at -20 or -80 °C and different buffer systems, were not successful. The analysis of the amino acid sequence of TgOAT for disorder propensity using the bioinformatics tool GeneSilico MetaDisorder Service [56] indicated a high level of intrinsic disorder in the N-terminus of the enzyme. Thus, on the basis of the disorder prediction consensus, a truncated variant by deleting the first 16 residues from the N-terminus was constructed. The resulted protein (residues 17-441) was purified with retention of activity and appeared stable when stored cold or frozen, and, therefore, was used for subsequent analysis. Notably, in all the macromolecular crystal structures of TgOAT deposited in the Protein Data Bank, even at very high resolution, the first 16 N-terminal residues are missing, likely due to excessive conformational disorder.

The purity of the N-terminal deletion variant of TgOAT (which we will subsequently refer to as TgOAT) was estimated by SDS-PAGE analyses. Purified TgOAT shows a protein band on SDS-PAGE with a relative molecular mass of 47 kDa, which closely matches its molecular mass calculated from the sequence information (47893 Da) (Figure 6A).

The native molecular mass of TgOAT is ~77 kDa as determined by gel filtration (Figure 6B), indicating that TgOAT is a homodimer in solution, in agreement with crystal structure information.

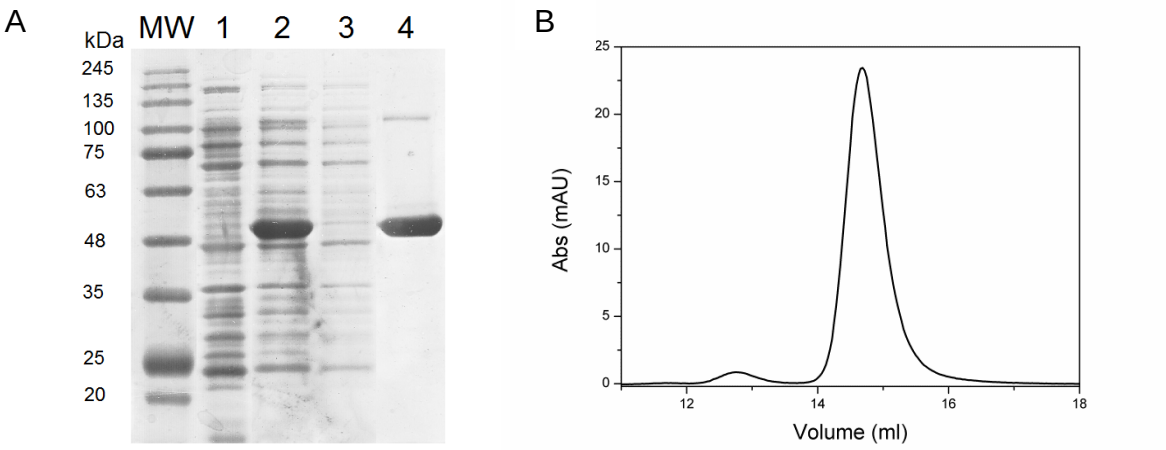

Figure 6. Production of recombinant TgOAT. (A) SDS-PAGE of TgOAT expression and purification. Lane MW, molecular mass standards; lane 1, uninduced control cells; lane 2, total *E.coli* proteins from cell lysate after overnight incubation at 24°C; lane 3, flow through fraction; lane 4, fraction of purified TgOAT. (B) SEC profile of TgOAT. Chromatogram recorded in 50 mM sodium phosphate buffer pH 8, 150 mM NaCl.

3.2 Spectral properties of recombinant TgOAT

Native purified holo-TgOAT binds 2 mol of PLP per dimer and shows, in addition to the band of aromatic amino acids centred at 278 nm, a major absorption band centred at 416 nm and a modest band at about 331 nm, which did not change in pH range 6.0 - 9.0. The 416 nm band is characteristic of the ketoenamine form of the internal aldimine between the active site lysine 286 and PLP, while the 331 nm band can likely be ascribed to a modest amount of the enolimine tautomer and/or to traces of PMP bound to the enzyme (Figure 7A) [57–60]. Several observations are consistent with the E-PMP presence. First of all, distinct preparations of TgOAT show a slight variable ratio of 331/416 nm absorbance (data not shown). Moreover, addition of a keto-acid substrate such as α-KG to the enzyme causes a modest decrease of 331 nm absorbance and an increase of the 416-nm absorbance band, in line with the conversion of E-PMP to E-PLP when a keto-acid substrate is present (Figure 5A). Thus, the absorbance at 331 nm is mainly due to the PMP form of the cofactor which is likely produced by conversion from *E. coli* of some endogenous amino acid to a keto acid. The same behavior has been observed for other transaminases, such as serine–glyoxylate aminotransferase from *Hyphomicrobium methylovorum* [61], and aminotransferase NikK from *Streptomyces tendae* [62].

The CD spectrum of holo-TgOAT shows a positive dichroic band at 423 nm and a modest signal around 340 nm (Figure 7B). Moreover, the enzyme displays positive dichroic bands between 260 and 290 nm, indicating the asymmetry of aromatic amino acids within the active site.

The fluorescence emission spectrum of holo-TgOAT, recorded for excitation at 280 nm, exhibits a pronounced peak at 338 associated to direct emission from Trp residues, and a much lower intensity emission band around 510 nm that can be attributed to emission from PLP, as a result of an energy-transfer process from the excited Trp residues to the ketoenamine tautomer of the internal Schiff base [63, 64] (Figure 7C). Direct excitation of the holo-enzyme at 331 or 416 nm gives a weak emission at about 384 and 528 nm, respectively (data not shown).

The emission spectrum of apo-TgOAT, upon excitation at 280 nm, displays a peak centered at 343 nm, with a 5 nm red-shift and a quantum yield ~60% higher compared to the holo-enzyme (Figure 7C). The apo-enzyme has no residual activity and does not exhibit absorbance bands in the visible region (Figure 7C, inset). Titration of apo-TgOAT with PLP resulted in a quenching of intrinsic fluorescence and yielded a K_D^{PLP} value for the enzyme of 60 ± 3 nM (Figure 7D).

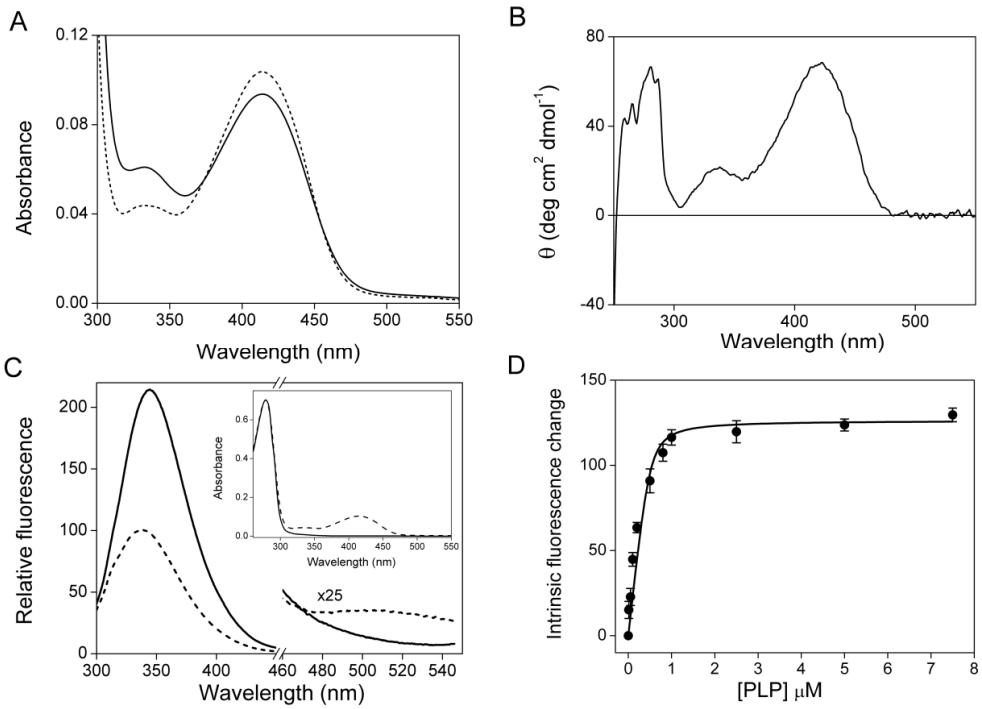

Figure 7. Spectroscopic features of TgOAT. (A) Absorption spectra of 20 μM TgOAT alone (solid line) and after addition of 1 mM α-KG (dashed line) in 50 mM Bis-Tris propane pH 8. (B) Dichroic spectra of TgOAT 30 μM in 20 mM sodium phosphate pH 8. (C) Intrinsic fluorescence emission spectra (excitation was at 280 nm) of apo-protein (solid line) and holo-enzyme (dashed line) in 50 mM Bis-Tris-propane pH 8.Inset: Absorption spectra of apo-TgOAT just after purification (solid line) and holo-TgOAT after saturation with PLP (dashed line) in 20 mM sodium phosphate pH 8. (D) Titration of the apo-TgOAT (0.5 μM enzyme dimer) at PLP concentration from 0.01 to 10 μM. The fluorescence emission variations were determined after excitation at 280 nm.

3.3 Steady state kinetic studies

The enzyme showed a temperature optimum for L-orn transamination at 46 °C (Figure 8A) and a relatively high thermal stability, with T_{50} value of ~65 °C (Figure 8B). The rate constant of TgOAT at various pH resulted in a maximum activity at pH 8.0.

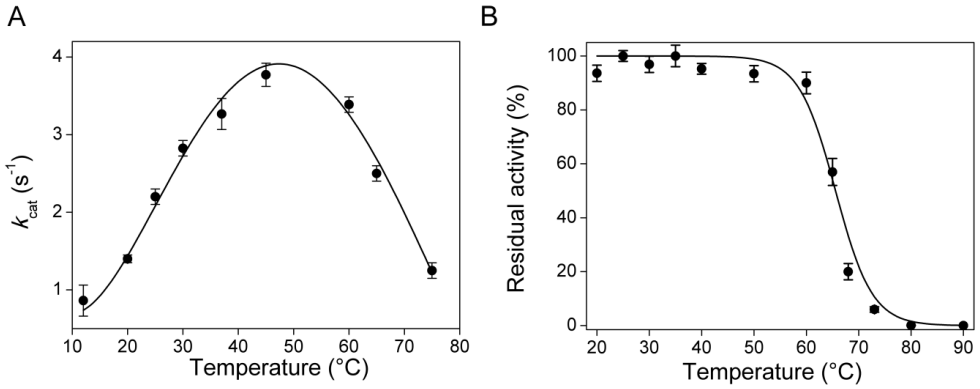

Figure 8. Kinetic properties of recombinant TgOAT. (A) Measurement of temperature optimum for L-orn transamination; TgOAT activity was examined from 10 to 75 °C in 50 mM Hepes buffer, pH 8.0. (B) Thermostability of TgOAT measured as residual activity following incubation of the enzyme at temperatures from 20 °C to 90°C for 10 min.

The kinetic parameters for transaminase reaction of TgOAT towards L-orn, under saturation with α-KG, were compared with those for other organisms and reported in Table 1. TgOAT had similar K_m value (~ 7 mM) for L-orn to those of the other organisms. However, when the k_{cat} of TgOAT (~2 s^{-1}) is compared with that of other OATs, it was significantly lower than that reported for the human (~ 74 s^{-1}) and Plasmodium (~ 10 s^{-1}) enzymes [48].

Table 1. Summary for kinetic parameters for L-orn transamination of TgOAT and OATs from other organisms.

Organism	**Specific activity (µmol mg^{-1} min^{-1})**	**k_{cat} (s^{-1})**	**K_m (mM)**	**k_{cat}/K_m ($M^{-1}s^{-1}$)**	**T (°C)**	**pH**	**References**
T.gondii[a]	2.6 ± 0.5	2.1 ± 0.1	6.9 ± 0.3	304	37	8	Present work
H.sapiens [b]	33.5 ± 4.2	73.7	11.7 ± 2.6	6300	37	7.4	[48]
P.falciparum[b]	2.0±0.7 (4.6±0.8)[d]	9.8	1.6 ± 0.1	6100	37	7.4	[48]
Pisum sativum[c]	3.6	4.3	15	287	37	8	[65]

[a] Kinetic parameters of *T. gondii* were determined by GOX-assay [47].
[b] Kinetic parameters of *P. falciparum* and human OATs were determined by ninhydrin assay [66].
[c] Kinetic parameters of pea OAT were determined with 2-aminobenzaldehyde method [67].
[d] When measured directly after purification.

Notably, when compared to the human enzyme, TgOAT showed a broad substrate specificity as in addition to L-orn it also readily accepted GABA and AcOrn as an amino group donor (Table 2). Based on k_{cat}/K_m values, GABA serves as a better substrate that AcOrn and L-orn

for TgOAT (Appendix, Figure A2). While the k_{cat} of the enzyme toward GABA (2.9 s^{-1}) was similar to that for L-orn, the K_m was ~6-fold higher. Moreover, comparison of relevant k_{cat}/K_m constants towards AcOrn and L-orn demonstrated that the enzyme had a two-fold preference for AcOrn due to a 2.2-fold increase in k_{cat} value. Interestingly, TgOAT can also act on D-orn, even if with low catalytic efficiency.

Table 2. Steady-state kinetic parameters of wild-type and V79Y variant of TgOAT at 37°C

Substrate	**Co-substrate**	k_{cat} **(s^{-1})**	K_m **(mM)**	k_{cat}/K_m **($M^{-1}s^{-1}$)**	K_i **(mM)**
Wild-type					
GABA	α-KG	2.91 ± 0.03	1.32 ± 0.02	2204 ± 56	−
AcOrn	α-KG	4.6 ± 0.3	7.4 ± 0.4	622 ± 74	−
L-orn	α-KG	2.1 ± 0.1	6.9 ± 0.3	304 ± 28	−
D-orn	α-KG	0.42 ± 0.05	4.2 ±0.5	1000 ± 23	−
α-KG	L-orn	2.51 ± 0.01	0.31 ± 0.03	8161 ± 815	17 ± 3
V79Y					
L-orn	α-KG	0.21 ± 0.01	3.9 ± 0.1	53 ± 4	−
GABA	α-KG	0.82 ± 0.04	18 ± 4	46 ± 12	−
AcOrn	α-KG	2.5 ± 0.1	496 ± 80	5 ± 1	−
α-KG	L-orn	0.41 ± 0.02	0.056 ± 0.004	7321 ± 880	20 ± 3

Under saturation with L-orn, the amino group acceptor α-KG provided a k_{cat} and K_m values of 2.51 ± 0.01 s^{-1} and 0.31 ± 0.03 mM, respectively, and showed substrate inhibition with K_i value of 17 ± 3 mM. Pyruvate and oxaloacetate do not appear to be adequate amino group acceptors. Their relative efficiency compared to α-KG in the reaction with L-orn was negligible, scarcely reaching 1% (data not shown). Even though the diamine putrescine and the polyamine spermidine were unproductive amino group donors, they were examined as inhibitor compounds of the enzyme.

Spermidine and putrescine act as non-competitive inhibitors with K_i values of 24 ± 4 mM and 93 ± 5 mM, respectively (Figure 9).

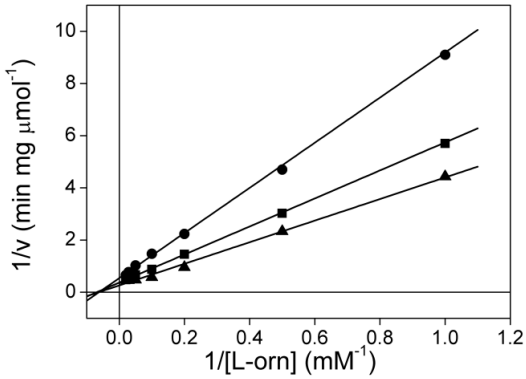

Figure 9. Determination of putrescine inhibition type. Double-reciprocal plot of enzyme kinetics in the absence (triangle) and presence of 60 mM (square) and 110 mM (circle) putrescine.

3.4 Absorption changes of TgOAT in the presence of substrates

The addition of L-orn to holo-TgOAT causes absorbance changes describing the complete conversion of the enzyme from the PLP into the PMP form. They consist in the immediate appearance of absorption band at 331 nm and the positive dichroic signals around 340 attributable to the PMP form of the enzyme, and the concomitant decrease of both the 416-nm absorbance band and the 423-nm dichroic band (Figures 10A and 10B), as well as an increase of the dichroic bands in the 280-290-nm region. No absorption from the internal aldimine of PLP is discernible in the visible range of the spectrum and PMP-TgOAT is pure with respect to the content of the cofactor. Also, the addition of GABA and AcOrn to the enzyme caused the conversion of PLP into PMP.

Following addition of α-KG to TgOAT-PMP, the original absorbance and dichroic bands of the holo-enzyme reappeared (Figures 10A and 10B).

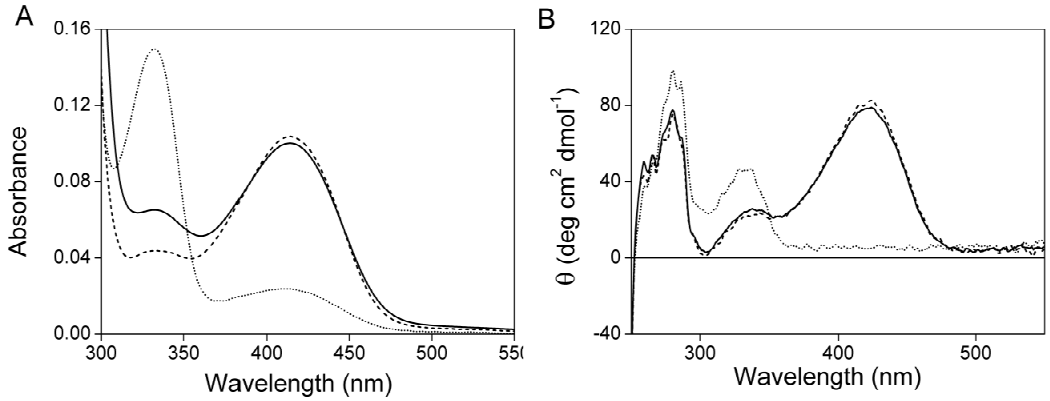

Figure 10. Absorption and CD spectra of TgOAT showing spectral changes upon addition of L-orn and α-KG (A) Absorption spectra of 10 μM TgOAT alone (solid line) in 50 mM Bis-Tris propane pH 8, in the presence of 30 mM L-orn (dotted line) and after addition of 1 mM α-KG (dashed line) to the enzyme pre-incubated with L-orn. (B) CD spectra in 20 mM sodium phosphate pH 8. Line style for enzyme alone, after addition of L-orn, and the following addition of α-KG is the same as for panel (A).

3.5 Rapid-scanning stopped-flow kinetics

In order to measure the kinetic parameters of each half-transamination reaction, we performed rapid scanning stopped-flow measurements of TgOAT-PLP with different concentrations of L-orn and TgOAT-PMP with different concentrations of α-KG at 12°C. This temperature was selected since it allows to follow spectral changes too rapid to be monitored at 37°C. We also determined the steady state parameters for the overall transamination with both substrates at the same temperature to allow suitable comparison (Table 3). Upon addition of saturating concentrations of L-orn, the visible spectrum of TgOAT-PLP exhibits a very rapid increase at 416 nm (within the dead time of the instrument, 3.6 ms, above 40 mM L-orn and only partially visible at the lowest concentrations) followed by a decrease at the same wavelength concomitant with an increase at 331 nm and no isosbestic point. Analysis of the absorbance changes at 300-550 nm fits well with a two-step, sequential first-order mechanism (Figure 11). The last, third irreversible phase corresponds to intermediate hydrolysis/product release:

$$E_{PLP} + L - orn \rightleftharpoons ES \rightleftharpoons EK \rightarrow E_{PMP} + P5C$$

where E_{PLP} is TgOAT-PLP, ES the external aldimine intermediate absorbing at 416 nm, EK the ketimine intermediate absorbing at 331 nm, E_{PMP} TgOAT-PMP, and P5C the cyclic irreversible product originating from L-glutamate-γ-semialdehyde.

The k_{obs} obtained as a function of L-orn concentration measured either as a 416 nm decrease or 331 nm increase follow a hyperbolic behaviour and fit to equation (4)

$$k_{obs} = \frac{k_{max}[S]}{K_m^{app} + [S]} \quad (4)$$

yielding k_{max} = 0.67 ± 0.05 s^{-1} and K_m^{app} = 7 ± 1 mM and k_{max} = 0.72 ± 0.09 s^{-1} and K_m^{app} = 7 ± 2 mM, respectively (inset of Figure 11, and Table 3).

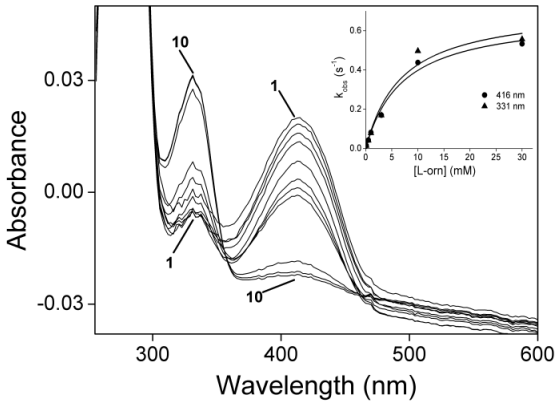

Figure 11. Rapid-scanning stopped-flow analysis of TgOAT at 12°C. Rapid-scanning stopped-flow spectra upon addition of 30 mM L-orn to 10 µM TgOAT-PLP. Ten spectra are displayed at 0, 0.03, 0.06, 0.09, 0.23, 0.51, 0.79, 1.07, 6.1, 11.7, and 17.3 s. Inset: rate constants for the 416 nm decrease (circle) or 331 nm increase (triangle up) as a function of L-orn concentration.

Notably, the value of k_{max} is coincident with that of k_{cat} of the overall L-orn/α-KG reaction at the same temperature (Table 3). Since k_{max} highly reflects the ketimine formation, it should be suggested that this step is rate limiting in this half-reaction. The catalytic efficiency k_{max}/K_m^{app} is 2-fold higher than k_{cat}/K_m, the latter being possibly correlated to ketimine hydrolysis or product release.

The addition of α-KG to TgOAT-PMP converts the PMP form of the enzyme, absorbing at 331 nm, into the PLP form absorbing at 416 nm in a single step with a clear isosbestic point (Figure 12).

Global fitting of the spectral changes at 300-550 nm fits well with a two-step, serial first-order mechanism (Figure 12)

$$E_{PMP} + \alpha KG \rightleftharpoons EK \rightleftharpoons ES \rightleftharpoons E_{PLP} + L - glu$$

where E_{PMP} is TgOAT-PMP, EK the ketimine intermediate absorbing at 331 nm, ES the external aldimine intermediate absorbing at 416 nm, and E_{PLP} TgOAT-PLP.

The rate constants obtained at the various concentrations determined as the increase at 416 nm (the spectral changes at 331 nm are slightly influenced by absorbance of α-KG) followed a hyperbolic behaviour (inset of Fig 12, and Table 3) and were fit to equation (4) yielding k_{max} = 103 ± 5 s^{-1} and K_m^{app} = 4.5 ± 0.5 mM.

The value of k_{max} is 86-fold higher than the k_{cat} measured under steady-state conditions, suggesting that external aldimine hydrolysis is rate limiting, and not its formation. Since K_m^{app} is 15-fold higher than K_m, the catalytic efficiency of external aldimine formation with L-glutamate is 7-fold higher than k_{cat}/K_m, as this value is highly affected by k_{cat}.

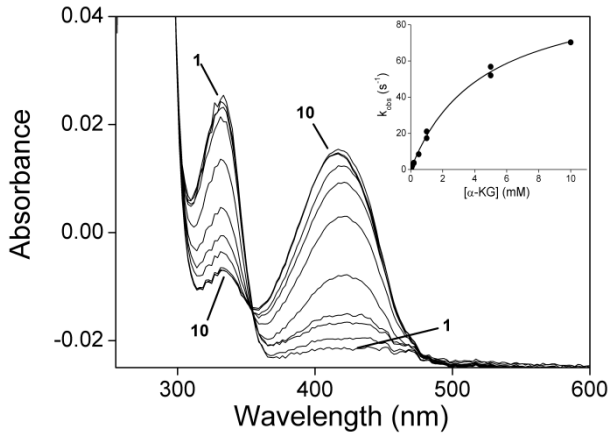

Figure 12. Rapid-scanning stopped-flow analysis of TgOAT at 12°C. Rapid scanning stopped-flow spectra upon addition of 1 mM α-KG to 10 µM TgOAT-PMP. Ten spectra are displayed at 0, 0.029, 0.057, 0.085, 0.23, 0.51, 0.79, 1.07, 2.35, 3.75, and 5.15 s. Inset: rate constants for the 416 nm increase as a function of α-KG concentration.

Table 3. Steady-state and pre-steady-state kinetic parameters of TgOAT at 12°C

Transamination half-reaction kinetic parameters				
	Substrate	k_{max} **(s^{-1})**	K_m^{app} **(mM)**	k_{max}/K_m^{app} **($M^{-1}s^{-1}$)**
Wild-type				
TgOAT-PLP	L-orn	0.67 ± 0.05[a]	7 ± 1[a]	96 ± 16[a]
		0.72 ± 0.09[b]	7 ± 2[b]	103 ± 42[b]
TgOAT-PMP	α-KG	103 ± 5	4.5 ± 0.5	22900 ± 3656
V79Y				
TgOAT-PLP	L-orn	--[c]	--[c]	--[c]
TgOAT-PMP	α-KG	1.23± 0.05	0.027 ± 0.007	45555 ± 13662
Steady-state kinetic parameters at 12°C				
Substrate	**Co-substrate**	k_{cat} **(s^{-1})**	K_m **(mM)**	k_{cat}/K_m **($M^{-1}s^{-1}$)**
Wild-type				
L-orn	α-KG	0.7 ± 0.1	15 ± 2	46 ± 13
α-KG	L-orn	1.2 ± 0.2	0.32 ± 0.01	3750 ± 742
V79Y				
L-orn	α-KG	0.08 ± 0.01	16 ± 1	5 ± 1
α-KG	L-orn	0.11 ± 0.02	0.030 ± 0.001	3667 ± 789

[a]measured as 416 nm decrease;
[b]measured as 331 nm increase;
[c]k_{on} = $7.3 \cdot 10^{-4} \pm 3 \cdot 10^{-5}$ $s^{-1}mM^{-1}$, k_{off} = 0.027 ± 0.002 s^{-1}, K_d = 37 ± 2 mM at 416 nm and k_{on} = $7.4 \cdot 10^{-4} \pm 3 \cdot 10^{-5}$ $s^{-1}mM^{-1}$, k_{off} = 0.032 ± 0.002 s^{-1}, K_d = 43 ± 2 mM at 331 nm.

3.6 Reaction of TgOAT with β-chloro-L-alanine

As β-elimination is a side reaction common to transaminases, we examined the lyase activity of TgOAT with β-chloro-L-alanine (BCA), a substrate with a good β-leaving group.

We collected spectra as a function of time upon addition of 50 mM BCA to 20 μM TgOAT, which caused a decrease of the absorption band at 416 nm and a broad increase in absorbance at wavelengths shorter than 350 nm (likely due to the pyruvate product), while the 416 band returned to the initial protein signal (Figure 13). The kinetic parameters determined for pyruvate production resulted in a k_{cat} of 0.51 ± 0.03 s^{-1} and a K_m of 24 ± 4 mM with a catalytic efficiency ~14-fold lower than that for L-orn transamination. Based on the knowledge that some aminotransferases become covalently inactivated by product(s) of β-elimination (syncatalytic inactivation) [68, 69], the residual L-orn transamination activity of TgOAT was determined following reaction with BCA. The activity was not reduced, indicating that the enzyme was not inactivated as a result of β-lyase reaction. Thus, it is unlikely that this reaction would have any biological meaning.

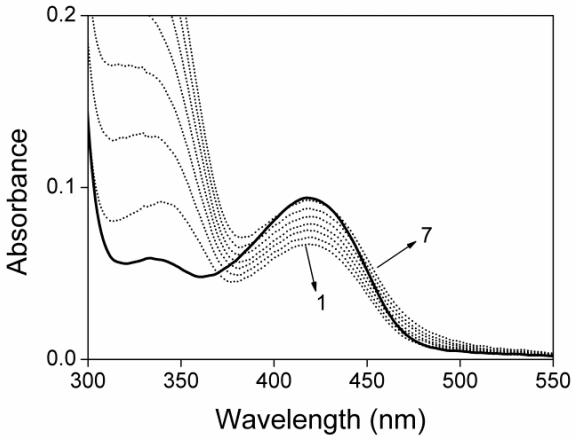

Figure 13. Spectral changes after addition of BCA to TgOAT. Absorption spectra of 10 μM TgOAT alone (solid line), and after addition of 50 mM BCA (dotted line) immediately (line 1) and after 5, 10, 15, 20, 25, and 30 min (line 7).

3.7 V79Y variant

To assess the contribution of the Val79 in determining TgOAT substrate specificity, we produced the TgOAT V79Y variant and analysed its spectroscopic and kinetic properties. The V79Y variant binds 2 mol of PLP per dimer, and exhibits absorbance, dichroic, and fluorescence features identical to those of TgOAT both alone and in the presence of substrates. The K_D^{PLP} values for V79Y variant was found to be 270 ± 20 nM, which is 4.5-fold higher than that of wild-type enzyme.

The steady-state kinetic parameters of V79Y are listed in Table 2. The V79Y mutation led to a small decrease in k_{cat} for GABA (3.7-fold) and for AcOrn (1.8-fold). This loss was accompanied by a 15-fold and 70-fold increase in K_m for GABA and AcOrn, respectively. By contrast, k_{cat} decreased 8-fold for L-orn, although K_m was reduced by 1.8-fold. The net result was a general decrease of the enzyme catalytic efficiency which is significant toward GABA (50-fold) and AcOrn (125-fold) compared to that of L-orn (6-fold).

In addition, the V79Y mutation led to a 8-fold decrease in k_{cat} for α-KG which is, however, countered by a 6-fold decrease in K_m, such that k_{cat}/K_m is reduced only 1.3-fold.

Of interest, when tested for β-elimination reaction, the protein variant showed the same behaviour as wild-type in terms of both kinetic parameters (k_{cat} 0.89 ± 0.01 s^{-1}, K_m 28 ± 2 mM) and spectroscopic changes, which would indicate that the substitution of Val79 with Tyr does not affect β-elimination reaction.

The half-reactions of V79Y with L-orn and α-KG were analyzed to understand the influence, if any, of the mutation with respect to the transamination catalytic mechanism. Rapid-scanning stopped-flow spectra/analyses of V79Y-PLP in the presence of L-orn or of V79Y-PMP in the presence of α-KG presented in both cases, a behaviour similar to that of the wild-

type enzyme. The global fitting of the absorbance spectra of both reactions fit to a two-step, serial first-order mechanism (Figures 14 and 15).

The addition of L-orn to V79Y-PLP determines a time-dependent decrease of absorbance at 416 nm with an increase at 331 nm without a clear isosbestic point (Figure 14). This could suggest the presence, as observed in the wild-type reaction (Figure 11), of multiple species besides external aldimine and ketimine, as Michaelis intermediate or the product PMP that has released the product L-glutamate-γ-semialdehyde. The rate constants k_{obs} for the conversion of the 416 nm peak to the 331 nm species yielded a straight line (inset of Figure 14) whose intercept and slope are the unimolecular rate dissociation constant and the bimolecular rate association constant of the species absorbing at 331 nm

$$E + S \underset{k_{off}}{\overset{k_{on}}{\rightleftharpoons}} ES$$

where E represents V79Y-PLP, S represents L-orn, k_{on} the bimolecular rate association constant, k_{off} the unimolecular rate dissociation constant and ES could be reasonably attributed to the ketimine intermediate. The k_{obs} values obtained at different concentrations were fitted to the following equation [70, 71]:

$$k_{obs} = k_{on}[S] + k_{off} \quad (5)$$

The comparison of the same pre-steady state values of the V79Y variant with those of the wild-type allowed for some interesting observations. First, the half-transamination of V79Y-PLP with different L-orn concentrations leads to spectral changes with rate constant values linearly correlated to L-orn increases. The absence of a hyperbolic behaviour of k_{obs} values implies that only k_{on} and k_{off} values could be calculated. This is quite unexpected since this means that no saturation occurs.

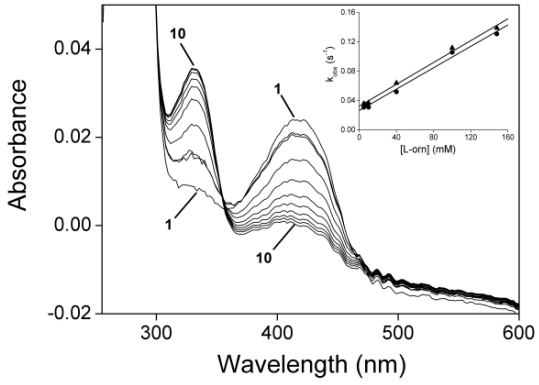

Figure 14. Rapid-scanning stopped-flow analysis of V79Y TgOAT at 12°C. (A) Rapid-scanning stopped-flow spectra following addition of 100 mM L-orn to 10 µM TgOAT-PLP. Ten spectra are displayed at 0, 0.03, 0.06, 0.09, 0.23, 0.51, 0.79, 1.07, 6.1, 11.7, and 17.3 s. Inset: rate constants for the 416 nm decrease (circle) or 331 nm increase (triangle up) as a function of L-orn concentration.

Since k_{on} could be regarded as k_{max}/K_m^{app} [72], a large decrease of the catalytic efficiency in V79Y was observed. A value of ~0.01 s^{-1} for k_{max} could be calculated, which is 8-fold lower than k_{cat} for overall transamination catalyzed by V79Y. This value is 70-fold lower than that measured for wildtype. However, this calculated k_{max} value is largely affected by the reverse reaction. The k_{off} value, instead, could reflect a destabilization of L-orn binding with respect to wild-type. The term K_d, given by k_{off}/k_{on}, is about 40 mM, 2.5-fold higher than K_m measured under steady state condition. In any case, the rate limiting step of the reaction has changed and the ketimine does not exhibit saturation behavior. The comparison of k_{cat}/K_m under steady state conditions for wild-type and V79Y showed that the catalytic efficiency is decreased by 9-fold for the V79Y variant.

Considering the other half-reaction, it is noteworthy that the rate constant values, k_{obs}, measured upon addition of α-KG to V79Y-PMP follow a hyperbolic behavior and were fitted to equation (4) (Figure 15 and inset), suggesting that the 416 nm species could be attributed to the external aldimine with L-glutamate, as the k_{max} value exceeds 12-fold the k_{cat} value, the latter probably reflecting aldimine hydrolysis/product release (Table 3). The coincidence of K_m^{app} and K_m explains the reason for a k_{max}/K_m^{app} value 14-fold higher than k_{cat}/K_m (Table 3). It could be inferred that the mutation has lowered L-glutamate aldimine hydrolysis more than external aldimine formation. Moreover, comparison of k_{max}/K_m^{app} for wild-type and V79Y showed that V79Y increased the efficiency of L-glutamate external aldimine formation by nearly 2-fold.

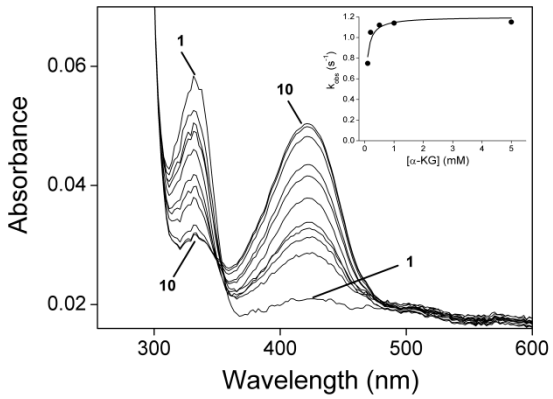

Figure 15. Rapid-scanning stopped-flow analysis of V79Y TgOAT at 12°C. Rapid scanning stopped-flow spectra upon addition of 1 mM α-KG to 10 µM TgOAT-PMP. Ten spectra are displayed at 0, 0.029, 0.057, 0.085, 0.23, 0.51, 0.79, 1.07, 2.35, 3.75, and 5.15 s. Inset: rate constants for the 416 nm increase as a function of α-KG concentration.

3.8 Molecular modelling

In the attempt to rationalize from a structural standpoint the unique substrate preference of TgOAT, we modelled the external aldimine of wild-type and the V79Y variant of TgOAT in complex with L-orn, AcOrn and GABA by docking means, starting from the crystal structure of TgOAT in its internal aldimine form (PDB ID code 4ZLV).

The predicted binding modes of L-orn in wild-type and V79Y TgOAT are shown in Figures 16A and 16B, respectively. With the δ-amino group of the substrate covalently bound to PLP, the carboxylate group is predicted to form an ion-pair with Arg174, similarly to what observed in the crystal structure of human OAT in complex with the substrate analogue 5-FMOrn (PDB ID code 2OAT) [43]. Another interaction involving the carboxylate moiety is represented by a hydrogen bond with the hydroxyl group of Tyr171. Finally, the carboxylate is bridged to the phosphate group of PLP through Tyr171 and a water molecule. Another Tyr residue of the active site, namely Tyr49, is predicted to interact with the amino group of L-orn. The presence of a third Tyr in the active site, as observed in the V79Y, is predicted to further stabilize L-orn in the active site, through: i) van der Walls interactions between the aliphatic tail of L-orn and the aromatic ring of Tyr; ii) a hydrogen bond between the α-amino group of L-orn and the hydroxyl group of Tyr.

Modelling of AcOrn in wild-type and V79Y forms of TgOAT suggests that the N-acetyl group of ornithine could be well accommodated in the pocket of the wild-type, but not as well in the variant, due to the potential steric hindrance with the Tyr residue (Figures 16C and 16D).

GABA is predicted to bind to wild-type TgOAT in two equally stable conformations, in which its carboxylic group can be oriented toward Arg174 or Arg409, respectively (Figure 16E). In the latter case, the presence of the less bulky Val79 in place of a Tyr residue, as observed in mammalian OATs (e.g., Tyr85 in human OAT) permits the formation of an additional ion-pair interaction between Arg409 and GABA, in addition to the GABA-Arg174 interaction. This is also possible thanks to the “switching” of Arg409 between Glu229 and GABA. On the other hand, the steric occupancy of a Tyr residue, as observed in V79Y (Figure 16F), greatly limits the conformational freedom of GABA and Arg409, potentially resulting in an unfavourable entropy loss upon binding. Therefore, as already pointed out [44], Val79 is a major determinant of specificity toward GABA versus L-orn.

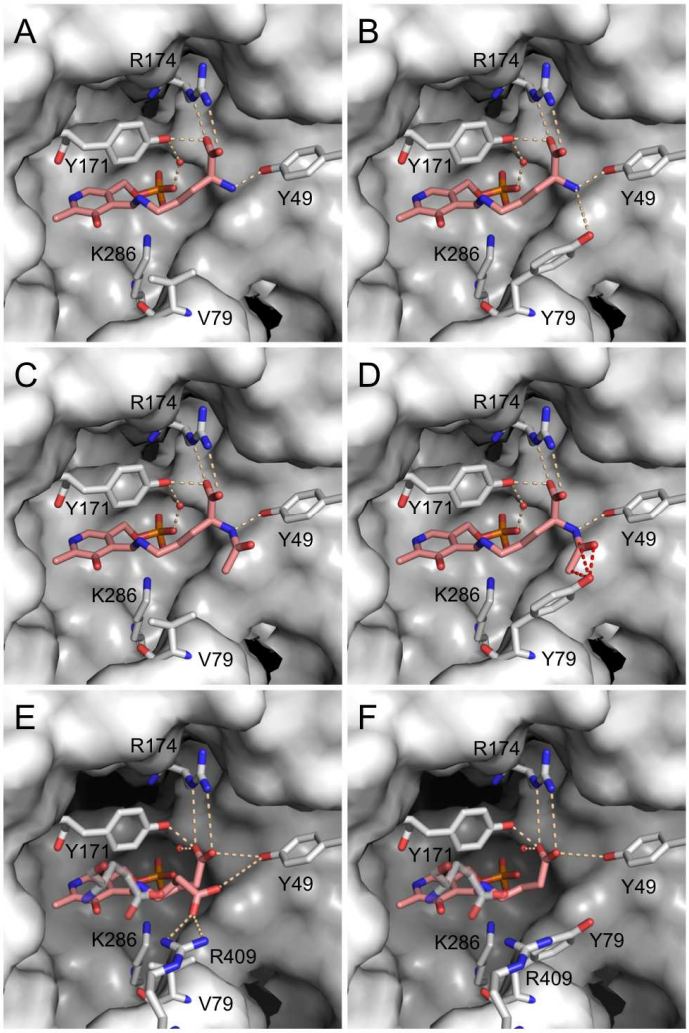

Figure 16. Modelling of the external aldimine of wild-type and the V79Y variant of TgOAT in complex with L-orn (A-B), AcOrn (C-D) and GABA (E-F). The external aldimines are shown as pink sticks. Residues described in text are labelled in single-letter code. Potential favourable and unfavourable interactions are depicted as pink and red dashes, respectively.

3.9 Regulation of TgOAT activity by reduced TgTrx

Recently, OAT from *P. falciparum* (PfOAT) has been shown to be positive regulated by Trx which is able to drastically enhance the activity of the parasitic enzyme. In particular, site-directed mutagenesis and functional analysis revealed that the interaction between PfOAT and Trx is mediated by two cysteine residues, Cys154 and Cys163, that are localized in the substrate binding loop [48].

Sequence alignment and structural comparison between PfOAT and TgOAT revealed that TgOAT also possesses two cysteine residues (Cys179 and Cys187) that are closed enough to form a disulfide bond and that are located in the loop involved in the substrate binding (Figure 17).

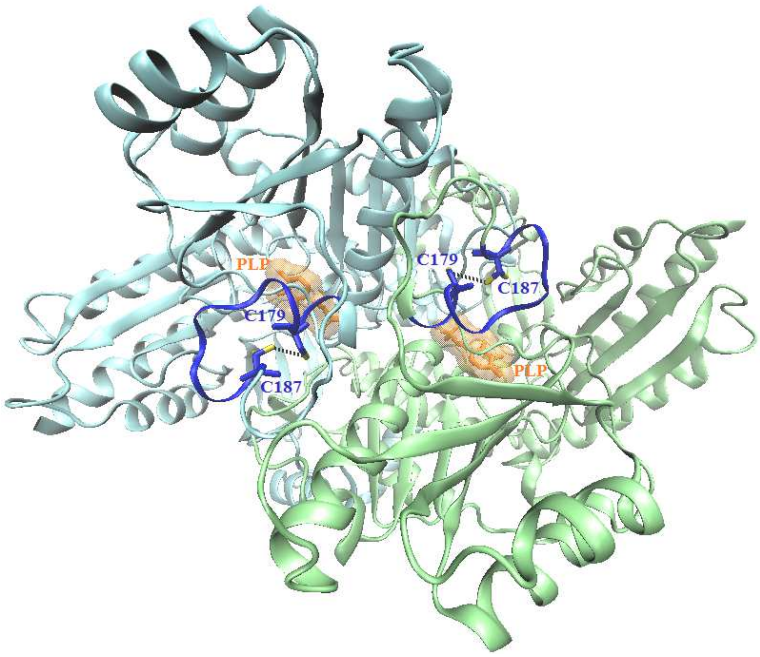

Figure 17. Dimeric structure of TgOAT. PLP is shown in orange, while Cys179 and Cys187 are labeled in blue. The substrate binding loop is shown in blue. Molecular graphics images were produced using VMD (Visual Molecular Dynamics).

Therefore, we decided to study whether also TgOAT activity could be regulated by TgTrx.

Recombinant TgTrx was purified as a His-tagged protein to greater than 98% purity as confirmed by SDS-PAGE; the size of the protein, calculated with a molecular size marker, was about 13 kDa that corresponds well to the molecular mass elucidated from the sequence information (12858 Da).

The effect of different concentration of reduced TgTrx was tested on the transaminase activity of TgOAT in the presence of saturating L-orn and α-KG as substrates. Five-min incubation of TgOAT with TgTrx in the assay buffer was necessary. We reduced TgTrx and oxidized

TgOAT as described in the experimental section. Importantly, oxidation treatment did not affect TgOAT activity.

Interestingly, reduced TgTrx increased the activity of TgOAT in a concentration-dependent manner (Figure 18). However, the increase was significantly lower compared to that observed in PfOAT for which a 10-fold increase in enzyme activity in the presence of reduced Trx was found. Notably, Trx did not cause any change in TgOAT activity when GABA or AcOrn where used as substrates (Figure 18).

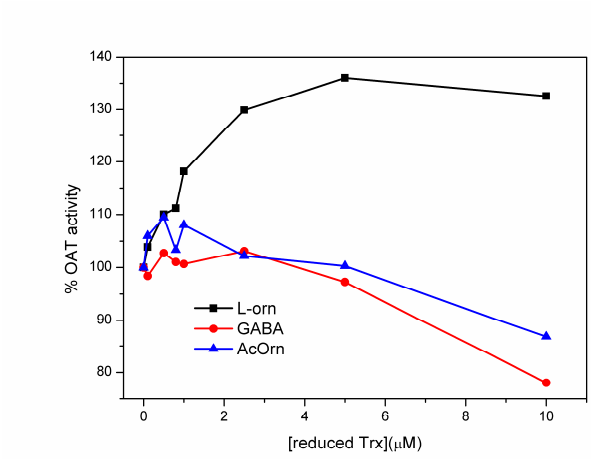

Figure 18. Representative curve of oxidized TgOAT in the presence of reduced TgTrx. Different concentrations of reduced Trx were added to the assay system under substrates saturation.

To analyze the specificity of this putative Trx regulation, we next tested the effect of oxidized TgTrx on TgOAT. As shown in figure 19, oxidized TgTrx was able to increase TgOAT activity even if to a lesser extent (~ 8 %) compared to reduced TgTrx (~ 25 %). The finding that the activity of TgOAT increased in the presence of TgTrx, independently from the redox state of the redoxin, raises the question if the *in vitro* observed Trx regulation of TgOAT might be relevant under *in vivo* physiological condition and if this regulation could be independent of the Trx redox state.

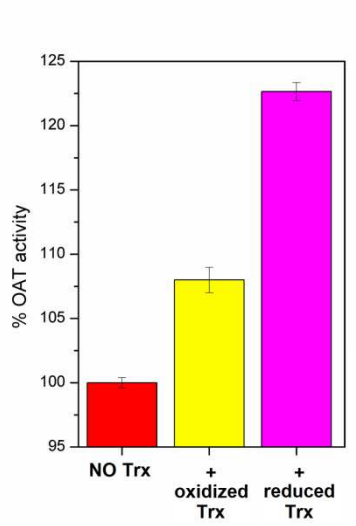

Figure 19. Activity of oxidized TgOAT in the absence and presence of reduced or oxidazied TgTrx (5µM).

It is known that Trx reduces protein disulfides via a disulfide-exchange mechanism through their active-site motif Cys-X-X-Cys. The N-terminal cysteine residue of the motif performs a nucleophilic attack towards the disulfide of the target protein, resulting in the formation of a mixed disulfide intermediate. Then the intermolecular disulfide bond is cleaved by the C-terminal resolving cysteine of the active-site motif, resulting in a reduced substrate and an oxidized redoxin (Figura 20) [73, 74].

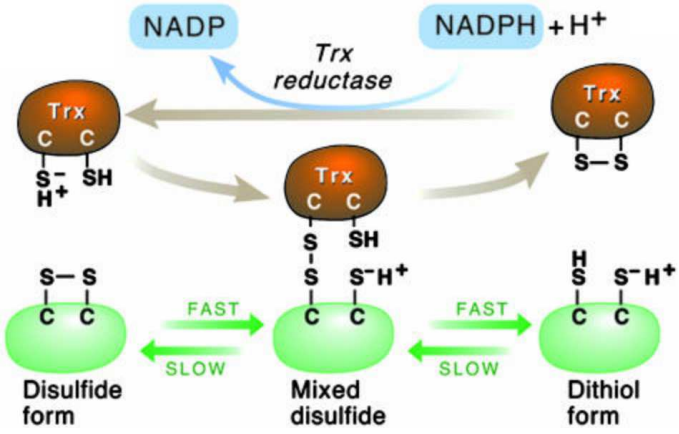

Figure 20. Mechanism for general disulfide reduction catalyzed by Trx [75].

Therefore, we created TgOAT mutants, with selected cysteines mutated to serine (C179S, C187S and C179S-C187S), in order to evaluate the role of this residues in the regulation of enzymatic activity by TgTrx. We measured the activity of the variants in the presence of different concentration of reduced TgTrx. Notably, all mutant proteins were not activated by Trx, suggesting a possible role of Cys179 and Cys187 in mediating the reversible thiol-

disulfide reaction, i.e., the typical mechanism of the control exerted by Trx over the activity of its target proteins (Figura 21).

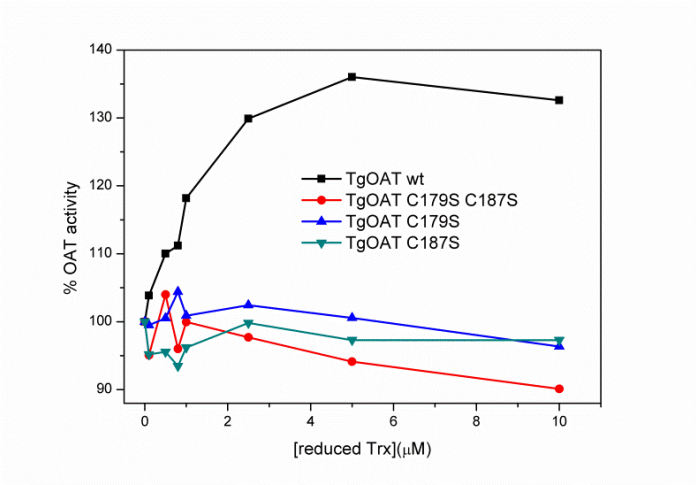

Figure 21. Representative curve of the activity of TgOAT cysteine mutant in the presence of TgTrx. Different concentrations of reduced TgTrx were added to the assay system under saturating condition of L-orn and α-KG.

Despite its importance in cellular redox homeostasis, the precise mechanism by which Trx recognizes target proteins, especially in the absence of any apparent signature binding sequence or motif, remains unknown. Recent studies revealed that the binding of Trx to its target does not depend on the redox-state of Trx as Trx recognizes the oxidized form of its target proteins with exquisite selectivity, compared with their reduced counterparts [45]. Therefore to gain deeper insight into Trx-TgOAT recognition modulating factors, the interaction between reduced and oxidized TgTrx and oxidized TgOAT variants was investigated also by ITC. Nevertheless, we did not determine the thermodynamic parameters of this putative binding because ITC measurements did not show a binding trend.

Altogether, our findings afford new insight into Trx-TgOAT recognition, which could be critical to understanding the enzyme function in normal metabolism. However, further studies will be necessary to verify the *in vitro* and *in vivo* interaction of the two proteins.

4. DISCUSSION

UV-Vis absorbance, fluorescence, and CD analysis indicate that TgOAT is largely similar to OATs from other species in term of spectral properties of PLP and mechanism of transamination in which the cofactor shuttles between PMP and PLP forms through two coupled half-reactions [76, 77].

However, the present work shows that TgOAT does not possess a specific ornithine aminotransferase activity, as suggested by the published genome of T.gondii (http://toxodb.org/toxo/) [78] but exhibits both AcOrn and GABA transaminase activity. Indeed, first of all GABA serves as a better substrate than L-orn for TgOAT. This property is peculiar to OAT from *T. gondii* as GABA is an ineffective amino group donor in OATs from other organisms such as *H. sapiens* [44], *P. sativum* [65], *P. falciparum* [79], and *Bacillus brevis* [80]. Furthermore, in addition to GABA, TgOAT utilizes AcOrn with higher efficiency than L-orn. This is another characteristic feature of TgOAT as no activity is detected for human, rat [81], or *B. brevis* OAT towards AcOrn [80], while *P. falciparum* OAT [79] and pea OAT [65] have a relative conversion rate for AcOrn that is significantly lower than that for L-orn. Modeling of L-orn, AcOrn, and GABA in complex with TgOAT provides a clear rationale for these unique features. The presence of Val79 of TgOAT in place of Tyr, as observed in mammalian homologs, provides the necessary room to accommodate AcOrn, and GABA in two equally stable conformations, resembling the active site arrangement of other GABA transaminases [23]. Interestingly, a recent work, which identifies a set of 13 amino acids in the active site within the ornithine transaminase-like family that could define substrate or reaction specificity [82], showed that TgOAT possesses higher sequence similarity, with respect to these “active site fingerprints”, to AcOAT than to OAT. OAT is highly specific to L-orn, while AcOAT accepts both L-orn and AcOrn [83, 84]. *T. gondii* OAT accepts both L-orn and AcOrn, with even higher efficiency towards AcOrn.

In light of our findings, TgOAT should more properly be considered as an enzyme with potential AcOrn and GABA transaminase function in the parasite cell, rather than an ornithine aminotransferase as annotated. The identification of an unanticipated functional GABA shunt in *T. gondii* tachyzoites by metabolite profiling studies [85] supported the possibility that TgOAT could have a role as GABA-transaminase in GABA-shunt. Notably, MacRae *et al* [85] suggests the presence in *T. gondii* of all the genes of GABA shunt, even a gene of glutamate transaminase, the second enzyme in the GABA shunt, which has putatively annotated as ornithine transaminase. Thus it is likely that TgOAT has a dual AcOrn

aminotransferase/GABA aminotransferase activity in vitro playing a role in both arginine and GABA metabolism in vivo. In line with this, the genome database for the genus Toxoplasma [78] results in both GABA-AT and AcOAT as missing enzymes. Broad specificity is a common property of aminotransferases and the extent of these enzymes promiscuity is not completely understood in any organism. In this respect, TgOAT resembles the *E.coli* ArgD enzyme, which has dual N-acetylornithine aminotransferase/N-succinyldiaminopimelate aminotransferase activity, with a function in both arginine and lysine biosynthesis [83].

Due to the possible involvement of TgOAT into two crucial amino acid metabolisms, the enzyme could represent a strong candidate for inhibitor design.

In this regard, we assessed the role of the active site residue Val79 of TgOAT, which is replaced by Tyr85 in human OAT, as structural differences between the two enzymes could account for inhibitor binding. Tyr85 of human OAT is presumed to be an essential determinant in distinguishing OAT from GABA-AT catalysis [44]. Change of Tyr85 to Ile72, as found in GABA-AT, converted the human enzyme, which has a 3200-fold preference for L-orn, to an enzyme with a 5-fold preference for GABA [44]. Exchange toward the human residue in TgOAT was accompanied with a general decrease of catalytic efficiency of *T. gondii* enzyme towards all substrates. Nevertheless, it was possible to notice an inversion in the substrate preference with L-orn becoming the preferred substrate. The effect of the V79Y mutation occurs mainly via K_m, showing a clear impact on substrate affinity by the mutation, especially towards AcOrn. The presence of Tyr79 in the substituted enzyme provides an additional anchor site of L-orn, while partially hampering, by steric hindrance, the binding of AcOrn (Figure 16B-D).

Determination of the pre-steady state kinetic parameters of the half-transamination reactions of wild-type and V79Y and their comparison to steady state values measured at the same temperature allowed us to reach some interesting considerations. First, while for the wild-type protein ketimine formation should be suggested as rate limiting in the L-orn half-reaction, for V79Y the rate of ketamine formation does not exhibit saturation and, therefore, the rate limiting step of the reaction has changed. On the contrary, the mutation does not affect the other half-reaction, from α-KG to L-glutamate, suggesting that for both protein variants external aldimine hydrolysis is rate limiting rather than its formation. Thus, pre-steady state and steady state kinetic data confirm the hypothesis that mutation impacts L-orn binding/processing more than α-KG half transamination.

In conclusion, our in vitro data demonstrate that TgOAT shows both AcOrn and GABA transaminase activities, highlighting its possible alternative role both in arginine and GABA

metabolism in vivo. The findings that TgOAT is likely involved into two important amino acid metabolisms and is significantly distinct from the well-characterized human enzyme with respect to substrate specificity could be considered as a first step towards exploring the possible use of TgOAT as an anti-toxoplasmosis drug target.

Chapter 3

The transsulfuration enzyme cystathionine γ-lyase is functional in *Toxoplasma gondii*

Abstract

Sulfur-containing amino acids play a central role in a variety of cellular functions in many organisms, therefore investigation of the enzymes involved in their metabolic pathways is of great interest. The protozoan parasite *T. gondii* includes the genes encoding enzymes of the reverse transsulfuration pathway, cystathionine β-synthase and CGL (previously annotated as cystathionine β-lyase) as well as the gene for the cysteine synthase involved in the de novo synthesis of L-cys. However, the functionality of none of these enzymes has so far been investigated.

Herein, TgCGL has been cloned, expressed and physiochemically and enzymatically characterized. We showed that TgCGL is a functional enzyme, which specifically catalyzes the cleavage at the CγS bond of cystathionine. This finding likely implies that the reverse transsulfuration pathway is operative in the parasite. The enzyme displays only marginal reactivity toward L-cysteine, which is also a mixed-type inhibitor of TgCGL activity, therefore indicating a tight regulation of cysteine intracellular levels in the parasite. Moreover, by employing structure-guided homology modelling we identified two main differences between the active sites of human and parasite enzymes: Glu59 and Ser340 in human to Ser77 and Asn360 in toxoplasma. Mutation of Asn360 to Ser revealed the importance of this residue in modulating the specificity of the parasitic enzyme for the catalysis of α,γ- versus α,β-elimination, suggesting a role in enforcing the appropriate binding conformation of the pseudo-symmetric L-cth substrate within the active site. Replacement of Ser77 by Glu completely abolished activity toward L-cth. Due to the presence of Tyr71, which is missing in human CGL, the side-chain of Glu77 is forced to occupy the same cleft of L-cth, likely interfering with its binding.

Our data, indicating that TgCGL exhibits notable differences with the human counterpart, might have far-reaching implications for the use of TgCGL as anti-toxoplasmosis drug target.

1. INTRODUCTION

1.1 Sulfur-containing amino acids metabolism

Sulfur-containing amino acids cysteine and methionine and their metabolic intermediates play essential roles in virtually all living organisms from bacteria to higher eukaryotes.

Due to the unique properties of sulfur and thiol, cysteine plays a relevant role in stability, structure, catalytic activity, and regulation of numerous proteins. Cysteine also takes part in the synthesis of glutathione, which plays a key role in protection from oxidative stress. Methionine is also a significance constituent of proteins and its oxidation and reduction in a protein are involved in the regulation of enzymatic activities. Moreover, methionine plays various roles through its activated intermediate S-adenosylmethionine (AdoMet) [86]. Despite the biological significance of the ubiquitous sulfur-containing amino acids, the distribution of their metabolic pathways is extremely diverse among organisms. Indeed, genome-wide and functional analyses of enzymes involved in the sulfur metabolic pathways have showed notable heterogeneity among protozoan parasites and between parasites and their mammalian hosts. Thus, the enzymes involved in sulfur-containing amino acids metabolic pathways are interesting drug targets.

Bacteria, fungi and plants possess the forward transsulfuration pathway, which is involved in the formation of methionine from cysteine. The enzymes implicated in these reactions are the cystathionine γ-synthase (CGS, EC 2.5.1.48), which converts cysteine and O-succinylhomoserine in cystathionine and succinate, and cystathionine β-lyase (CBL EC 4.4.1.8), which catalyzes an α,β-elimination of cystathionine to produce homocysteine and pyruvate. These organisms are also capable of *de novo* production of cysteine by sulfur assimilation. This pathway is catalyzed by two steps, initiated by serine acetyltransferase (SAT, EC 2.3.1.30) to form O-acetylserine (OAS) from L-serine and acetyl-coenzyme A. Subsequently, OAS reacts with sulfide to produce cysteine in an alanyl-transfer reaction catalyzed by cysteine synthase (CS, OAS thiolyase, EC 2.5.1.47) (Figure 22).

In mammals, cysteine is synthesized from methionine via cystathionine by the so-called reverse transsulfuration pathway. This pathway is considered to be the unique route for cysteine synthesis in vertebrates and involves two PLP-dependent enzymes, cystathionine β-synthase (CBS, EC 4.2.1.22), which synthesizes cystathionine from homocysteine and serine via a β-replacement reaction, and CGL (EC 4.4.1.1), which catalyzes the hydrolysis of cystathionine via an α,γ- elimination reaction, to yield cysteine, α-ketobutyrate, and ammonia (Figure 22) [87].

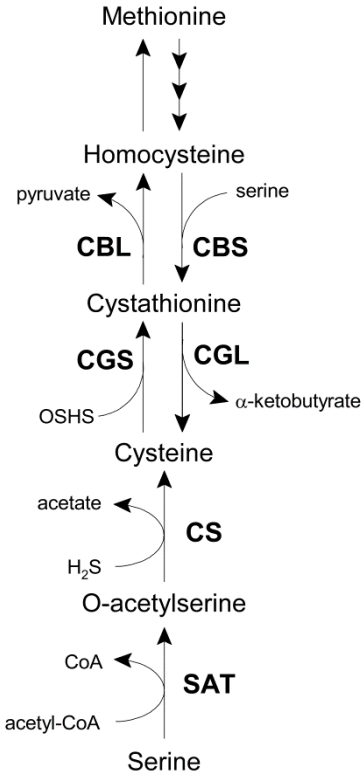

Figure 22. Sulfur-containing amino acid metabolism. CBS, cystathionine β-synthase; CBL, cystathionine β-lyase; CGS, cystathionine γ-synthase; CGL, cystathionine γ-lyase; CS, cysteine synthase; SAT, serine acetyltransferase; OSHS, O-succinylhomoserine.

Parasitic protozoa are characterized by remarkable differences in the above described transsulfuration pathways. For example, it has been demonstrated that *Entamoeba histolytica* lacks genes encoding enzymes of the transsulfuration pathway in both directions [88], *Giardia duodenalis*, *Trichomonas vaginalis*, *P. falciparum* and *C. parvum* lack both CBS and CGL of the reverse transsulfuration pathway [86, 89, 90]. In *T. cruzi* the enzymes CBS, CS and CGL have been identified and characterized [91, 92], thus indicating that in this pathogen cysteine could be produced by the de novo synthesis processes as well as by the reverse transsulfuration pathway.

The presence of genes for the enzymes CBS (TGME49_059180), CGL (TGME49_112930), and CS (TGME49_078910) in the genome of the intracellular protozoan parasite *T. gondii* raises the possibility that this parasite possesses both the reverse transsulfuration and the assimilatory cysteine biosynthetic pathways. However, although sequence analysis is an invaluable tool for unraveling the function of a gene product, further enzymatic and biochemical characterization of the encoded protein is necessary to unequivocally identify its function and properties. Moreover, since the main transsulfuration enzymes belong to the same so-called fold-type I of PLP-dependent enzymes [93], gene function prediction and gene

nomenclature assignment based only on phylogenetics and sequence alignment are often complicated [94].

1.2 Cystathionine γ-lyase

CGL catalyzes the γ-cleavage of cystathionine to yield cysteine, α-ketobutyrate, and ammonia. This enzyme is present in actinobacteria, fungi, and mammals. CGLs are homotetramers and carry one PLP cofactor per monomer covalently bound through a Schiff base to an active-site lysine.

A molecular mechanism was deduced on the basis of the structural similarity to the *E. coli* CBL active site (Scheme 3). In the first step, substrate binds to the active-site PLP cofactor by formation of a Schiff base. α-Proton abstraction by the active-site lysine residue, followed by reprotonation at C4' leads to the reversible formation of a ketamine intermediate. This species subsequently undergoes β-proton abstraction by the same lysine which is responsible for the proton transfer from Cα to C4' of the cofactor and the subsequent deprotonation of Cβ to initiate the γ-cleavage [95].

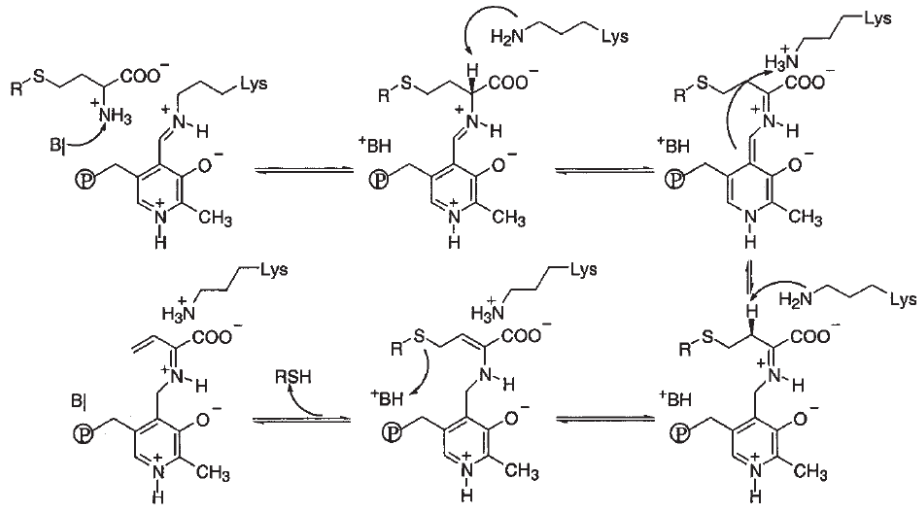

Scheme 3. Reaction scheme for CGL up to the point of the release of cysteine [95].

Human CGL displays an interesting substrate specificity with clear preference of C–S over S–S bond breakage: L-cys and L-cystine are converted orders of magnitudes more slowly than the natural substrate L-cth. The yeast enzyme attacks the C–β–S bond of L-cystine or L-cys. In humans, L-cth is split almost exclusively in a CGL-specific manner, whereas the yeast enzyme harbors pronounced CBL activity. A CGL enzyme from *Lactococcus lactis* was reported to consist of at least six identical subunits and have a broad substrate specificity and relatively low specific activity toward L-cth compared to bacterial CGL. The reaction

specificity seems context-dependent, such that the reaction catalyzed *in vivo* depends on the substrate supplied.

Despite the high degree of conservation of CGL among different organisms, inspection of human and *T. gondii* active sites overlays by structure-guided homology modelling identified two striking amino acid differences (Glu59 and Ser340 in human to Ser77 and Asn360 in toxoplasma).

In particular, sequence alignment of CGL from different organisms resulted in the presence of conserved acidic Glu or Asp residue at position 59 and Ser residue at position 340 in all organisms except protozoa, e.g. trypanosomes in general, *Lehismania major*, and *T. gondii*, in which a serine and an asparagine residues respectively were found (Figure 23).

Herein, we have cloned, expressed in *E. coli*, and characterized the putative CGL from *T. gondii* (TgCGL) with the aim to expand the very limited knowledge about the transsulfuration and cysteine biosynthesis routes in this pathogen and to explore the potential of TgCGL as anti-toxoplasmosis drug target.

Furthermore, in order to in-depth understand the structure–function relationships that control substrate and reaction specificity, which is a necessary step to develop novel therapeutics, we substituted the non-conserved serine and asparagine residues of TgCGL to glutamate and serine residues respectively, as found in human enzyme, and we examined their influence on enzyme function.

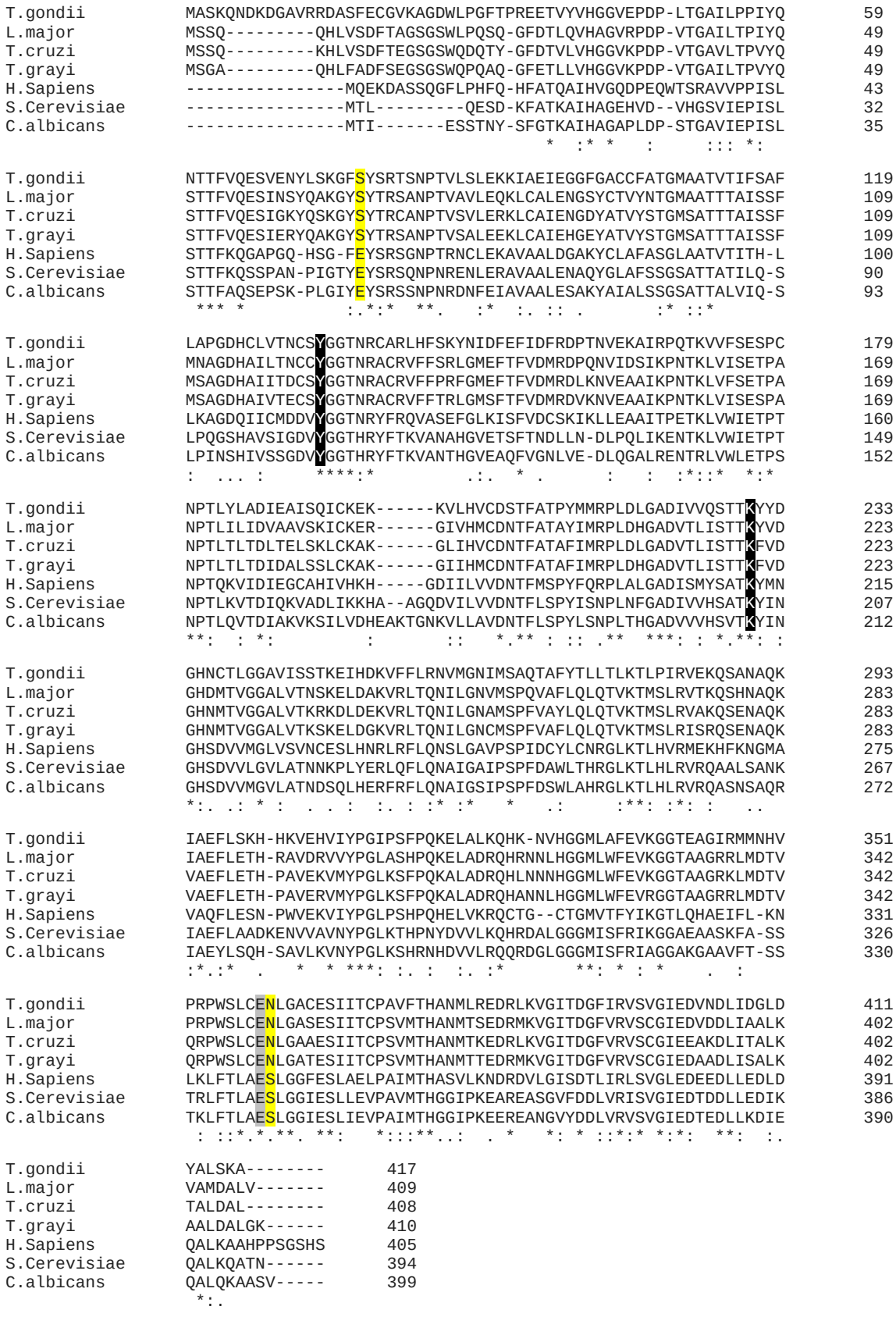

Figure 23. Sequence alignment of CGL from different organisms. Black shading indicates the PLP-binding lysine and the tyrosine involved in aromatic stacking interaction with PLP pyridine ring. Gray shading indicates Glu339 (hCGL numbering) which is conserved in 100% CGLs. The target residue for mutational analysis is highlighted in yellow. The CGLs used in this alignment (NCBI accession number) are XP_002364505.1, *T. gondii* ME49; XP_003722717.1, *L. major*; EKG03141.1, *T. cruzi*; XP_009313447.1, *T. grayi*; NP_666065.1, *Homo sapiens*; NP_009390.1, *S. cerevisiae*; XP_716241.1, *Candida albicans*. All sequence alignments were carried out using the Clustal OMEGA program.

2. EXPERIMENTAL PROCEDURES

2.1 Protein production

The complete cDNA of TgCGL (accession number: XM_002364464) in pMA-T vector was obtained from Invitrogen Corporation with a tag of six His at the N-terminal. The gene was cloned into the vector pET21a for the expression in *E. coli* Rosetta (DE3) cells. Cell cultures were grown at 37°C to an absorbance at 600 nm of 0.6. The expression of TgCGL was induced with 0.5 mM IPTG at 24°C for 20 h. Vitamin B6 (0.1 g/L) was added to the cell culture during induction in order to favour the proper protein folding and increase the protein stability. Cells were isolated by centrifugation, resuspended in 20 mM sodium phosphate pH 8, 150 mM NaCl buffer containing 1X protease inhibitor EDTA free, and lysed by sonication. Cell debris were removed by centrifugation (30000 xg for 15 min) and 1% streptomycin was added to supernatant to remove nucleic acid contamination. After centrifugation the supernatant was loaded onto an Ni-affinity column previously equilibrated with 20 mM sodium phosphate at pH 8, 150 mM NaCl, 0.1 mM DTT and 10 mM imidazole. The concentration of imidazole was increased stepwise, first to 80 mM to remove no specifically bound proteins, and then to 500 mM to elute the enzyme. Soluble TgCGL eluted between 200 and 250 mM imidazole. After addition of 100 μM PLP, the fraction containing TgCGL were concentrated and washed with 20 mM sodium phosphate buffer pH 8, 0.1 mM DTT using Vivaspin concentrators (Sartorius) to remove imidazole and unbound PLP.

The extinction coefficient was used to calculate the monomer concentration of the purified protein (ε_{280nm} = 30745 M^{-1} cm^{-1}; http://web.expasy.org/protparam/). The PLP content of the holo-enzyme was determined by addition of 0.1 M NaOH and using ε_{388nm} = 6600 M^{-1} cm^{-1} as described [96].

The S77E, S77A and N360S TgCGL variants was produced by site specific mutagenesis on the pET21a-TgCGL construct using the QuikChange® site-directed mutagenesis kit (Agilent Technologies). The mutated sequences were confirmed by DNA sequence analysis. Expression and purification of the S77E, S77A and N360S variants were performed as described for wild-type TgCGL. The yield from a one-liter purification was approximately 20 mg for all enzyme variants.

2.2 Size exclusion chromatography (SEC)

Gel filtration chromatography (Superdex 200 HR 10⁄300 GL) was used to analyze the oligomeric state of TgCGL. Chromatography was performed using 50 mM sodium phosphate

buffer pH 8.5, 150 mM NaCl, 0.1 mM DTT. The calibration curve was obtained as described [46]. In order to investigate the quaternary structure stability, the protein was incubated with increased concentration of urea (0 - 5.5 M) for 1 h, and loaded on the gel filtration column previously equilibrated with the specific urea concentration. The percentage of tetrameric protein was measured by integration of the area under the curve (absorbance at 280 nm) using the Evaluation module of Unicorn 7.0.2 software. The data were fit by sigmoidal curves and the concentration of urea at which 50% of TgCGL is tetrameric (C_m) was determined.

2.3 Apo-proteins preparation

Apo-proteins were obtained following the protocol in [94, 97]. The apo-proteins showed no absorption peak at 421 nm and no residual activity. The equilibrium dissociation constant for PLP (K_D^{PLP}) was obtained by measuring the fluorescence emission at 330 nm upon excitation at 280 nm in the presence of PLP ranging from 0.05 to 40 μM at 25 °C in 50 mM Bis-Tris propane pH 8 at apo-proteins concentration of 1 μM. The values of fluorescence intensity at 330 nm were plotted as a function of PLP concentration and fit to a non-linear binding equation to obtain the dissociation constant K_D.

2.4 Limited proteolysis

Fifty micrograms of holo- and apo-TgCGL were digested with trypsin (1:200 w/w) in 50 mM Tris-HCl pH 7.5 at 25 °C. At various time intervals (0, 1, 5, 10, 20, 40, 60 and 120 min), 8μl aliquots were taken for electrophoretic analysis. The digestion reaction was ended by boiling the sample for 5 min and adding reducing Laemmli buffer. After staining the gel with Coomassie blue, the bands intensities analysis was performed as described [98].

2.5 Differential scanning calorimetry

Differential scanning calorimetry (DSC) experiments were conducted using a TA Instrument Nano-DSC (New Castle, Delaware, USA). TgCGL samples of 50-100 μM were dissolved in in 20 mM sodium phosphate pH 8, and were heated from 10 °C to 120 °C at a scan rate of 1°C/min. All the samples were degassed prior to analysis.

2.6 Enzyme activity assays

Enzyme activity was determined using a Jasco-V560 UV-Vis spectrophotometer (Easton, Maryland, USA) via two spectrophotometric assays: the reaction of 5,5′-dithiobis-(2-nitrobenzoic acid) (DTNB) with the free thiol of the product (ε_{412} = 13600 M^{-1} s^{-1}), and by

monitoring the pyruvate formation with the coupling enzyme NADH-dependent lactate dehydrogenase (LDH) (ε_{340} = 6200 M^{-1} cm^{-1}), as described [49]. All enzymatic assays were carried out at 37°C in 50 MOPS, bicine, proline (MBP) buffer pH 9 in the presence of 20 μM PLP. Reactions were initiated by the addition of the enzyme at a final concentration of 1, 5 or 10 μM, depending on the activity of the enzyme variant. A background reading was recorded before initiation of the reaction by the addition of TgCGL.

Data were fitted to the Michaelis–Menten equation to obtain values of k_{cat} and K_m . For site-directed variants for which saturation was not observed, k_{cat}/K_m values were obtained by linear regression, based on the assumption that $K_m \gg$ [substrate]. The L-cys hydrolysis data were fitted to equation (5), which modifies the Michaelis-Menten equation taking into account the K_i term for substrate inhibition by L-cysteine [99]:

$$\frac{v}{E} = \frac{k_{cat}}{1 + \frac{K_m}{S} + \frac{S}{K_i}} \qquad (5)$$

where *E* is the total enzyme concentration, k_{cat} the rate constant, *S* the substrate concentration, K_m the apparent Michaelis-Menten constant and K_i the dissociation constant.

To evaluate the effect of temperature on α,γ-lyase activity, the enzyme was incubated for 10 min at temperatures between 20 °C and 90 °C, cooled on ice for 5 min, and the residual enzymatic activity was determined as described above.

2.7 Inhibition assays

The inhibitory activity of L-cys was evaluated through LDH assay and was expressed as the inhibitor concentration required for 50% inhibition of the α,β-eliminase activity (IC_{50}). The IC_{50} value was measured by a plot of percent activity versus log of L-cys concentration.

The kinetic parameters of α,β-eliminase inhibition by L-cys were evaluated by the Lineweaver–Burk plots and its secondary plots. The double-reciprocal plots were constructed with enzyme reaction initial velocity (V) versus substrate (S) concentration in the absence (control) or presence of L-cys at different concentrations. The type of inhibition, K_m and V_{max} values were determined from the plots. Slopes and Y-intercepts of these reciprocal plots were also replotted against the inhibitor concentration, respectively [100]. Data analysis was performed by OriginLab software.

Inactivation of TgCGL by DL-proparglyglycine (PAG) was evaluated by reacting 5 mM L-cth with TgCGL (2 μM), pre-incubated with different concentration of the inhibitor for 15 min at room temperature. Reactions were monitor through DTNB assay. Residual activity, remaining after 15 min incubation, was plotted against the relative concentration of PAG.

2.8 Spectroscopic measurement

Absorption measurements were performed on a Jasco-V560 UV-Vis spectrophotometer (Easton, Maryland, USA) in a buffer solution containing 50 MBP buffer pH 9, at protein concentration of 12 μM.

In order to evaluate the the equilibrium dissociation constant for TgCGL-L-cys complex formation (K_{app}), absorption spectra of TgCGL were recorded upon addition of different L-cysteine concentrations: 0, 0.04, 0.1, 0.15, 0.16, 0.2, 0.3, 0.4, 0.5, 0.8, 1, 2, and 3 mM. The plots of the absorbance changes at 335 and 421 nm against the L-cys concentration could be fitted to a hyperbolic relationship such as equation (6) :

$$\Delta A = \frac{\Delta A_{max} * [cysteine]}{K_{app} + [cysteine]} \quad (6)$$

where ΔA and ΔA_{max} are the absorption changes at given and infinite L-cys concentrations respectively, and K_{app} the equilibrium dissociation constant for TgCGL-L-cys complex formation.

2.9 Statistical analysis

Each experiment was performed at least in triplicate and reported values are representative of two or more independent determinations using different batches of protein that were purified separately. Data were analyzed using Origin 8.0 (OriginLab Corporation, Northampton, MA) and expressed as mean ± standard error.

2.10 Thin layer chromatography

Amino acid standards (1 mg/mL) were prepared in 20 mM sodium phosphate buffer, pH 8.0. These solutions were spotted, 1 μL at a time, on chromatographic plates, comprised of a 0.1-mm thick layer of silica gel on an aluminum support, and developed with a mobile phase of n-propanol/water (70:30, v/v), for a distance of 13 cm. TLC plates were subsequently dried, sprayed with a solution of 2 mg/mL ninhydrin in ethanol and dried, prior to heating for 5 min at 100°C.

2.11 Molecular modelling studies

The crystal structure of Methionine γ-lyase from *Citrobacter Freundii* in its internal aldimine form (PDB ID code 5E4Z) and human cystathionase (Cystathionine γ-lyase) in complex with PAG (PDB ID code 3COG) were used as a starting point to generate the model of the wt, N360S and S77E TgCGL enzyme, using the “homology modeling” tool of PyMod 2.0,

followed by energy minimization with the BIOPOLYMER package from InsightII (V.2000, MSI, Los Angeles), as already described [53, 101].

The Dundee PRODRG2 Server [54] was used to build the energy minimized three-dimensional structures of the PLP-Cystathionine and PLP-PAG external aldimines complexes, which were then docked into the active site of wt form of TgCGL, using the template-based molecular docking approach of Molegro Virtual Docker (MVD) software (CLCbio®). Flexible torsions of the external aldimines were automatically detected by MVD, and manually checked for consistency. A search space of 15 Å radius, centered on the active site cavity, was used for docking. The PLP in its internal aldimine form, as found in 3COG, was taken as pharmacophoric group for template-based docking. In the latter, if an atom of the ligand matches a group definition, it is rewarded by using a weighted score that depends on its distance to the group centers. The grid-based MolDock score with a grid resolution of 0.30 Å was used as scoring function and MolDock SE was used as docking algorithm [55]. For each ligand, ten runs were defined. Similar poses (RMSD $\leq$ 1.0 Å) were clustered, and the best scoring one was taken as representative. Other docking parameters were fixed at their default values. After docking, energy optimization of hydrogen bonds was performed.

3. RESULTS

3.1 Expression and purification of recombinant TgCGL

The recombinant TgCGL was expressed in *E. coli* cells with a 6xHis-Tag fused to the N-terminus and purified using Ni^{2+}-affinity chromatography. The yield from a standard purification was approximately 20 mg of recombinant protein per liter of bacterial culture.

The purity of enzyme was confirmed by SDS-PAGE and the band size of the recombinant protein, calculated with a molecular size marker, was 46 kDa that well corresponds to the protein molecular mass calculated from the sequence information (45926 Da) (Figure 24A).

Determination of enzyme-bound PLP indicated that the TgCGL binds ~1 mol of PLP/mol of monomer.

In its native form, TgCGL displayed a tetrameric quaternary structure both in apo- and holo-state as demonstrated by analytical size exclusion chromatography (Figure 24B).

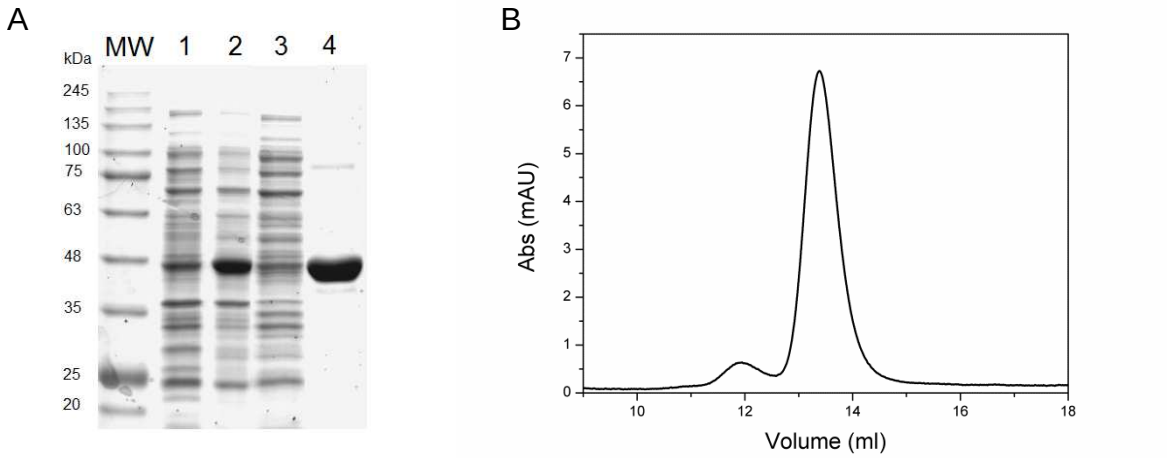

Figure 24. Production of recombinant TgCGL. (A) SDS-PAGE of TgCGL wt expression and purification. Lane MW, molecular mass standards; lane 1, uninduced control cells; lane 2, total E.coli proteins from cell lysate after overnight incubation at 24°C; lane 3, flow through fraction; lane 4, fraction of purified TgCGL. (B) SEC profile of TgCGL wt. Chromatogram recorded in 50 mM sodium phosphate buffer pH 8.5, 150 mM NaCl, 0.1 mM DTT

3.2 Properties of recombinant TgCGL

Recombinant native TgCGL exhibited an absorption spectrum with a major peak at 421 nm and a 280:421 nm ratio of about 4.6 (Figure 25A). The band in the 420 nm region is typical of protonated internal aldimine species that PLP forms with Lys230 in the active site.

The fluorescence emission spectrum of TgCGL upon excitation at 280 nm showed a pronounced peak at 336 nm, ascribable to the emission of Trp residues, and a much lower intensity and broader peak around 500 nm, which is the result of energy transfer from Trps to the ketoenamine tautomer of the internal Schiff base [63, 64] (Figure 25B). Excitation at 421

nm led to a single emission peak with a maximum at ~500 nm, thus further confirming the assignment of the 421 absorbance band to the ketoenamine tautomer (data not shown).

The emission spectrum of the apo-TgCGL following excitation at 280 nm had an emission band at 331 nm with an intensity approximately 1.5-fold greater than that of holoenzyme, as a consequence of the quenching of the emission fluorescence due to the bound PLP in the holo-form (Figure 25B). The dissociation constant (K_D) for the binding of PLP to TgCGL was measured by titrating apo-TgCGL with increasing amounts of PLP and following the fluorescence signal upon excitation at 280 nm. This analysis yielded a K_D value for the TgCGL–PLP complex of 0.17 ± 0.04 µM.

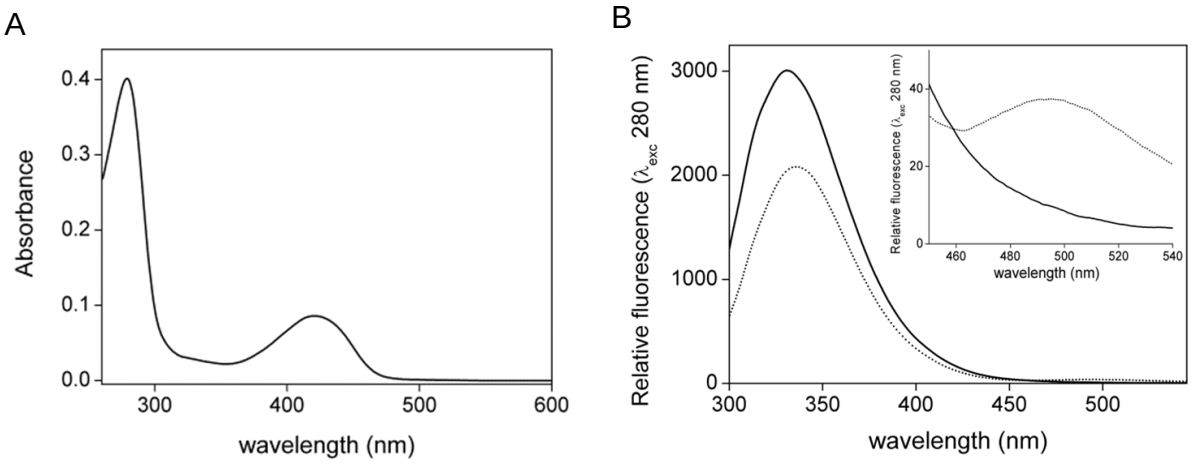

Figure 25. Spectral properties of TgCGL. (A) Absorption spectrum of purified TgCGL recorded on a solution containing 12 µM protein in 50 mM MBP buffer pH 9. (B) Fluorescence spectra (excitation was at 280 nm) of holo-TgCGL (dotted line) and apo-TgCGL (solid line) in 20 mM Bis-Tris-propane pH 8.3, at a concentration of 1 µM.

Limited trypsin proteolysis experiments on the holo- and apo-forms of TgCGL provided evidence for a protective effect of PLP. After 10 minutes of reaction, the 70% of apo-protein was already digested by protease; by contrast, after the same time, a 40% decrease in the 46 kDa-band intensity of holo-protein was observed. In the holo-state TgCGL was stable to proteolysis for more than 120 min. (Figures 26A and 26B).

Moreover, the holo-enzyme exhibited a higher thermal stability (T_m of about 71°C at pH 8.0) compared to the apo-protein (T_m value at about 55 °C) as observed by DSC (Figures 26C and 26D).

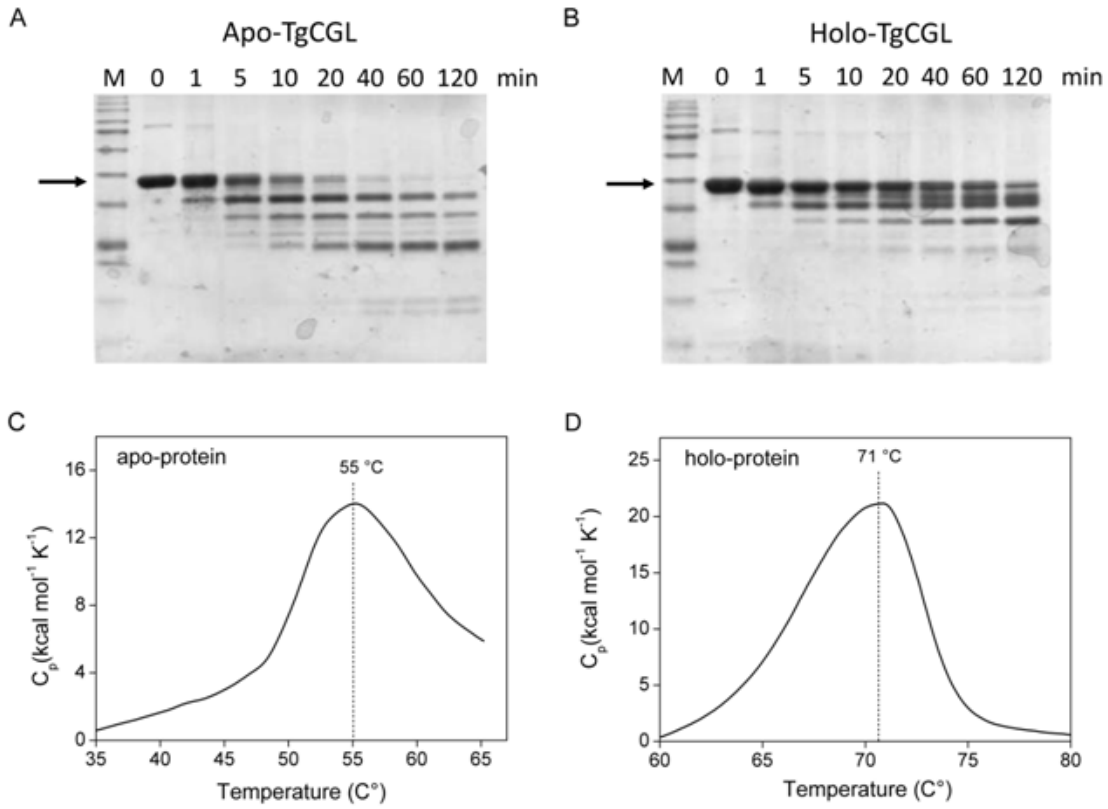

Figure 26. Properties of apo-TgCGL. (A) and (B) Trypsin digestion profile of holo- (A) and apo-TgCGL (B) after incubation of TgCGL with trypsin 1:200 (w/w) for 0, 1, 5, 10, 20, 40, 60 and 120 min, respectively. The intensity of the untreated with trypsin TgCGL band (lane 0 min) was assumed as 100%. The arrow indicates the untreated 46 kDa band. Lane M represents a molecular mass marker. (C) and (D) Representative DSC thermograms of apo- (C) and holo-TgCGL (D), respectively after baseline-correction.

3.3 Steady State Kinetic Parameters of TgCGL

To verify the appropriate reaction conditions for the enzyme, we firstly determined the effect of pH (MBP buffer in the pH range 6-10) and temperature (between 20-70 °C) on the L-cth hydrolysis of TgCGL. The purified enzyme revealed an optimum activity at pH 9 and 37°C (Figures 27A and 27B). Moreover, the enzyme exhibits a relatively high thermal stability with a T_{50} value of ~ 64 °C (Figure 27C).

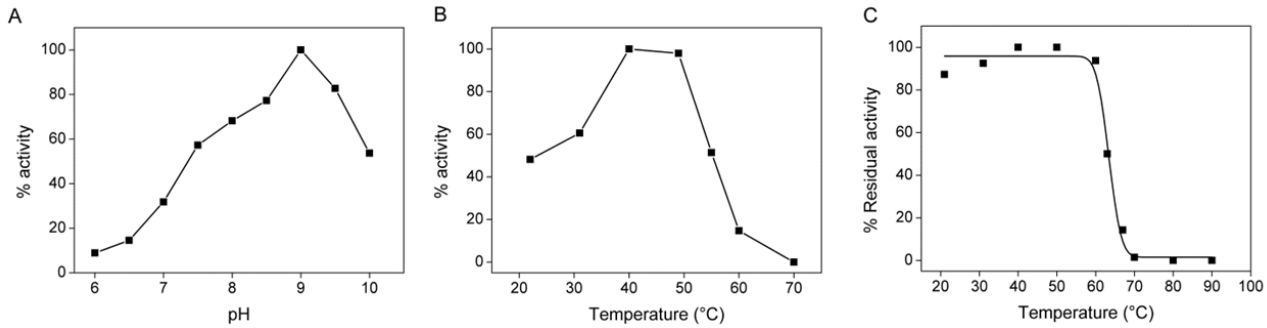

Figure 27. Activity of TgCGL: pH and temperature optima with L-cth substrate. (A) Representative profile of the effect of pH on purified TgCGL in MBP buffer in the pH range 6-10 at 37 °C. (B) Representative curve of the effect of temperature on the activity of purified TgCGL at pH 9. (C) Representative thermal stability curve for purified TgCGL, held at temperature range from 20 to 90 °C for 15 min.

The L-cth hydrolysis activity of the TgCGL was measured with both the DTNB and LDH assays. Indeed, the DTNB-based assay does not distinguish between the products of L-cth hydrolysis, which are L-homocysteine (L-hcys) and L-cys for the β- and γ-elimination reactions, respectively. Therefore, we employed also the LDH assay to monitor the formation of L-pyruvate product by specific L-cth α,β-elimination. Determination of L-cth hydrolysis via DTNB assay at pH 9 resulted in k_{cat} and K_m values of 2.0 ± 0.1 s^{-1} and 0.9 ± 0.1 mM, respectively, whereas a negligible activity was detected via LDH-coupled assay (the enzyme specific activity was < 0.4% compared to that measured by DTNB assay). Thus, TgCGL resulted highly specific for α,γ-elimination of L-cth, like in *T. cruzi* [92] and in human [102], [103], where L-cth is split almost exclusively in a CGL-specific manner, whereas the yeast enzyme harbors pronounced CBL activity [104].

Besides its role in the conversion of L-cth into L-cys, we found that TgCGL can also utilize djenkolic acid (Appendix, Figure A3), and amino-ethyl-L-cysteine, to a lesser extent (k_{cat} 0.037 ± 0.001 s^{-1} and K_m 1.3 ± 0.1 mM), via an α,β-elimination reaction (Table 4). L-cys served as a very poor substrate with a maximum velocity only 1 % of the value with the natural substrate L-cth. Substrate inhibition was also observed (k_{cat} 0.024 ± 0.001 s^{-1}, K_m 0.7 ± 0.2 mM and K_i 0.17 ± 0.02 mM).

Table 4. Steady-state kinetic parameters of TgCGL variants [a] at pH 9 and 37°C

	Assay	***k_{cat}*** **[b] (s^{-1})**	**K_m [b] (mM)**	***k_{cat}*****/ K_m ($mM^{-1}s^{-1}$)**
Hydrolysis of L-cystathionine				
wt	DTNB	2.0 ± 0.1	0.9 ± 0.1	2.2 ± 0.4
N360S	DTNB	0.24 ± 0.02	6.1 ± 1.2	0.04 ± 0.01
	LDH	0.08 ± 0.01	1.1 ± 0.1	0.07 ± 0.02
S77A	DTNB	0.7 ± 0.1	2.4 ± 0.3	0.29 ± 0.08
S77E	LDH/DTNB	n.d.[b]	n.d. [b]	-
Hydrolysis of djenkolic acid				
wt	LDH	0.24 ± 0.01	0.51 ± 0.01	0.47 ± 0.03
N360S	LDH	0.19 ± 0.01	0.86 ± 0.03	0.22 ± 0.02
S77E	LDH	n.s.[c]	n.s. [c]	0.0022 ± 0.0006
S77A	LDH	0.22 ± 0.02	1.5 ± 0.2	0.15 ± 0.03

[a] TgCGL at 1, 5 or 10 μM was used, depending on the activity of the specific enzyme variant.
[b] not detected.
[c] The notation n.s. indicates that S77E does not display saturation kinetics within the solubility limit of the djenkolic acid substrate, such that k_{cat}/K_m was determined via linear regression with the assumption that $K_m \gg$ [djenkolic acid].

Moreover, L-cys showed an inhibitory effect when assessed via LDH assay on djenkolic acid β-elimination by TgCGL. Plot of percentage inhibition versus log of L-cys concentration resulted in an IC_{50} value of 0.27 ± 0.05 mM (Figure 28A). We next estimated the K_i for L-cys by measuring the dependence of the initial velocity on djenkolic acid concentration (from 0.1 to 12 mM). (Appendix, Figure A4). The data were analyzed in double reciprocal (Lineweaver-Burk) plot and were interpolated by four straight lines resulting in a common intersection point in the second quadrant characteristic of mixed-type inhibition (Figure 28B). k_{cat} value decreases from 0.24 (no-inhibitor) to 0.12 s^{-1} and K_m value increases from 0.53 to 1.19 mM with increasing concentration of L-cys. Secondary plots of the slope and Y-intercept values, obtained from each line in the primary Lineweaver-Burk plot versus L-cys concentrations (Figure 28C), allowed extrapolation of enzyme inhibitor dissociation constants K_i (the enzyme inhibitor (EI) constant) and K_i' (the enzyme substrate complex (ESI) constant), respectively. The smaller value of K_i (160 ± 30 μM) than K_i' (370 ± 50 μM) indicates that L-cys binds with higher affinity to the free enzyme in comparison with the enzyme-substrate complex.

The availability of large amounts of the recombinant protein allowed us to analyze directly the interaction between TgCGL and L-cys by collecting absorption spectra. Upon addition of L-cys to TgCGL we observed an immediate decrease in the absorption at 421 nm (Figure 28D). Such decrease was concomitant with the appearance of a new maximum at 335 nm, which is characteristic of a thiazolidine adduct between L-cys and the PLP cofactor [105]. Indeed, it is well known that L-cys, in addition to the general ability to work as substrate for most CGL enzymes [102, 104], may bind to the aldehyde group PLP cofactor to form thiazolidine [106]. The recording of the spectra obtained for increasing concentrations of L-cys (Figure 28D) showed an isosbestic point at 370 nm, indicating the presence of only two species in the mixture, free TgCGL and L-cys-complexed enzyme. The plots of the absorbance changes at 335 and 421 nm against the L-cys concentration (Figure 28D inset), fitted to equation (6), yielded K_{app} values of 306 ± 41 μM and 273 ± 52 μM, respectively. The average value for K_{app} (290 μM) is consistent with those determined from the enzyme-inactivation data.

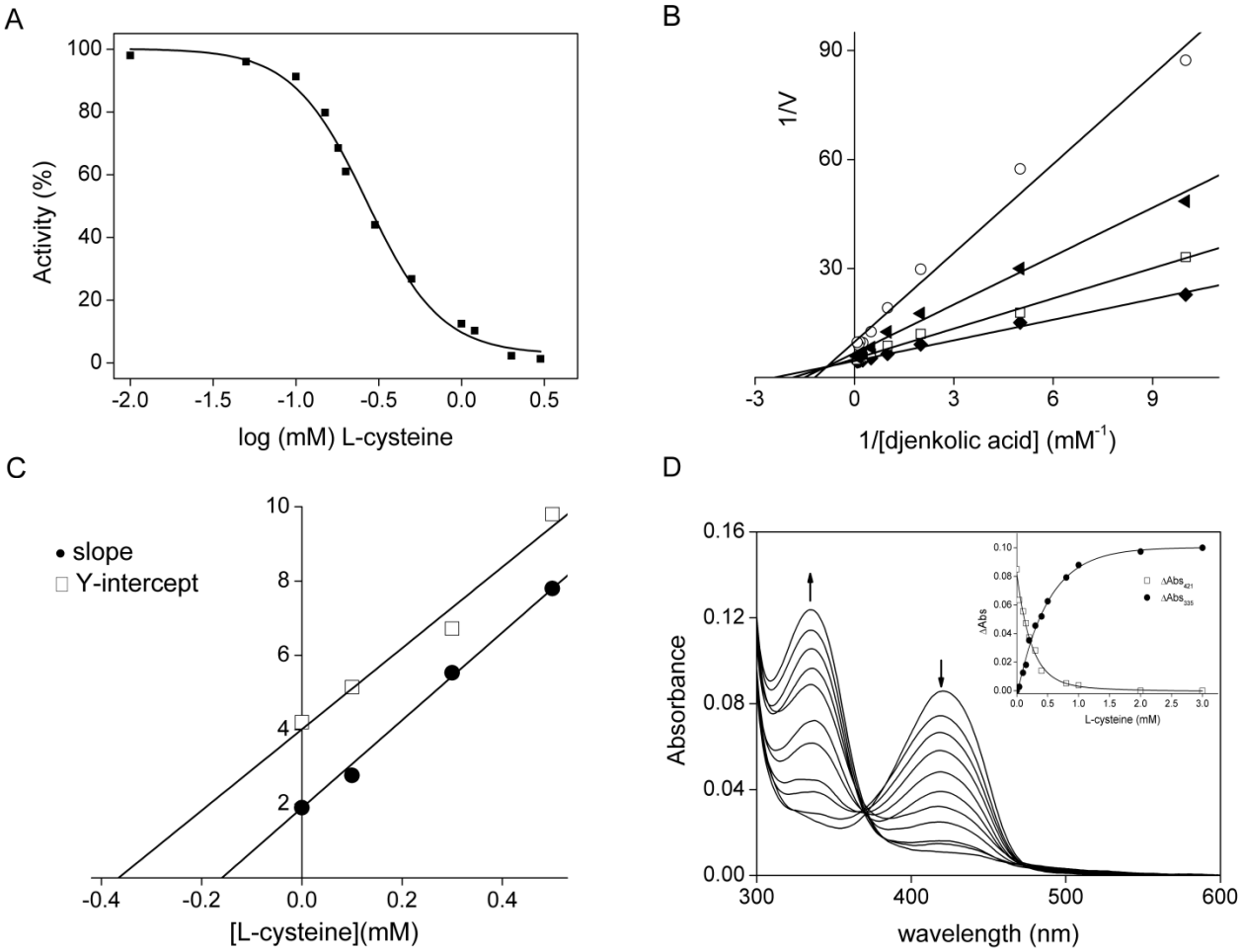

Figure 28. Inhibition of TgCGL β-eliminase activity by L-cys. (A) Representative profile of IC_{50} determination. The enzymatic activity of TgCGL was related to the activity in the absence of inhibitor (100%). The *in vitro* inhibition of enzyme by L-cys was performed in the presence of 6 mM djenkolic acid substrate via LDH assay. (B) Lineweaver-Burk plot analysis of the kinetics of TgCGL inhibition exerted by L-cys. (C) Slope and Y-intercept values from primary Lineweaver-Burk plot (panel B) versus L-cys concentrations; K_i, and K_i' were obtained as the absolute values of the concentration-axis intercepts of slope and Y-intercept plots, respectively. (D) Absorption spectra of 12 µM TgCGL upon addition of the following L-cys concentrations: 0, 0.04, 0.1, 0.15, 0.16, 0.2, 0.3, 0.4, 0.5, 0.8, 1, 2, and 3 mM. *Inset.* Absorbance changes at 335 (solid circle) and 421 nm (open square) plotted against L-cys concentration.

We also analyzed the behavior of TgCGL in the presence of PAG as it is the most widely used *in vivo* inhibitor of H_2S production by human CGL. The irreversible inactivation of human CGL by PAG has been well described [102, 103, 107]. We found that PAG inhibited also TgCGL. Because of the rapidity of the inactivation (PAG inactivated the enzyme faster than the manual mixing time for the samples), we measured the residual activity after a 15-min incubation of TgCGL with increasing concentrations of PAG (Figure 29). The very fast inactivation of TgCGL by PAG was not surprising, since the same behaviour was observed for human CGL [102, 103]. Notably, enzymatic activity of TgCGL could not be recovered by extensive dialysis, therefore confirming the irreversible inhibition.

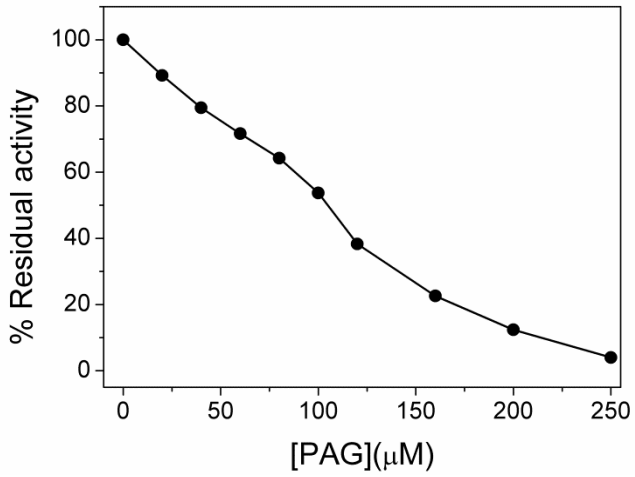

Figure 29. Residual activity of TgCGL after incubation with PAG. The inhibition of enzyme by PAG was measured in the presence of saturating concentrations of L-cth (5 mM) via the DTNB assay following pre-incubation with different concentration of the inhibitor for 15 min at room temperature.

3.4 Molecular modelling

We modelled the external aldimine of the wt enzyme in complex with L-cth and PAG, starting from the homology-modelled tetramer structure of TgCGL (residues 35-417) in its internal aldimine state. To this end, we used the crystal structures of methionine γ-lyase from Citrobacter Freundii (PDB ID code 5E4Z; % identity ≈ 44.2) and human CGL in complex with PAG (PDB ID code 3COG; % identity ≈ 41.3) as structural templates.

The predicted binding mode of L-cth in wt TgOAT is shown in Figure 30A. With the α-amino group of the substrate covalently bound to PLP, the carboxylate group of L-cth is well positioned to form an ion-pair with Arg395 and hydrogen-bonds with Asn180 and the N main-chain atom of Asn360. These interactions are also well conserved in the crystal structure of human CGL (residues Arg375, Asn161, Ser340; PDB ID code 3COG), where a nitrate ion occupies approximately the same position of the carboxylate group of L-cth in the predicted docked model. Moreover, and similarly to what observed in the crystal structure of human CGL, the ζ-amino and ζ-carboxyl groups of L-cth are predicted to share with the carboxyl and amino moieties of PAG the same interactions with two arginine residues (i.e., Arg80 and Arg138 of TgCGL and Arg62 and Arg119 in human CGL) and a glutamic acid (i.e., Glu359 of TgCGL and Glu339 in human CGL). Another interaction involving the ζ-amino moiety is represented by a water-bridged hydrogen bond with the hydroxyl group of Tyr71. The latter residue has no homologous counterpart in the human CGL, and its water-bridged hydrogen bond interaction with L-cth is replaced by the carboxyl group of human CGL Glu59.

When comparing the modelled position of PLP- L-cth and its interacting residues into the active site of TgCGL with the corresponding residues in human and yeast CGL, one striking differences is the replacement of the conserved residues of Ser334/Ser340 and Glu48/Glu59 (numbering refers to the yeast and human CGL, respectively) with Asn360 and Ser77 in TgCGL (Figure 30A). Therefore, we decided to exchange these two positions in TgCGL with the corresponding residues of human and yeast enzymes to test their effect on substrate and reaction specificity.

We also modelled wt form of TgCGL in complex with PAG and the modelling reveals that this covalent inhibitor could act as already observed in the human enzyme (covalent bond with Tyr133), since the residues interacting with the inhibitor are all well conserved between human CGL and TgCGL (Figure 30B).

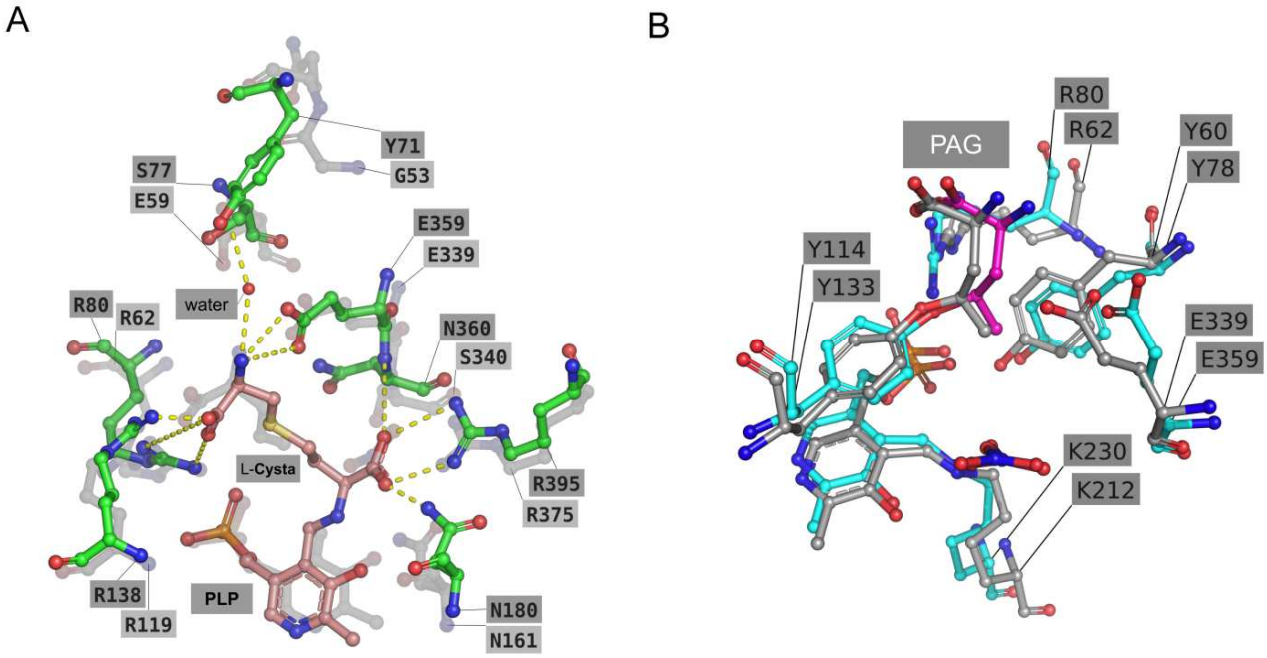

Figure 30. Modelling of the external aldimine of wt TgCGL in complex with L-cth (A) and PAG (B). (A) TgCGL is shown as green sticks, and superposed to human CGL (PDB:3COG; transparent gray sticks). The external aldimine is shown as pink sticks. Residues described in text are labeled in single-letter code. Potential favorable interactions are depicted as yellow. (B) The covalent bond between PAG (purple sticks) and Tyr133 of TgCGL (cyan sticks) is shown superposed with the corresponding residues of human CGL (PDB: 3COG; gray sticks).

3.5 N360S variant

The absorbance spectrum of N360S showed a major peak at 421 nm, as the wt protein, and a minor peak at ~500 nm, which is not present in wt enzyme but it has been already seen in the human CGL protein preparations [102, 103, 108]. This 500 nm absorption band disappeared by reconstitution of TgCGL N360S with PLP following the generation of apo-protein (Figure 31), therefore it is tentative to speculate that it could be ascribed to a quinonoid species formed by a bound amino acid that co-purifies with TgCGL. As for wt enzyme, the N360S variant binds ~1 mol of PLP/mol of monomer.

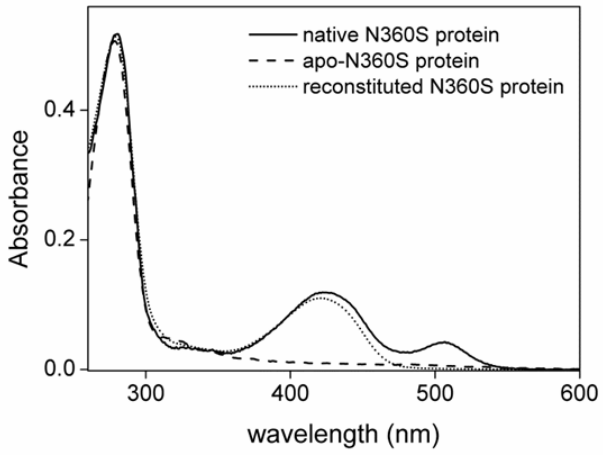

Figure 31. UV–visible absorption spectra of TgCGL N360S variant. Spectra are for native enzyme after purification (solid line), apo-protein (dashed line), and reconstituted holoenzyme (dotted line).

Substitution of N360 with Ser led to a ~56-fold decrease in catalytic efficiency for L-cth hydrolysis when analyzed via DTNB assay compared to the wt enzyme, and the change was influenced by matched ~10-fold decrease in k_{cat} and ~7-fold increase in K_m. Most importantly, α,β-cleavage of L-cth estimated via LDH-based assay was significantly increased (from negligible activity < 0.4% of that detected by DTNB assay in the wt enzyme to ~ 33% in N360S variant), and the K_m for β-elimination of L-cth was reduced by ~ 6-fold compared to the one obtained by DTNB analysis (Table 4), suggesting that the binding of L-cth in a conformation suitable for α,β-elimination is favored. The α,β-hydrolysis of L-cth was also assayed at different pH and the optimum was at 9 (data not shown).

Qualitative comparison of the reaction products with L-cth, L-hcys and L-cys standards via thin layer chromatography (TLC) analysis confirmed the production of both L-hcys and L-cys when L-cth was used as substrate for the N360S enzyme, thus confirming the ability of this variant to catalyze both α,β and α,γ-elimination toward L-cth (Figure 32).

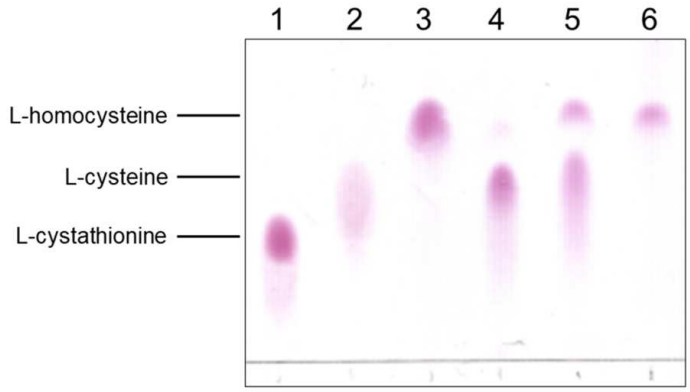

Figure 32. Product analysis of the amino acid products of L-cth hydrolysis by wt and N360S variants TgCGL. Reaction products and amino acid standards were separated by TLC and derivatized with ninhydrin. Lane 1-3, amino acids standards. Lane 1: 1 mg/mL L-cth; lane 2: 1 mg/mL L-cys; lane 3: 1 mg/mL L-hcys; lane 4: 5 mM L-cth + 100 µM wt TgCGL; lane 5: 5 mM L-cth + 100 µM N360S TgCGL; lane 6: 5 mM L-cth + 10 µM cystathionine β-lyase from *Corynebacterium diphtheriae* which catalyzes the β-elimination of L-cth to generate ammonia, pyruvate, and homocysteine.

The replacement of Asn360 by Ser had no significant effect on α,β-elimination activity towards L-cys and djenkolic acid, since for these substrates the enzyme variant showed near wt kinetic parameters (Table 4). L-cys also inhibited TgCGL N360S with an IC_{50} of 0.43 ± 0.02 mM (Figure 33A). Accordingly, the average K_{app} for TgCGL N360S-L-cys complex formation determined from spectral analyses was 333 µM (K_{app} of 335 ± 15 µM at 335 nm, K_{app} of 331 ± 20 µM at 421 nm) (Figure 33B).

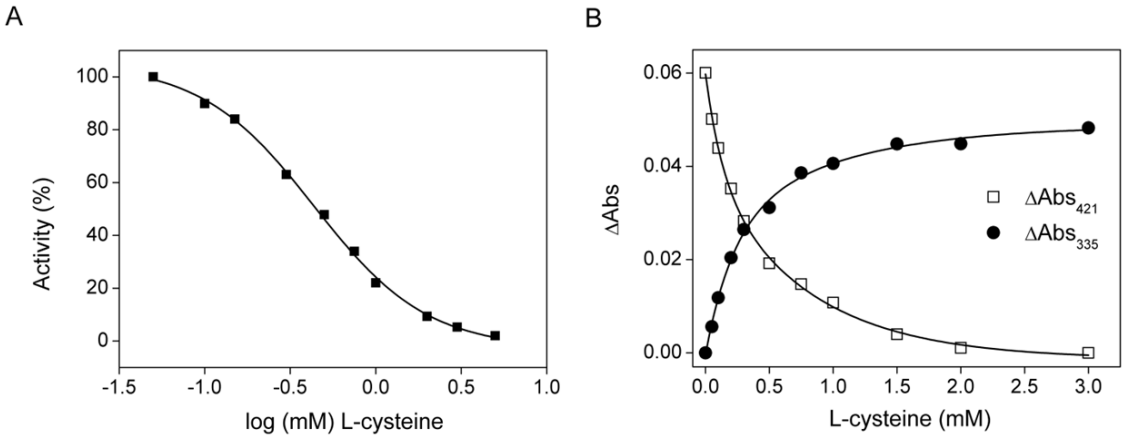

Figure 33. Inhibition profiles of TgCGL N360S variant by L-cys. (A) Representative curve for IC_{50} determination. The enzymatic activity of TgCGL N360S variant was related to the activity in the absence of inhibitor (100%). The in vitro inhibition of enzyme by L-cys was performed in the presence of djenkolic acid substrate via LDH assay. (B) Absorbance changes at 335 (solid circle) and 421 nm (open square) plotted against L-cys concentration.

The modelled N360S enzyme in its external aldimine form in complex with the L-cth substrate bound in opposite orientation (in agreement with the distinct α,β versus α,γ-elimination reaction specificity requirements) allowed us to rationalize the TgCGL N360S behavior. Notably, in the presence of N360, the binding of L-cth in a conformation suitable for α,β-elimination is partially hindered (see Figure 34A and compare with the orientation of L-cth shown in Figure 30A), due to the slight steric clash with the bulky S atom in position γ of L-cth. On the contrary, the N360S mutant is predicted to accommodate well both binding modes of L-cth (Figure 34B). Accordingly, the sulfur atom of the L-cth substrate was proposed to be an important determinant of the orientation of substrate binding and, therefore, reaction specificity in yeast CGL [95].

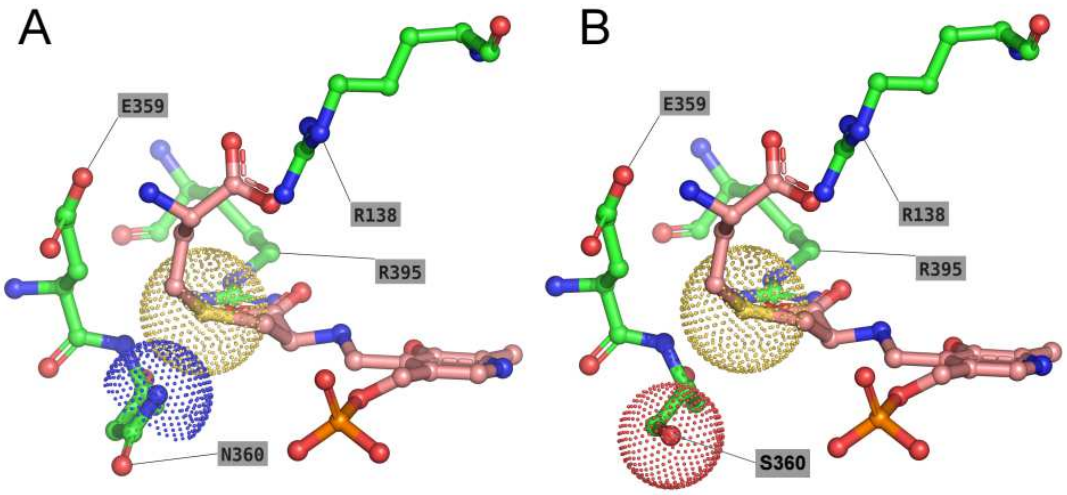

Figure 34. Modelling of the external aldimine of PLP-L-cth in complex with wild-type TgCGL (A) and N360S mutant TgCGL (B). The external aldimine of PLP-L-cth is shown as pink sticks, and the surrounding residues as green sticks. Residues described in text are labeled in single-letter code. The Van der Waals radius of the Sγ atom of L-cth is shown as yellow dots. The Van der Waals radii of Nγ N360 and Oβ S360 are shown as blue and red dots, respectively.

3.6 S77E variant

We found no difference in the absorption spectrum of S77E and in the stoichiometry of PLP-bound (~1 mol of PLP per monomer) compared to wt enzyme.

Notably, replacement of Ser77 by glutamate completely abolished activity toward L-cth. We made different attempts to determine enzymatic activity, including long incubation times, and increased substrate and enzyme concentrations, but none α,γ and α,β-elimination activities were detected.

Also the α,β-elimination activity of S77E variant was also seriously compromised. Only by increasing enzyme concentration in the assay we were able to determine the steady-state kinetic parameters of S77E towards djenkolic acid and amino-ethyl-L-cysteine, which however showed a net decrease of S77E enzyme catalytic efficiency (by 214- and 90-fold for djenkolic acid and amino-ethyl-L-cysteine, respectively) compared to wt enzyme.

The potential of the active-site residue S77 to influence L-cth hydrolysis was also explored *via* characterization of the S77A substitution. However, the near wt kinetic parameters for S77A variant did not support a direct and key role for this residue in catalysis (Table 4).

When testing the L-cys inhibitory effect on djenkolic acid β-elimination by TgCGL S77E, we found a IC_{50} value of 0.55 ± 0.09 mM (Figure 35A). Moreover, a K_{app} of 797 µM for TgCGL S77E-L-cys complex formation was determined from spectral analyses (K_{app} of 677 ± 180 µM at 335 nm, K_{app} of 874 ± 87 µM at 421 nm) (Figure 35B).

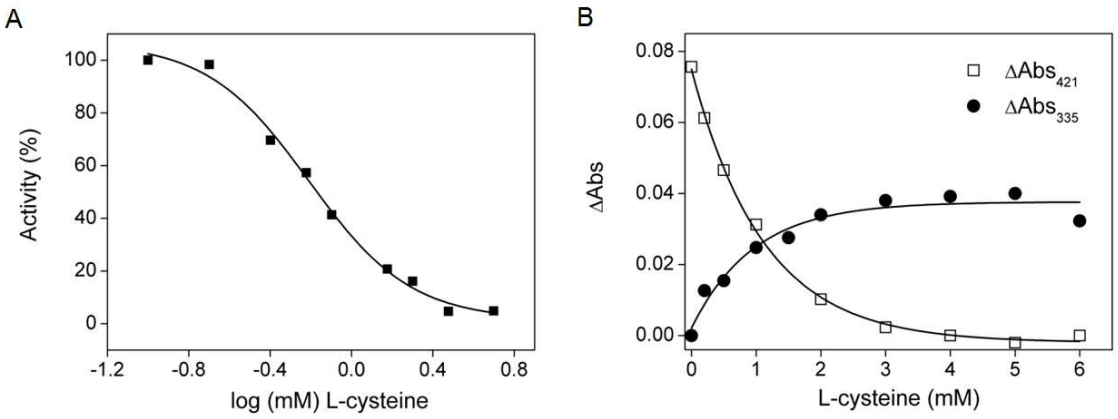

Figure 35. Inhibition profiles of TgCGL S77E variant by L-cys. (A) Representative curve for IC_{50} determination. The enzymatic activity of TgCGL S77E variant was related to the activity in the absence of inhibitor (100%). The in vitro inhibition of enzyme by L-cys was performed in the presence of djenkolic acid substrate via LDH assay. (B) Absorbance changes at 335 (solid circle) and 421 nm (open square) plotted against L-cys concentration.

Due to the presence of Tyr71, which is missing in human CGL, in the modelled S77E mutant the side-chain of Glu77 is unable to occupy the same position of the homologous Glu59 of human CGL, since this would cause a steric clash with Tyr71 (Figure 36). Instead, the side-chain of Glu77 is forced to occupy the same cleft of L-cth, possibly interfering with its binding. The overall effect of the S77E mutation could affect also the stability of the quaternary structure of the enzyme, since this residue is placed on a loop making close contacts with two other monomers of TgCGL (Figure 36, inset window).

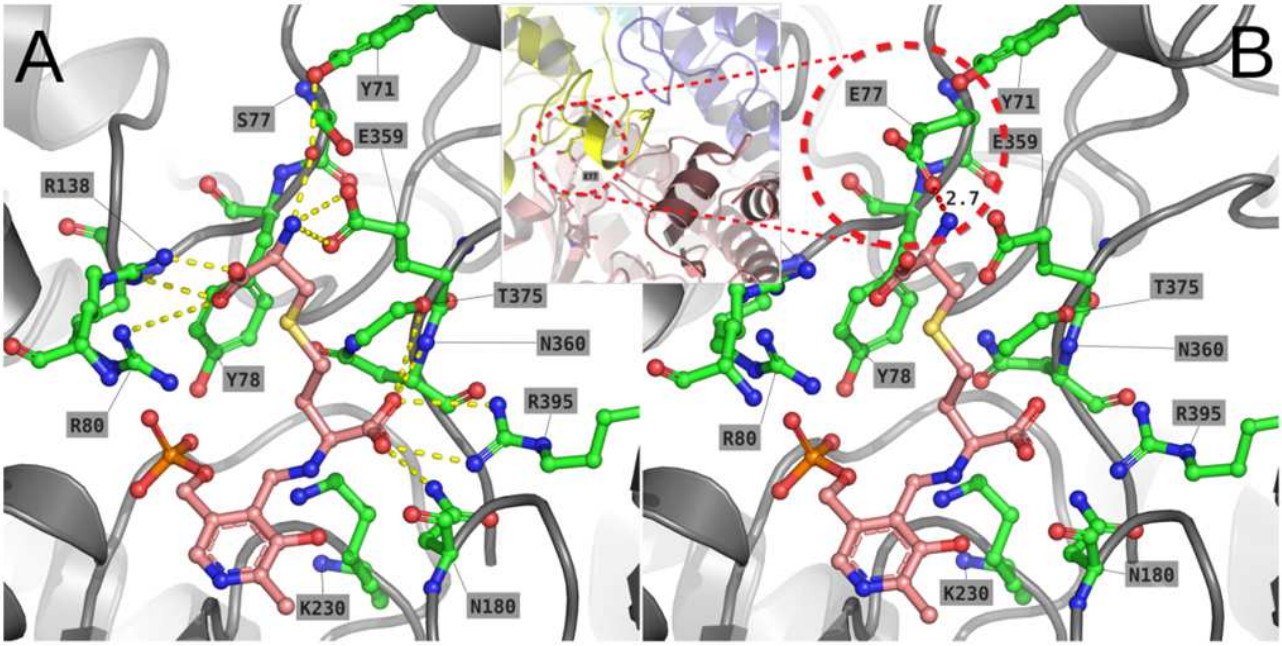

Figure 36. Modelling of the external aldimine of wild-type (A) and the S77E mutant (B) of TgCGL in complex with L-cystathionine. The external aldimines are shown as pink sticks. Residues described in text are labelled in single-letter code. Potential favourable and unfavourable interactions are depicted as yellow (A) and red (B) dashes, respectively. The position of the loop hosting E77 relatively to the other chains (A=yellow; B=pink; C=cyan; D=blue) of the quaternary structure is shown in the inset of panel (B).

The effect of mutation on structure stability of TgCGL was probed by analyzing the thermal stability of the protein both in apo- and holo-state by DSC. The holo-S77E variant showed a T_m value of about 66°C at pH 8.0, therefore indicating that the single amino acid substitution is associated with a 5 °C decrease in the protein thermal stability (Figure 37A). In contrast, the thermogram of apo-S77E variant displayed a profile identical to that of apo-wt protein with T_m value of about 55 °C (data not shown). Moreover, we evaluated the quaternary structure stability of wt and S77E enzyme variants by chemical denaturation with urea. The loss of TgCGL quaternary structure was measured by monitoring changes in protein size on a gel filtration column as a function of changes in the concentration of urea. Figure 37B shows representative unfolding curves for the wt and S77E isoforms in urea. The data were fitted by sigmoidal dose-response curves with variable slope. The midpoint transition values (C_m) between tetramer/nontetramer were 2.9 ± 0.1 M and 2.4 ± 0.2 M for the wt and S77E variants, respectively.

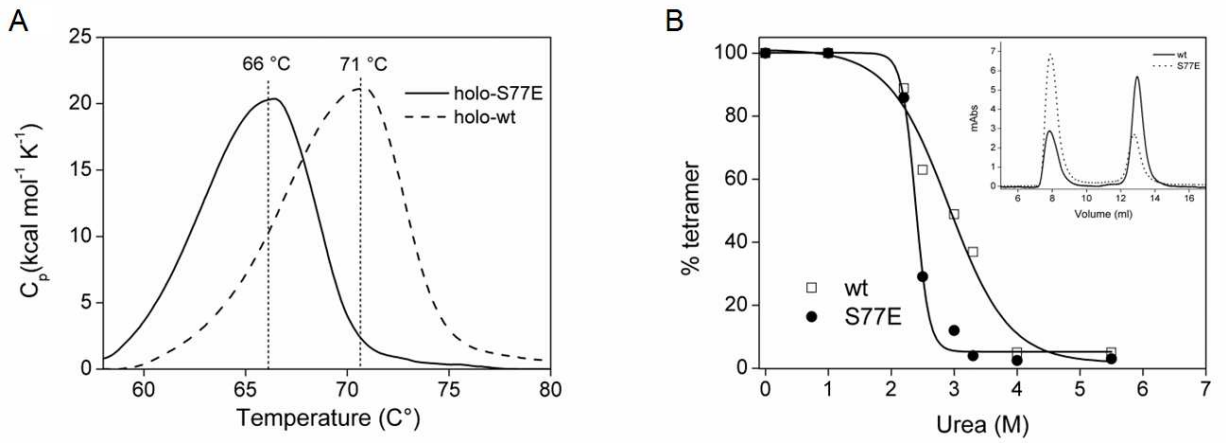

Figure 37. Effect of S77E mutation on thermal stability and quaternary structure of TgCGL. (A) Representative DSC thermograms of holo-S77E (solid line) and holo-wt (dashed line), respectively after baseline-correction. (B) Plot of percent tetrameric (% T) TgCGL wt (open square) and S77E (solid circle) as a function of the urea concentration. Inset: chromatograms of wt (solid line) and S77E (dotted line) TgCGL at 2.5 M urea.

4. DISCUSSION

The present work shows that *T. gondii* possesses a functional CGL which specifically catalyzes the cleavage at the CγS bond of L-cth, producing L-cys, α-ketobutyrate and ammonia. This finding likely implies that the reverse transsulfuration pathway is operative in the parasite. Furthermore, TgCGL was shown to convert L-cys orders of magnitudes more slowly than the natural substrate L-cth. Cysteine is an inhibitor of TgCGL, which likely suggests that, at a physiological cysteine:cystathionine ratio, the parasitic enzyme might be inhibited. This would permit tight regulation of cysteine intracellular levels, preventing its intracellular accumulation.

The enzymes of the γ-subfamily of fold-type I, especially CGS, CBL and CGL, represent and ideal model for the investigation of the structure-function relationship in terms of substrate and reaction specificity [109]. Some residues that are proposed to participate in substrate binding and catalysis are well conserved among these enzymes, even though these enzymes catalyze mechanistically distinct reactions.

Due to the high degree of similarity between TgCGL and human CGL (e.g. 40% sequence identity) it constitutes a tremendous task to design inhibitors that can distinguish between the nearly superimposable active sites of CGL. However, by structure-guided homology modelling and mutational analysis, we identified the residues Asn360 and Ser77 of TgCGL as important for the reaction and substrate specificity of the parasitic enzyme.

Mutation N360 to the corresponding residue in human (Ser) was found to influence the reaction preference of the parasitic enzyme, such that the N360S mutant harbors a significant L-cth β-lyase activity. It is an intriguing question what determines the reaction specificity for the catalysis of α,γ- versus α,β-elimination of the same substrate L-cth.

It is known that both CBL and CGL catalyze the hydrolysis of L-cth, but split the substrate at β- and γ- positions, producing homocysteine and cysteine, respectively. The pseudo-symmetric L-cth substrate, containing the equivalent of two Cα atoms, binds in opposite orientations in the active sites of CBL and CGL to allow β- versus γ-elimination [87]. Messerschmidt *et al* [95] suggested that the orientation of the L-cth in yCGL is partially due to its sulfur atom. Indeed, as demonstrated by our molecular modelling analysis, the substituted Ser allows a better accommodation of L-cth for the β-cleavage than wt, in which the Asn residue create steric obstruction.

Furthermore, Messerschmidt *et al* [95, 110] predicted that the reaction specificity of the enzyme for the α,γ- elimination versus α,β- elimination would depend on a pair of residues

located in the substrate entrance region. These residues are very conserved among CGLs and corresponds to a pair of glutamate residues (E48-E333 in yeast CGL and E59-E339 in human CGL). CBL enzymes generally possess aromatic residues in those positions, that lead to more hydrophobicity in the active site. Replacement of C-term Glu in yeast and human CGL indicated that this residue plays a unique role in the reaction specificity. In particular, the replacement of Glu333 in yeast CGL indicated that this residue interacts with distal amino moiety of L-cth and plays a unique role in the substrate binding [104]. Moreover, in human CGL, substitution of Glu339 with a hydrophobic residue increased the α,β elimination reaction toward L-cys [111]. On the other hand, mutational analysis of Glu48 in yeast CGL suggested a role into active site architecture or substrate positioning, therefore subtly and not directly influencing reaction specificity. Replacement of the corresponding D45 of CGS from *E.coli* with alanine or asparagine also results in only 2–9-fold changes in kinetic parameters, but enables a minor transamination activity, suggesting a subtle role into active site architecture or substrate positioning [112]. Notably, the mutation S77E in TgCGL completely abolished the activity toward L-cth, probably due to a complete rearrangement of the active site that prevents the binding of L-cth. However, the analysis on S77A mutant showed that this is not a catalytic residue. Molecular modelling results demonstrated that the presence of Tyr71, which has no homolog in human CGL, forces the Glu77 of the S77E variant to occupy the same cleft of L-cth This finding reinforces the importance of the structural contest of parasitic and human enzymes in defining the architecture of the active sites. Moreover, the mutation has a significant impact on the structural stability of TgCGL, as demonstrated by DSC and SEC analysis, according to the fact that this residue is placed on a loop in close contact with two other monomers.

These results provide support for the theory, proposed by Clausen [113], that the conformation and orientation of substrate(s) within the active site as well as the degree of freedom of rotation about the Cα–Cβ bond of the substrate covalently bound to the cofactor are determinants of reaction specificity among the enzymes of the γ-subfamily.

Moreover, despite the high similarity of CGL enzymes among different organisms, there are subtle differences in active site architecture which have important implications for enzyme functionality. We must await data on the three-dimensional structure of TgCGL for a thorough interpretation of these differences..

General conclusions

In this work we investigated the possible use of TgOAT and TgCGL as anti-toxoplasmosis drug targets and we contributed to gain knowledge about two metabolic pathways that are still poorly explored in *T. gondii*. However, our *in vitro* and *in silico* analysis could be considered only a first step toward the structure-based selective drug design development. First of all, the respective PLP-dependent host enzymes as well as the likely broad specificity of target inhibition have to be taken into account. In this regard, the effect of known inhibitors has to be investigated in order to provide new insights into the inhibition mechanism of the enzyme. Moreover, a virtual screening approach will lead to the rational design of more selective inhibitors that, subsequently, can be chemically synthesized and *in vitro* tested. Finally, future *in vivo* studies will be necessary to examine in depth the effective roles of these enzymes in the parasitic cell processes and infection.

Appendix

Figure A1

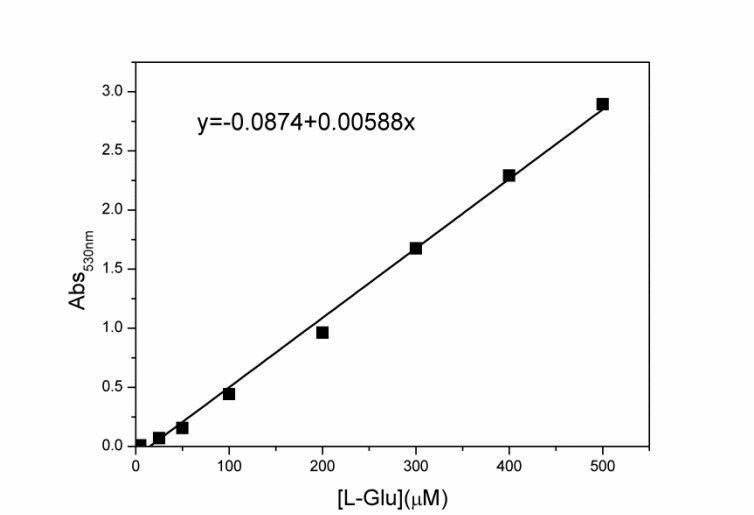

Figure A1. GOX-coupled assay calibration curve. The straight line obtained is y = -0.0874 + 0.00588x, in presence of L-glutamate, ranging from 10 to 500 μM, α-KG 5 mM, PLP 0.05 mM and phosphoric acid 14 mM.

Figure A2

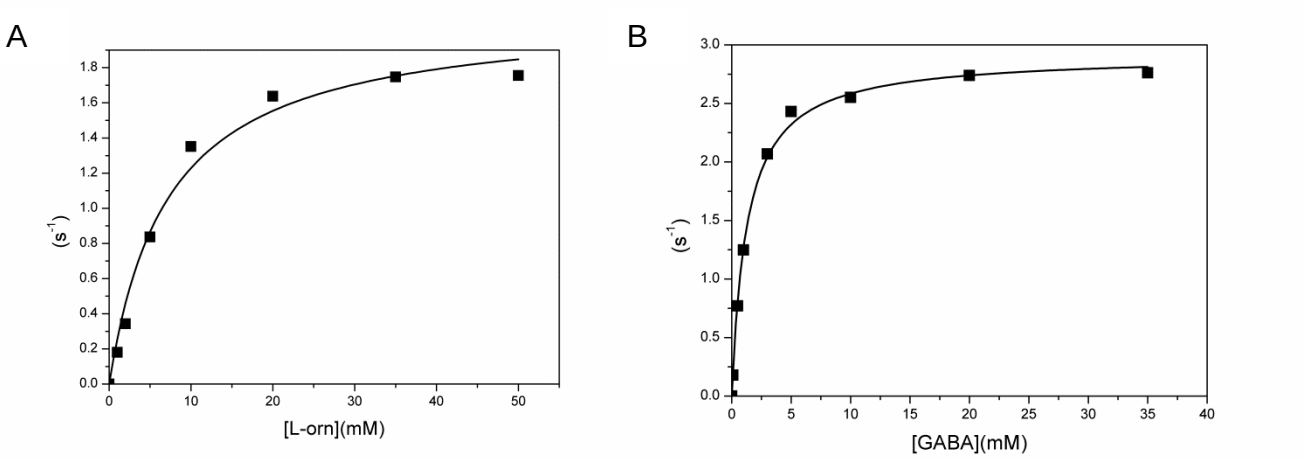

Figure A2. Michaelis – Menten profiles of TgOAT. Representative curve of TgOAT activity towards L-orn (A) and GABA (B) in the presence of 5 mM α-KG, 50 μM PLP in 50 mM Hepes pH 8 at 37 °C.

Figure A3

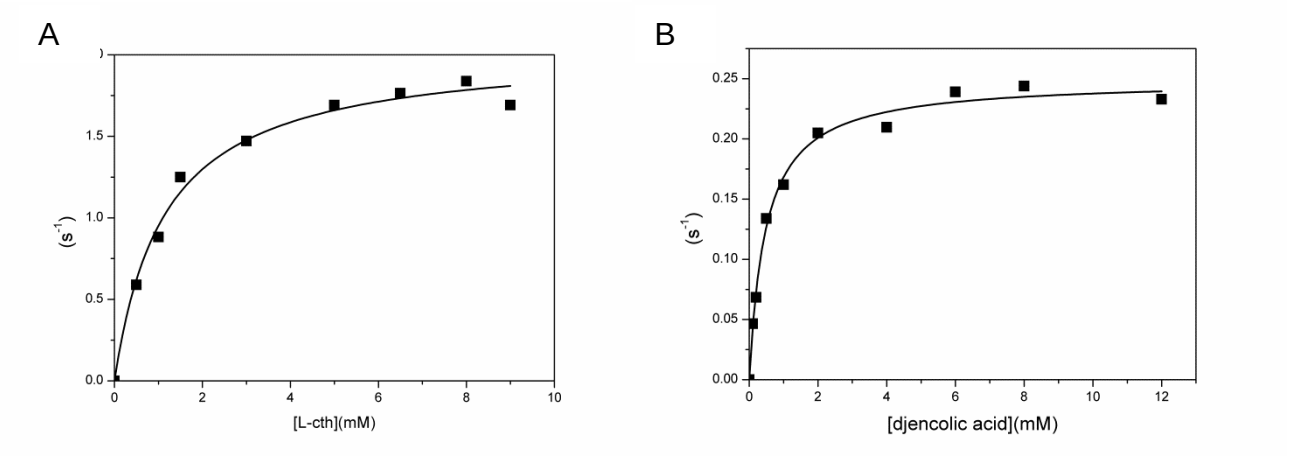

Figure A3. Michaelis – Menten profiles of TgCGL wt. Representative curve of TgCGL activity towards L-cth (A) and djencolic acid (B) at 37°C in 50 MBP buffer pH 9 in the presence of 20 μM PLP.

Figure A4

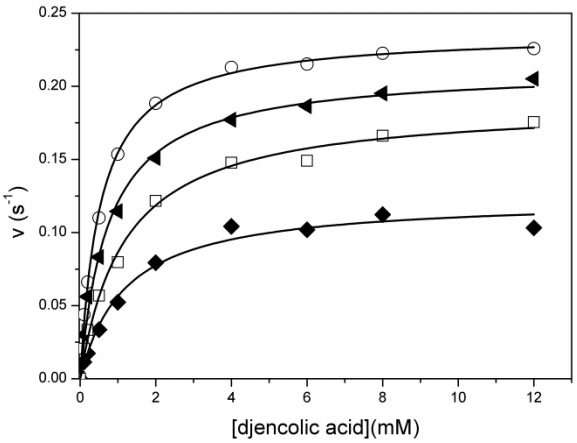

Figure A4. Inhibitory effect of L-cys on TgCGL activity. The initial velocity of enzymatic reaction was measured as a function of djencolic acid concentration at 0 (○), 100 (◀), 300 (□) and 500 (♦) μM of L-cys.

References

[1] A. Possenti *et al.*, 'Global proteomic analysis of the oocyst/sporozoite of Toxoplasma gondii reveals commitment to a host-independent lifestyle', *BMC Genomics*, vol. 14, no. 1, p. 1, 2013.

[2] G. I. McFadden and E. Yeh, 'The apicoplast: now you see it, now you don't', *Int. J. Parasitol.*, vol. 47, no. 2–3, pp. 137–144, 2017.

[3] F. Robert-Gangneux and M. L. Dardé, 'Epidemiology of and diagnostic strategies for toxoplasmosis', *Clin. Microbiol. Rev.*, vol. 25, no. 2, pp. 264–296, 2012.

[4] D. Schlüter, W. Däubener, G. Schares, U. Groß, U. Pleyer, and C. Lüder, 'Animals are key to human toxoplasmosis', *Int. J. Med. Microbiol.*, vol. 304, no. 7, pp. 917–929, 2014.

[5] A. M. Tenter, A. R. Heckeroth, and L. M. Weiss, 'Toxoplasma gondii: from animals to humans.', *Int. J. Parasitol.*, vol. 30, no. 12–13, pp. 1217–58, 2000.

[6] C. A. Hunter and L. D. Sibley, 'Modulation of innate immunity by Toxoplasma gondii virulence effectors', *Nat Rev Microbiol.*, vol. 10, no. 11, pp. 766–778, 2012.

[7] H. Denton, C. W. Roberts, J. Alexander, K. W. Thong, and G. H. Coombs, 'Enzymes of energy metabolism in the bradyzoites and tachyzoites of Toxoplasma gondii.', *FEMS Microbiol. Lett.*, vol. 137, no. 1, pp. 103–108, Mar. 1996.

[8] F. Dzierszinski, M. Mortuaire, N. Dendouga, O. Popescu, and S. Tomavo, 'Differential expression of two plant-like enolases with distinct enzymatic and antigenic properties during stage conversion of the protozoan parasite Toxoplasma gondii', *J. Mol. Biol.*, vol. 309, no. 5, pp. 1017–1027, 2001.

[9] H. M. Fritz, P. W. Bowyer, M. Bogyo, P. A. Conrad, and J. C. Boothroyd, 'Proteomic analysis of fractionated toxoplasma oocysts reveals clues to their environmental resistance', *PLoS One*, vol. 7, no. 1, 2012.

[10] T. Fleige, K. Fischer, D. J. P. Ferguson, U. Gross, and W. Bohne, 'Carbohydrate metabolism in the Toxoplasma gondii apicoplast: Localization of three glycolytic isoenzymes, the single pyruvate dehydrogenase complex, and a plastid phosphate translocator', *Eukaryot. Cell*, vol. 6, no. 6, pp. 984–996, 2007.

[11] C. A. Speer, S. Clark, and J. P. Dubey, 'Ultrastructure of the oocysts, sporocysts, and sporozoites of Toxoplasma gondii.', *J. Parasitol.*, vol. 84, no. 3, pp. 505–512, Jun. 1998.

[12] J. G. Montoya and O. Liesenfeld, 'Toxoplasmosis', *Lancet*, vol. 363, pp. 1965–1976, 2004.

[13] H. Alday and J. Doggett, 'Drugs in development for toxoplasmosis: advances, challenges, and current status', *Drug Des. Devel. Ther.*, vol. Volume11, pp. 273–293, 2017.

[14] J. N. Jansonius, 'Structure, evolution and action of vitamin B6-dependent enzymes', *Proteins*, vol. 8, pp. 759–769, 1998.

[15] A. Amadasi *et al.*, 'Pyridoxal 5'-phosphate enzymes as targets for therapeutic agents', *Curr. Med. Chem.*, vol. 14, no. 12, pp. 1291–1324, 2007.

[16] H. C. Dunathan, 'CONFORMATION AND REACTION SPECIFICITY IN PYRIDOXAL PHOSPHATE ENZYMES', *Proc. Natl. Acad. Sci. U. S. A.*, vol. 55, no. 4, pp. 712–716, 1966.

[17] R. Percudani and A. Peracchi, 'The B6 database: A tool for the description and classification of vitamin B6-dependent enzymatic activities and of the corresponding protein families', *BMC Bioinformatics*, vol. 10, p. 273, 2009.

[18] M. L. Di Salvo, N. Budisa, and R. Contestabile, 'PLP-dependent Enzymes : a Powerful Tool for Metabolic Synthesis of non-canonical amino acids', *Beilstein Bozen Symp. Mol. Eng. Control*, pp. 27–66, 2012.

[19] G. Schneider, H. Käck, and Y. Lindqvist, ‘The manifold of vitamin B6 dependent enzymes’, *Structure*, vol. 8, no. 1, pp. 1–6, 2000.
[20] P. Christen and P. K. Mehta, ‘From cofactor to Ezymes. The Molecular Evolution of Pyridoxal-5’-Phosphate-Dependent Ezymes’, *Chem. Rec.*, vol. 1, no. 6, pp. 436–447, 2001.
[21] F. Daidone *et al.*, ‘Identification by virtual screening and in vitro testing of human DOPA decarboxylase inhibitors’, *PLoS One*, vol. 7, no. 2, 2012.
[22] M. A. Azam and U. Jayaram, ‘Inhibitors of alanine racemase enzyme: A review’, *J. Enzyme Inhib. Med. Chem.*, vol. 31, no. 4, pp. 517–526, 2016.
[23] P. Storici *et al.*, ‘Structures of γ-Aminobutyric Acid (GABA) Aminotransferase, a Pyridoxal 5′-Phosphate, and [2Fe-2S] Cluster-containing Enzyme, Complexed with γ-Ethynyl-GABA and with the Antiepilepsy Drug Vigabatrin’, *J. Biol. Chem.*, vol. 279, no. 1, pp. 363–373, 2004.
[24] B. Kappes, I. Tews, A. Binter, and P. MacHeroux, ‘PLP-dependent enzymes as potential drug targets for protozoan diseases’, *Biochim. Biophys. Acta - Proteins Proteomics*, vol. 1814, no. 11, pp. 1567–1576, 2011.
[25] R. Singh, F. Spyrakis, P. Cozzini, A. Paiardini, S. Pascarella, and A. Mozzarelli, ‘Chemogenomics of pyridoxal 5′-phosphate dependent enzymes’, *J. Enzyme Inhib. Med. Chem.*, vol. 28, no. 1, pp. 183–194, 2013.
[26] A. Ö. Gevrekci, ‘The roles of polyamines in microorganisms’, *World J. Microbiol. Biotechnol.*, vol. 33, no. 11, pp. 1–7, 2017.
[27] L.-M. Birkholtz, M. Williams, J. Niemand, A. I. Louw, L. Persson, and O. Heby, ‘Polyamine homoeostasis as a drug target in pathogenic protozoa: peculiarities and possibilities’, *Biochem. J.*, vol. 438, no. 2, pp. 229–244, 2011.
[28] J. S. Keithly, G. Zhu, S. J. Upton, K. M. Woods, M. P. Martinez, and N. Yarlett, ‘Polyamine biosynthesis in Cryptosporidium parvum and its implications for chemotherapy’, *Mol. Biochem. Parasitol.*, vol. 88, no. 1–2, pp. 35–42, 1997.
[29] S. Muller *et al.*, ‘In the human malaria parasite Plasmodium falciparum, polyamines are synthesized by a bifunctional ornithine decarboxylase, S-adenosylmethionine decarboxylase.’, *J. Biol. Chem.*, vol. 275, no. 11, pp. 8097–8102, 2000.
[30] C. J. Bacchi, H. C. Nathan, and S. H. Hutner, ‘Polyamine metabolism: a potential therapeutic target in trypanosomes’, *Science (80-.).*, vol. 210, no. 4467, pp. 332–334, 1980.
[31] A. Sjoerdsma and P. J. Schechter, ‘Eflornithine for African sleeping sickness.’, *Lancet (British Ed.*, vol. 354, no. 9174, p. 254, 1999.
[32] C. Burri and R. Brun, ‘Eflornithine for the treatment of human African trypanosomiasis’, *Parasitol. Res.*, vol. 90, no. 1, pp. S49--S52, 2003.
[33] O. Heby, L. Persson, and M. Rentala, ‘Targeting the polyamine biosynthetic enzymes: A promising approach to therapy of African sleeping sickness, Chagas’ disease, and leishmaniasis’, *Amino Acids*, vol. 33, no. 2, pp. 359–366, 2007.
[34] T. Kronenberger *et al.*, ‘Vitamin B6-dependent enzymes in the human malaria parasite plasmodium falciparum: A druggable target?’, *Biomed Res. Int.*, vol. 2014, 2014.
[35] I. B. Müller, R. Das Gupta, K. Lüersen, C. Wrenger, and R. D. Walter, ‘Assessing the polyamine metabolism of Plasmodium falciparum as chemotherapeutic target’, *Mol. Biochem. Parasitol.*, vol. 160, no. 1, pp. 1–7, 2008.
[36] S. Müller, G. H. Coombs, and R. D. Walter, ‘Targeting polyamines of parasitic protozoa in chemotherapy’, *Trends Parasitol.*, vol. 17, no. 5, pp. 242–249, 2001.
[37] T. Cook *et al.*, ‘Divergent polyamine metabolism in the Apicomplexa’, *Microbiology*, vol. 153, no. 4, pp. 1123–1130, 2007.
[38] B. A. Fox, J. P. Gigley, and D. J. Bzik, ‘Toxoplasma gondii lacks the enzymes required for de novo arginine biosynthesis and arginine starvation triggers cyst formation’, *Int.*

J. Parasitol., vol. 34, no. 3, pp. 323–331, 2004.
[39] S. H. Seabra, R. A. DaMatta, F. G. de Mello, and W. de Souza, 'ENDOGENOUS POLYAMINE LEVELS IN MACROPHAGES IS SUFFICIENT TO SUPPORT GROWTH OF TOXOPLASMA GONDII', *J. Parasitol.*, vol. 90, no. 3, pp. 455–460, 2004.
[40] R. Montioli, C. Zamparelli, C. Borri Voltattorni, and B. Cellini, 'Oligomeric State and Thermal Stability of Apo- and Holo- Human Ornithine δ-Aminotransferase', *Protein J.*, vol. 36, no. 3, pp. 174–185, 2017.
[41] B. W. Shen, M. Hennig, E. Hohenester, J. N. Jansonius, and T. Schirmer, 'Crystal structure of human recombinant ornithine aminotransferase.', *J. Mol. Biol.*, vol. 277, no. 1, pp. 81–102, 1998.
[42] S. A. Shah, B. W. Shen, and A. T. Brunger, 'Human ornithine aminotransferase complexed with L-cananline and gabaculine: structural basis for substrate recongnition', *Structure*, vol. 5, no. 8, pp. 1067–1075, 1997.
[43] P. Storici, G. Capitani, R. Müller, T. Schirmer, and J. N. Jansonius, 'Crystal structure of human ornithine aminotransferase complexed with the highly specific and potent inhibitor 5-fluoromethylornithine', *J. Mol. Biol.*, vol. 285, no. 1, pp. 297–309, 1999.
[44] M. Markova, C. Peneff, M. J. E. Hewlins, T. Schirmer, and R. A. John, 'Determinants of substrate specificity in ω-aminotransferases', *J. Biol. Chem.*, vol. 280, no. 43, pp. 36409–36416, 2005.
[45] P. B. Palde and K. S. Carroll, 'A universal entropy-driven mechanism for thioredoxin–target recognition', *Proc. Natl. Acad. Sci.*, vol. 112, no. 26, pp. 7960–7965, 2015.
[46] A. Astegno, G. Capitani, and P. Dominici, 'Functional roles of the hexamer organization of plant glutamate decarboxylase', *Biochim. Biophys. Acta - Proteins Proteomics*, vol. 1854, no. 9, pp. 1229–1237, 2015.
[47] E. Passera *et al.*, 'Human kynurenine aminotransferase II - Reactivity with substrates and inhibitors', *FEBS J.*, vol. 278, no. 11, pp. 1882–1900, 2011.
[48] E. Jortzik, K. Fritz-Wolf, N. Sturm, M. Hipp, S. Rahlfs, and K. Becker, 'Redox regulation of Plasmodium falciparum ornithine δ-aminotransferase', *J. Mol. Biol.*, vol. 402, no. 2, pp. 445–459, 2010.
[49] A. Astegno, A. Giorgetti, A. Allegrini, B. Cellini, and P. Dominici, 'Characterization of C-S lyase from C. diphtheriae: A possible target for new antimicrobial drugs', *Biomed Res. Int.*, vol. 2013, 2013.
[50] R. A. Copeland, *Enzymes: A Practical Introduction to Structure, Mechanism, and Data Analysis*. 2000.
[51] A. Astegno *et al.*, 'Structural plasticity of calmodulin on the surface of CaF2 nanoparticles preserves its biological function.', *Nanoscale*, vol. 6, no. 24, pp. 15037–47, 2014.
[52] W. DeLano, 'The PyMOL Molecular Graphics System'. DeLano Scientific, San Carlos, CA, USA, 2002.
[53] E. Oppici *et al.*, 'Crystal structure of the S187F variant of human liver alanine: Aminotransferase associated with primary hyperoxaluria type I and its functional implications', *Proteins Struct. Funct. Bioinforma.*, vol. 81, no. 8, pp. 1457–1465, 2013.
[54] A. W. Schüttelkopf and D. M. F. Van Aalten, 'PRODRG: A tool for high-throughput crystallography of protein-ligand complexes', *Acta Crystallogr. Sect. D Biol. Crystallogr.*, vol. 60, no. 8, pp. 1355–1363, 2004.
[55] R. Thomsen and M. H. Christensen, 'MolDock: a new technique for high accuracy molecular docking', *J. Med. Chem.*, vol. 49, pp. 3315–3321, 2006.
[56] L. P. Kozlowski and J. M. Bujnicki, 'MetaDisorder: a meta-server for the prediction of intrinsic disorder in proteins', *BMC Bioinformatics*, vol. 13, no. 1, p. 1, 2012.
[57] X. Zhou and M. D. Toney, 'pH Studies on the mechanism of the pyridoxal phosphate-

dependent dialkylglycine decarboxylase', *Biochemistry*, vol. 38, no. 1, pp. 311–320, 1999.
[58] Y. Li, L. Feng, and J. F. Kirsch, 'Kinetic and Spectroscopic Investigations of Wild-Type and Mutant Forms of Apple', *Society*, vol. 2960, no. Scheme 2, pp. 15477–15488, 1997.
[59] H. Ikushiro, H. Hayashi, Y. Kawata, and H. Kagamiyama, 'Analysis of the pH- and ligand-induced spectral transitions of tryptophanase: Activation of the coenzyme at the early steps of the catalytic cycle', *Biochemistry*, vol. 37, no. 9, pp. 3043–3052, 1998.
[60] P. F. Cook and R. T. Wedding, 'A reaction mechanism from steady state kinetic studies for O-acetylserine sulfhydrylase from Salmonella typhimurium LT-2.', *J. Biol. Chem.*, vol. 251, no. 7, pp. 2023–2029, 1976.
[61] W. E. Karsten and P. F. Cook, 'Detection of a gem-diamine and a stable quinonoid intermediate in the reaction catalyzed by serine-glyoxylate aminotransferase from Hyphomicrobium methylovorum', *Biochim. Biophys. Acta - Gen. Subj.*, vol. 1790, no. 6, pp. 575–580, 2009.
[62] A. Binter *et al.*, 'Characterization of the PLP-dependent aminotransferase NikK from Streptomyces tendae and its putative role in nikkomycin biosynthesis', *FEBS J.*, vol. 278, no. 21, pp. 4122–4135, 2011.
[63] G. D. J. McClure and P. F. Cook, 'Product binding to the alpha-carboxyl subsite results in a conformational change at the active site of O-acetylserine sulfhydrylase-A: evidence from fluorescence spectroscopy.', *Biochemistry*, vol. 33, no. 7, pp. 1674–1683, Feb. 1994.
[64] G. B. Strambini, P. Cioni, A. Peracchi, and A. Mozzarelli, 'Characterization of tryptophan and coenzyme luminescence in tryptophan synthase from Salmonella typhimurium.', *Biochemistry*, vol. 31, no. 33, pp. 7527–7534, Aug. 1992.
[65] J. Stránská, M. Tylichová, D. Kopečný, J. Snégaroff, and M. Šebela, 'Biochemical characterization of pea ornithine-δ-aminotransferase: Substrate specificity and inhibition by di- and polyamines', *Biochimie*, vol. 92, no. 8, pp. 940–948, 2010.
[66] H. R. Kim, H. W. Rho, J. W. Park, B. H. Park, J. S. Kim, and M. W. Lee, 'Assay of ornithine aminotransferase with ninhydrin.', *Anal. Biochem.*, vol. 223, no. 2, pp. 205–207, Dec. 1994.
[67] C. Peraino and H. C. Pitot, 'Ornithine-δ-transaminase in the rat I. Assay and some general properties', *Biochim. Biophys. Acta - Spec. Sect. Enzymol. Subj.*, vol. 73, no. 2, pp. 222–231, 1963.
[68] Y. Morino, H. Kojima, and S. Tanase, 'Affinity Labeling of Alanine Aminotransferase by 3-Chloro-L-alanine', *J. Biol. Chem.*, pp. 279–85, 1979.
[69] Y. Morino and M. Okamoto, 'Labeling of the active site of cytoplasmic aspartate aminotransferase by -chloro-L-alanine.', *Biochem. Biophys. Res. Commun.*, vol. 50, no. 4, pp. 1061–1067, Feb. 1973.
[70] X. Zhou, X. Jin, R. Medhekar, X. Chen, T. Dieckmann, and M. D. Toney, 'Rapid kinetic and isotopic studies on dialkylglycine decarboxylase', *Biochemistry*, vol. 40, no. 5, pp. 1367–1377, 2001.
[71] S. Sun, C. K. Bagdassarian, and M. D. Toney, 'Pre-steady-state kinetic analysis of the reactions of alternate substrates with dialkylglycine decarboxylase', *Biochemistry*, vol. 37, no. 11, pp. 3876–3885, 1998.
[72] B. Cellini, M. Bertoldi, R. Montioli, A. Paiardini, and C. Borri Voltattorni, 'Human wild-type alanine:glyoxylate aminotransferase and its naturally occurring G82E variant: functional properties and physiological implications', *Biochem. J.*, vol. 408, no. 1, pp. 39–50, 2007.
[73] A. Holmgren, 'Thioredoxin structure and mechanism: conformational changes on oxidation of the active-site sulfhydryls to a disulfide', *Structure*, vol. 3, no. 3, pp. 239–

243, 1995.
[74] A. Holmgren, ‘Thioredoxin and Glutaredoxin systems’, *Biochemistry*, vol. 264, no. 25, pp. 13963–13966, 1989.
[75] J. K. Kumar, S. Tabor, and C. C. Richardson, ‘Proteomic analysis of thioredoxin-targeted proteins in Escherichia coli.’, *Proc. Natl. Acad. Sci. U. S. A.*, vol. 101, no. 11, pp. 3759–64, 2004.
[76] J. a Williams, G. Bridge, L. J. Fowler, and R. a John, ‘The reaction of ornithine aminotransferase with ornithine.’, *Biochem. J.*, vol. 201, no. 1, pp. 221–5, 1982.
[77] R. a John and L. J. Fowler, ‘Kinetic and spectral properties of rabbit brain 4-aminobutyrate aminotransferase.’, *Biochem. J.*, vol. 155, no. 3, pp. 645–51, 1976.
[78] B. Gajria *et al.*, ‘ToxoDB: An integrated toxoplasma gondii database resource’, *Nucleic Acids Res.*, vol. 36, no. SUPPL. 1, pp. 553–556, 2008.
[79] C. Gafan, J. Wilson, L. C. Berger, and B. J. Berger, ‘Characterization of the ornithine amino transferase from Plasmodium falciparum’, *Mol. Biochem. Parasitol.*, vol. 118, no. 1, pp. 1–10, 2001.
[80] M. Takechi, M. Kanda, K. Hori, T. Kurotsu, and Y. Saito, ‘Purification and properties of L-ornithine delta-aminotransferase from gramicidin S-producing Bacillus brevis’, *J. Biochem.*, vol. 116, no. 5, pp. 955–959, 1994.
[81] T. Ohura, E. Kominami, K. Tada, and N. Katunuma, ‘Crystallization and properties of human liver ornithine aminotransferase.’, *J. Biochem.*, vol. 92, no. 6, pp. 1785–1792, 1982.
[82] F. Steffen-Munsberg *et al.*, ‘Bioinformatic analysis of a PLP-dependent enzyme superfamily suitable for biocatalytic applications’, *Biotechnol. Adv.*, vol. 33, no. 5, pp. 566–604, 2015.
[83] R. Ledwidge and J. S. Blanchard, ‘The dual biosynthetic capability of N-acetylornithine aminotransferase in arginine and lysine biosynthesis’, *Biochemistry*, vol. 38, no. 10, pp. 3019–3024, 1999.
[84] J. T. Billheimer, H. N. Carnevale, T. Leisinger, T. Eckhardt, and E. E. Jones, ‘Ornithine delta-transaminase activity in Escherichia coli: its identity with acetylornithine delta-transaminase’, *J. Bacteriol.*, vol. 127, no. 3, pp. 1315–1323, 1976.
[85] J. I. MacRae, L. Sheiner, A. Nahid, C. Tonkin, B. Striepen, and M. J. McConville, ‘Mitochondrial metabolism of glucose and glutamine is required for intracellular growth of Toxoplasma gondii.’, *Cell Host Microbe*, vol. 12, no. 5, pp. 682–692, Nov. 2012.
[86] T. Nozaki, V. Ali, and M. Tokoro, *Sulfur-containing amino acid metabolism in parasitic protozoa*, vol. 60, no. 5. Elsevier Masson SAS, 2005.
[87] S. M. Aitken, P. H. Lodha, and D. J. K. Morneau, ‘The enzymes of the transsulfuration pathways: Active-site characterizations’, *Biochim. Biophys. Acta - Proteins Proteomics*, vol. 1814, no. 11, pp. 1511–1517, 2011.
[88] M. Tokoro, T. Asai, S. Kobayashi, T. Takeuchi, and T. Nozaki, ‘Identification and characterization of two isoenzymes of methionine gamma-lyase from Entamoeba histolytica: a key enzyme of sulfur-amino acid degradation in an anaerobic parasitic protist that lacks forward and reverse trans-sulfuration pathways.’, *J. Biol. Chem.*, vol. 278, no. 43, pp. 42717–42727, Oct. 2003.
[89] V. Ali and T. Nozaki, ‘Current therapeutics, their problems, and sulfur-containing-amino-acid metabolism as a novel target against infections by “amitochondriate” protozoan parasites’, *Clin. Microbiol. Rev.*, vol. 20, no. 1, pp. 164–187, 2007.
[90] D. Beri, B. Balan, S. Chaubey, S. Subramaniam, B. Surendra, and U. Tatu, ‘A disrupted transsulphuration pathway results in accumulation of redox metabolites and induction of gametocytogenesis in malaria’, *Sci. Rep.*, vol. 7, no. July 2016, pp. 1–13, 2017.
[91] T. Nozaki, Y. Shigeta, Y. Saito-Nakano, M. Imada, and W. D. Kruger,

‘Characterization of transsulfuration and cysteine biosynthetic pathways in the protozoan hemoflagellate, Trypanosoma cruzi: Isolation and molecular characterization of cystathionine β-synthase and serine acetyltransferase from trypanosoma’, *J. Biol. Chem.*, vol. 276, no. 9, pp. 6516–6523, 2001.

[92] D. Marciano, M. Santana, and C. Nowicki, ‘Functional characterization of enzymes involved in cysteine biosynthesis and H2S production in Trypanosoma cruzi’, *Mol. Biochem. Parasitol.*, vol. 185, no. 2, pp. 114–120, 2012.

[93] P. K. Mehta, T. I. Hale, and P. Christen, ‘Aminotransferases: demonstration of homology and division into evolutionary subgroups.’, *Eur. J. Biochem.*, vol. 214, no. 2, pp. 549–561, Jun. 1993.

[94] A. Allegrini, A. Astegno, V. La Verde, and P. Dominici, ‘Characterization of C-S lyase from Lactobacillus delbrueckii subsp. bulgaricus ATCC BAA-365 and its potential role in food flavour applications’, *J. Biochem.*, vol. 161, no. 4, pp. 349–360, 2017.

[95] A. Messerchmidt *et al.*, ‘Determinants of enzymatic specificity in the cys-met-metabolism PLP-dependent enzymes family: Crystal structure of cystathionine γ-lyase from yeast and intrafamiliar structure comparison’, *Biol. Chem.*, vol. 384, no. 3, pp. 373–386, 2003.

[96] H. Gut *et al.*, ‘A Common Structural Basis for pH- and Calmodulin-mediated Regulation in Plant Glutamate Decarboxylase’, *J. Mol. Biol.*, vol. 392, no. 2, pp. 334–351, 2009.

[97] M. Bertoldi, B. Cellini, T. Clausen, and C. B. Voltattorni, ‘Spectroscopic and kinetic analyses reveal the pyridoxal 5′-phosphate binding mode and the catalytic features of Treponema denticola cystalysin’, *Biochemistry*, vol. 41, no. 29, pp. 9153–9164, 2002.

[98] R. Vallone, V. La Verde, M. D’Onofrio, A. Giorgetti, P. Dominici, and A. Astegno, ‘Metal binding affinity and structural properties of calmodulin-like protein 14 from *Arabidopsis thaliana*’, *Protein Sci.*, vol. 25, no. 8, pp. 1461–1471, 2016.

[99] R. A. Copeland, ‘Kinetics of Single-Substrate Enzyme Reactions’, in *Enzymes: A Practical Introduction to Structure, Mechanism, and Data Analysis*, John Wiley & Sons, Inc., 2002, pp. 109–145.

[100] C. Tavani *et al.*, ‘Nitro-substituted tetrahydroindolizines and homologs: Design, kinetics, and mechanism of α-glucosidase inhibition’, *Bioorganic Med. Chem. Lett.*, vol. 27, no. 17, pp. 3980–3986, 2017.

[101] G. Janson, C. Zhang, M. G. Prado, and A. Paiardini, ‘PyMod 2.0: improvements in protein sequence-structure analysis and homology modeling within PyMOL.’, *Bioinformatics*, vol. 33, no. 3, pp. 444–446, Feb. 2017.

[102] Q. Sun *et al.*, ‘Structural basis for the inhibition mechanism of human cystathionine γ-lyase, an enzyme responsible for the production of H2S’, *J. Biol. Chem.*, vol. 284, no. 5, pp. 3076–3085, 2009.

[103] C. Steegborn *et al.*, ‘Kinetics and Inhibition of Recombinant Human Cystathionine’, *J Biol Chem*, vol. 274, no. 18, pp. 12675–12684, 1999.

[104] E. M. S. Hopwood, D. Ahmed, and S. M. Aitken, ‘A role for glutamate-333 of Saccharomyces cerevisiae cystathionine γ-lyase as a determinant of specificity’, *Biochim. Biophys. Acta - Proteins Proteomics*, vol. 1844, no. 2, pp. 465–472, 2014.

[105] P. Liu, M. P. Torrens-Spence, H. Ding, B. M. Christensen, and J. Li, ‘Mechanism of cysteine-dependent inactivation of aspartate/glutamate/cysteine sulfinic acid alpha-decarboxylases.’, *Amino Acids*, vol. 44, no. 2, pp. 391–404, Feb. 2013.

[106] S. Yamagata, M. Isaji, T. Yamane, and T. Iwama, ‘Substrate inhibition of L-cysteine alpha,beta-elimination reaction catalyzed by L-cystathionine gamma-lyase of Saccharomyces cerevisiae.’, *Biosci. Biotechnol. Biochem.*, vol. 66, no. 12, pp. 2706–2709, 2002.

[107] R. H. Abeles and C. T. Walsh, ‘Acetylenic Enzyme Inactivators. Inactivation of

gamma-Cystathionase, in Vitro and in Vivo, by Propargylglycine', *J. Am. Chem. Soc.*, vol. 95, no. 18, pp. 6124–6125, 1973.
[108] W. Zhu, A. Lin, and R. Banerjee, 'Kinetic properties of polymorphic variants and pathogenic mutants in human cystathionine gamma-lyase.', *Biochemistry*, vol. 47, no. 23, pp. 6226–6232, Jun. 2008.
[109] A. L. Manders, A. F. Jaworski, M. Ahmed, and S. M. Aitken, 'Exploration of structure-function relationships in Escherichia coli cystathionine γ-synthase and cystathionine β-lyase via chimeric constructs and site-specific substitutions', *Biochim. Biophys. Acta - Proteins Proteomics*, vol. 1834, no. 6, pp. 1044–1053, 2013.
[110] T. Clausen, R. Huber, L. Prade, M. C. Wahl, and A. Messerschmidt, 'Crystal structure of Escherichia coli cystathionine gamma-synthase at 1.5 A resolution.', *EMBO J.*, vol. 17, no. 23, pp. 6827–38, 1998.
[111] S. Huang *et al.*, 'Site-Directed Mutagenesis on Human Cystathionine-γ-Lyase Reveals Insights into the Modulation of H2S Production', *J. Mol. Biol.*, vol. 396, no. 3, pp. 708–718, 2010.
[112] A. F. Jaworski, P. H. Lodha, A. L. Manders, and S. M. Aitken, 'Exploration of the active site of Escherichia coli cystathionine γ-synthase.', *Protein Sci.*, vol. 21, no. 11, pp. 1662–71, 2012.
[113] T. Clausen, R. Huber, A. Messerschmidt, H. D. Pohlenz, and B. Laber, 'Slow-binding inhibition of Escherichia coli cystathionine β-lyase by L- aminoethoxyvinylglycine: A kinetic and X-ray study', *Biochemistry*, vol. 36, no. 41, pp. 12633–12643, 1997.